8-2017

Wide-Area Measurement-Driven Approaches for Power System Modeling and Analytics

Hesen Liu
University of Tennessee, Knoxville, hliu24@vols.utk.edu

To the Graduate Council:

I am submitting herewith a dissertation written by Hesen Liu entitled "Wide-Area Measurement-Driven Approaches for Power System Modeling and Analytics." I have examined the final electronic copy of this dissertation for form and content and recommend that it be accepted in partial fulfillment of the requirements for the degree of Doctor of Philosophy, with a major in Electrical Engineering.

Yilu Liu, Major Professor

We have read this dissertation and recommend its acceptance:

Joshua S. Fu, Fangxing Li, Wei Gao

Accepted for the Council:

Dixie L. Thompson

Vice Provost and Dean of the Graduate School

(Original signatures are on file with official student records.)

Wide-Area Measurement-Driven Approaches for Power System Modeling and Analytics

A Dissertation Presented for the

Doctor of Philosophy

Degree

The University of Tennessee, Knoxville

Hesen Liu

August 2017

DEDICATION

This dissertation is dedicated to my beloved parents, Yansheng Liu and Guilin He, whose love and encouragement make it possible for me to finish this work.

ACKNOWLEDGEMENTS

I would like to express my thanks to those who helped me with various aspects of conducting research and writing this dissertation.

Primarily, I would like to express my deepest gratitude to my advisor, Dr. Yilu Liu for her continuous guidance and persistent help for this dissertation and all other research during my Ph.D. study at the University of Tennessee, Knoxville (UTK). I am also grateful that she can fund my Ph.D. study.

I am very thankful to Dr. Joshua S. Fu， Dr. Fangxing "Fran" Li and Dr. Wei Gao for their time and efforts in serving as the members of my dissertation committee.

Moreover, I would like to express my special thanks to all the students and scholars in our group, Dr. Lin Zhu, Dr. Wenpeng Yu, Dr. Yong Liu, Dr. Jiahui Guo, Dr. Jidong Chai, Dr. Gefei Kou, Dr. Zhuohong Pan, Dr. Feifei Bai, Dr. Dao Zhou, Shutang You, Micah Joel Till, Ling Wu and Wenxuan Yao for being supportive to my research. I would like to thank Dr. Matthew Gardner, Dr. Tao Xia, and Dr. Rui Sun in Dominion Virginia Power for their guidance. In addition, I would like to thank all my friends and professors in the Center for Ultra-Wide-Area Resilient Electric Energy Transmission (CURENT) who create a loving and friendly atmosphere for conducting research.

ABSTRACT

This dissertation presents wide-area measurement-driven approaches for power system modeling and analytics. Accurate power system dynamic models are the very basis of power system analysis, control, and operation. Meanwhile, phasor measurement data provide first-hand knowledge of power system dynamic behaviors. The idea of building out innovative applications with synchrophasor data is promising.

Taking advantage of the real-time wide-area measurements, one of phasor measurements' novel applications is to develop a synchrophasor-based auto-regressive with exogenous inputs (ARX) model that can be updated online to estimate or predict system dynamic responses.

Furthermore, since auto-regressive models are in a big family, the ARX model can be modified as other models for various purposes. A multi-input multi-output (MIMO) auto-regressive moving average with exogenous inputs (ARMAX) model is introduced to identify a low-order transfer function model of power systems for adaptive and coordinated damping control. With the increasing availability of wide-area measurements and the rapid development of system identification techniques, it is possible to identify an online measurement-based transfer function model that can be used to tune the oscillation damping controller. A demonstration on hardware testbed may illustrate the effectiveness of the proposed adaptive and coordinated damping controller.

In fact, measurement-driven approaches for power system modeling and analytics are also attractive to the power industry since a huge number of monitoring devices are deployed in substations and power plants. However, most current systems for collecting and monitoring data are isolated, thereby obstructing the integration of the various data into a holistic model. To improve the capability of utilizing big data and leverage wide-area measurement-driven approaches in the power industry, this dissertation also describes a comprehensive solution through building out an enterprise-level data platform based on the PI system to support data-driven applications and analytics. One of the applications is to identify transmission-line parameters using PMU data. The identification can obtain more accurate parameters than the current parameters in PSS®E and EMS after verifying the calculation results in EMS state estimation. In addition, based on temperature information from online asset monitoring, the impact of temperature change can be observed by the variance of transmission-line resistance.

TABLE OF CONTENTS

LIST OF TABLES

LIST OF FIGURES

CHAPTER 1 INTRODUCTION OF MEASUREMENT-DRIVEN APPROACHES

1.1 Background

Since identification technologies and mathematic algorithms are developing rapidly and the number of measurement devices in power systems is increasing dramatically, measurement-driven approaches for solving power system problems are becoming hot topics. Compared to existing circuit-based models for power system calculation and analysis, measurement-driven approaches can create an updated model to reflect operating conditions of power systems promptly. Moreover, the obvious disadvantage of circuit-based models is that they can never include details of power systems. However, measurement-driven approaches can avoid the drawback. Therefore, calculation results of measurement-driven approaches may be more reliable and accurate than current circuit-based models.

Assuming the identification algorithms only depend on pure measurement data and prior knowledge, these algorithms can be viewed as black box models when details of a power system are unknown or not concerned. To derive a measurement-driven model, the construction of the model from data involves three basic entities: a data set, a set of candidate models and a rule by which candidate models can be assessed using the data. Based on datasets of inputs and outputs, the identification procedure has a natural logical flow: first collect data, then select a model set, and then pick the "best" model in this set. According to empirical data and knowledge, it is quite likely, though, that the model which is first obtained would not pass the model validation tests. If that happens, the training loop must go back to the starting point and revise the various steps of the procedure.

1.2 Introduction of Applications in This Dissertation

In this dissertation, two different linear auto-regressive models are introduced and discussed, respectively. The first linear auto-regressive model is applied to estimate system dynamic responses and another is for identifying a transfer function model for designing an adaptive wide-area oscillation damping controller. Furthermore, to exhibit the performance of linear auto-regressive models, the comparison among various identification methods is provided in terms of the time consumption, order and accuracy. In these applications, the linear auto-regressive models not only have low-order structures for the sake of updating speed, but also can obtain the acceptable results.

After discussing applications based on linear auto-regressive models, this dissertation also demonstrates an enterprise-level data platform with its data-driven applications. Taking advantage of raw data from the data platform, the identification of transmission-line parameters can be implemented by a data-driven model which is a black box model. The comparison between the parameters from both the data-driven model and the circuit-based model emphasizes that the outcome of the data-driven model has high accuracy.

Measurement-driven models in this dissertation are mainly created by synchrophasor data. Synchrophasor data can be fed into power system situational awareness applications to analyze the dynamic behavior of power systems. Thus, as an important support system for operators to reveal system dynamics and enhance the operator’s situational awareness, wide-area monitoring systems (WAMS) are built in the electric transmission network with extensive installation effort and overwhelming manufacture cost. In order to reduce cost and create flexible and robust platforms, WAMS for power grids have been extended from the transmission to distribution level in the past few years [1]. As a pioneering WAMS deployed at the distribution level, the frequency monitoring network FNET/GridEye [2]–[6] has been providing independent observation of U.S. and other worldwide electrical grid dynamic performance continuously since 2004.

Since FNET/GridEye is designed to be deployed at the distribution level, It collects power grid data (frequency, voltage magnitude, voltage phase angle, as well as power quality information) using low-cost high-accuracy frequency disturbance recorders (FDRs) [7]. An FDR can be roughly viewed as a single-phase PMU device. It utilizes voltage waveforms at standard 120 V electrical outlets as input, which is different from the much higher transmission-level voltages that need to be transduced by potential transformers (PTs) before PMUs can use them. Taking advantage of the obvious ease of installation, FDRs can be deployed virtually anywhere, such as offices, schools, and personal residences.

FNET/GridEye is widely welcomed by the industry and academia—as well as the U.S. government—and serves more than twenty main power grids in the world as of 2015. Figure 1–1 presents the existing FDR installation spots in the North America. Figure 1–2 shows the map of worldwide FDR coverage.

Figure 1–1 Map of FDR locations in North America

Figure 1–2 Map of worldwide FDR coverage

1.2.1 System Dynamic Response Estimation

Dynamic models of power systems play an important role in power system operations and planning. An accurate dynamic model can reveal system dynamic behaviors to various disturbances and help establish a mechanism of early warning of impeding instability. Traditional circuit-based models for screening transient instability are very complex and inaccurate due to limited details of a power system. In addition, even for a high-order power system, a limited number of system models in the system are critical to determine its dynamic responses. Therefore, the method for generating a low-order reduced system dynamic model by means of a measurement-driven model would be very promising to tackle the system dynamic response estimation.

In Chapter 2, a linear auto-regressive model, which is an auto-regressive with exogenous input (ARX) model, is proposed to estimate the system dynamic response using FNET/GridEye data. The model is calculated by least squares (LS) optimization to reflect the change of operating condition in a bulky power system. Case studies are conducted to test the reliability and accuracy of the model with ambient data and event data.

1.2.2 Identification of Transfer Function Model

Inter-area oscillation is a significant issue limiting the power transfer capability between areas of power systems and it also threatens power system stability. Therefore, damping of inter-area oscillations is one of the main concerns for improving power system stability and power transmission. Conventional design of oscillation damping controllers is based on system circuit-based models around a specific operating condition. This approach requires detailed dynamic models and parameters for each component, such as the generator, load, and transmission line.

However, existing circuit-based models cannot include enough detailed information of a power system. To design a wide-area adaptive oscillation damping controller to adjust the change of operating condition, a measurement-based transfer function model describing oscillatory behaviors of the power system needs to be developed.

Base on the ARX model from Chapter 2, it can be modified to a multi-input multi-output (MIMO) auto-regressive moving average exogenous inputs (ARMAX) model, which also belongs to the family of linear auto-regressive models. In Chapter 3, The methodology to identify the transfer function is described and then the performance of the MIMO ARMAX model for identifying the transfer function of a power system is presented in case studies as well.

Meanwhile, the performance comparison among different MIMO identification models to estimate inter-area oscillation modes is exhibited in Chapter 4. Study cases are conducted to test models in terms of the accuracy, order and time consumption. The results may indicate that linear auto-regressive models seem to be effective in identifying a transfer function of a power system. In addition, the cost of linear auto-regressive models is, by contrast, still very low. It would be a good method to be applied into the online environment.

1.2.3 Implementation of the Enterprise-Level Data Platform

The increasing data categories and quantities in power systems facilitate that electric utilities implement advanced data platforms to integrate data, consolidate models and enhance existing analytics and applications using data-driven methods. Chapter 5 describes the ongoing project in Dominion Virginia Power (DVP) which is an example to implement analytics with data at various resolutions. Taking advantage of integrated information and data, the data-driven visualizations for generating one-line displays are also exhibited in Chapter 5.

1.2.4 Identification of Transmission-Line Parameters

The transmission-line parameters in today's power systems still depend on the calculation from a circuit model through conductor dimension, tower geometry, line length and other factors. However, transmission-line parameters can be affected by various factors like environment factors, modeling inaccuracies and even human errors. Thus, measurement-driven approaches to estimate the transmission-line parameters are very promising to improve the accuracy of parameters.

Taking advantage of synchrophasor data from the enterprise-level platform and prior knowledge regarding the circuit model of a transmission line, a black box model in Chapter 6 can represent the model of a transmission line by input and output signals. LS method can be applied to calculate the coefficients of the measurement-based model for obtaining transmission-line parameters. Furthermore, since the platform can store the ambient temperature of transmission lines, it is possible to exhibit the impact of temperature changes on the variance of transmission-line resistance which is seldom discussed in extensive studies before.

CHAPTER 2 SYSTEM DYNAMIC RESPONSE ESTIMATION

2.1 Introduction

In this chapter, a measurement-driven approach is introduced for system dynamic response estimation. Accurate power system dynamic models are the very basis of power system analysis, control and operation [8]–[10]. Traditionally, power system dynamic responses can be obtained by the time-domain simulation package that models a power system using theoretical models and parameters for a given operating condition. However, the time-domain simulation approach has two major limitations: 1) the simulated dynamic model can never include all the details of the power system; 2) the topology and the operating point of the power system change constantly. Neither of these two aspects can be captured completely by existing circuit-based models. System identification is a good method for capturing dynamic behaviors of the power system based on pure measurement data. An auto-regressive with exogenous inputs (ARX) model, a kind of measurement-based model, has already been introduced to estimate dynamic responses. Past work with the model uses an event simulated in PSS®E (such as a generation trip or a load shedding) for training and another event response is estimated to be compared with further PSS®E simulation [11]. Taking advantage of real measurement data collected by FNET/GridEye, it is good attempt to examine and validate the performance and accuracy of the ARX model.

Validation using real measurement data is conducted in this chapter. Furthermore, the ARX model trained by ambient signals is used to estimate system responses. Few previous works have addressed the use of ambient data for estimating dynamic responses in power systems [12], [13]. The basic assumption for this improvement is that there are constant random changes occurring in power systems (such as random load variations), and these changes may provide small excitations to train the ARX model. This discovery may allow the proposed algorithm to have a near real-time estimation of dynamic responses through updating the model continuously. Accurate real-time dynamic information can form the basis for many future operation and control algorithms.

This chapter is organized as follows. The following part introduces the ARX model; and the validation methodology is also presented. After that, FDR measurement data [14] are applied to estimate and verify the ARX model. The conclusion is provided at the end of this chapter.

2.2 Model Construction

The abundant information of system dynamics is carried by synchrophasor measurements. A reasonable hypothesis is that a large power system may exhibit linear-system behaviors for most of time. The features of the power system are very linear for a small event, such as a 1500 MW generation trip or load shedding happening in the East Interconnection (EI) system. Therefore, a linear model can be utilized to estimate system dynamic responses. In other words, the ARX model is used as a linear power system dynamic model to estimate dynamic responses with real measurements.

2.2.1 ARX Model Structure

The mathematical structure expression of a single-input, single-output (SISO) ARX model is described by the equation:

$$\boldsymbol{\bar{y}(t) + \sum_{k=1}^{n} a_k\, \bar{y}(t-k) = \sum_{j=1}^{n} b_j u(t-j) + e(t)} \tag{2–1}$$

where k and j are the sampled data index, $e(t)$ is a white noise process. u and $\bar{y}$ are the model input and output, respectively. Both a_k and b_j are the ARX coefficients.

The SISO ARX model can be extended to the multi-input, single-output (MISO) ARX model as follows:

$$\boldsymbol{\begin{bmatrix} \bar{y}(t) \\ a_1\bar{y}(t-1) \\ \vdots \\ a_n\bar{y}(t-m) \end{bmatrix} = \begin{bmatrix} b_1 & \ldots & r_1 \\ b_2 & \cdots & r_2 \\ \vdots & \ddots & \vdots \\ b_n & \cdots & r_n \end{bmatrix} \begin{bmatrix} u_1(t) & \cdots & u_1(t-n) \\ u_2(t) & \cdots & u_2(t-n) \\ \vdots & \ddots & \vdots \\ u_n(t) & \cdots & u_n(t-n) \end{bmatrix} + e(t)} \tag{2–2}$$

The model parameters of the ARX model can be estimated by a linear Least squares (LS) approach. The least squares estimation problem is solved by using QR factorization to optimize the ARX model parameters and minimizing the following function:

$$\boldsymbol{V_{LS} = \sum_{t=n_s+1}^{N} \varepsilon_{ARX}(t)^2} \tag{2–3}$$

where the error criterion ε_{ARX} is described by:

$$\boldsymbol{\varepsilon_{ARX} = \bar{y}(t) + \sum_{k=1}^{n} a_k\, \bar{y}(t-k) - \sum_{j=1}^{n} b_j u(t-j)} \tag{2–4}$$

2.2.2 ARX Model Accuracy Index

To evaluate the identified ARX model, accuracy index can be performed as follows:

$$\boldsymbol{Accuracy\ Index} = \left(\mathbf{1} - \frac{\|\boldsymbol{Y_i} - \widehat{\boldsymbol{Y}}_{\boldsymbol{i}}\|}{\|\boldsymbol{Y_i} - \overline{\boldsymbol{Y}}_{\boldsymbol{i}}\|}\right)\times\mathbf{100} \qquad (2\text{–}5)$$

where Y_i, $\bar{Y}_i$, $\hat{Y}_i$ are the measured response, the estimated response, and the mean value of the measured response, respectively. This index is used to reflect the accuracy of the model for describing system dynamic characteristics. An accuracy index of 100 means a perfect fit between the estimated response and measured response, while an accuracy index of 0 means the estimated response is no better than the mean value of the measured response.

2.2.3 Correlation Coefficient Index

In power systems, a widely used measurement-based coherency function [15]–[17] is defined as:

$$\boldsymbol{\gamma_{xy}}(\boldsymbol{f}) = \frac{|\boldsymbol{S_{xy}}(\boldsymbol{f})|}{\sqrt{\boldsymbol{S_{xx}}(\boldsymbol{f})\boldsymbol{S_{yy}}(\boldsymbol{f})}} \qquad |\boldsymbol{\gamma_{xy}}| \le \mathbf{1} \qquad (2\text{–}6)$$

where f is the frequency, γ_{xy} is the coherent relationship between power system measured signals $\{x(t)\}$ and $\{y(t)\}$. $S_{xy}(f)$ is the cross-spectral density (CSD) function between $\{x(t)\}$ and $\{y(t)\}$, $S_{xx}(f)$ and $S_{yy}(f)$ are the power-spectral density (PSD) of $\{x(t)\}$ and $\{y(t)\}$, respectively.

These two signals can be assumed as the wide-sense stationary random processes. The coherency function literally presents the linear correlation between two output signals in the power system as a function of the frequency. However, the frequency domain function is not convenient when dealing with many signals. The following equations may be used to obtain the time domain correlation function which is correlation coefficient index (CCI) for a wide frequency.

The cross-correlation function $R_{xy}(\tau)$, self-correlation functions $R_{xx}(\tau)$ and $R_{yy}(\tau)$ are given by the inverse Fourier transform of $S_{xy}(f)$, $S_{xx}(f)$and$S_{yy}(f)$, respectively.

$$\boldsymbol{R_{xy}(\tau) = \int_{-\infty}^{+\infty} S_{xy}(f) e^{j2\pi f\tau} df} \tag{2–7}$$

$$\boldsymbol{R_{xx}(\tau) = \int_{-\infty}^{+\infty} S_{xx}(f) e^{j2\pi f\tau} df} \tag{2–8}$$

$$\boldsymbol{R_{yy}(\tau) = \int_{-\infty}^{+\infty} S_{yy}(f) e^{j2\pi f\tau} df} \tag{2–9}$$

where τ is the time delay.

Applying the inverse Fourier transform to (2–6) and using (2–7), (2–8), and (2–9), the correlation function in the time domain is:

$$\boldsymbol{r_{xy}(\tau) = \int_{-\infty}^{+\infty} \gamma_{xy}(f) e^{j2\pi f\tau} df = \frac{R_{xy}(\tau)}{\sqrt{R_{xx}(\tau) R_{yy}(\tau)}}} \tag{2–10}$$

The mathematical expectations of these two signals are $u_x = E\{x(t)\}$ and $u_y = E\{y(t)\}$, respectively. Thus, the cross-correlation function $R_{xy}(\tau)$ and cross-covariance function $C_{xy}(\tau)$ are defined:

$$\boldsymbol{R_{xy}(\tau) = E\{x(t)y(t+\tau)\} = \lim_{T\to\infty}\frac{1}{T}\int_0^T x(t)y(t+\tau)dt} \tag{2–11}$$

$$\boldsymbol{C_{xy}(\tau) = \lim_{T\to\infty}\frac{1}{T}\int_0^T \{x(t)-\mu_x\}\{y(t+\tau)-\mu_y\}dt = R_{xy}(\tau)-\mu_x\mu_{xy}} \tag{2–12}$$

For the special case where $x(t) = y(t)$, the self-covariance function of $C_{xx}(\tau)$ and $C_{yy}(\tau)$ are:

$$\boldsymbol{C_{xx}(\tau) = R_{xx}(\tau) - \mu_x^2} \qquad \boldsymbol{C_{yy}(\tau) = R_{yy}(\tau) - \mu_y^2} \tag{2–13}$$

If $\mu_x = \mu_y = 0$ in (2–10), it can be obtained:

$$\boldsymbol{C_{xy}(\tau) = R_{xy}(\tau)} \qquad \boldsymbol{C_{xx}(\tau) = R_{xx}(\tau)} \qquad \boldsymbol{C_{yy}(\tau) = R_{yy}(\tau)} \tag{2–14}$$

Assuming the time delay $\tau = 0$ and using (2–10) and (2–14), the correlation coefficient function can be obtained:

$$\boldsymbol{\gamma_{xy}(0) = \frac{C_{xy}(0)}{\sqrt{C_{xx}(0)C_{yy}(0)}}} \tag{2–15}$$

where γ_{xy} is the correlation coefficient between signal $\{x(t)\}$ and $\{y(t)\}$ in time domain, which ranges from -1 (complete linear inverse correlation) to 1 (complete linear correlation) with $\gamma_{xy} = 0$ meaning lack of linear interdependence. The sign of γ_{xy} indicates the direction of correlation: $\gamma_{xy} < 0$ implies inverse correlation, while $\gamma_{xy} > 0$ implies direct correlation.

The CCI between the ith input signal x_i and the jth output signal y_i is defined as:

$$\boldsymbol{\gamma_{ij}} = \frac{\boldsymbol{C(x_i, x_j)}}{\sqrt{\boldsymbol{C(x_i, x_i)C(y_j, y_j)}}} \tag{2–16}$$

where i and j are the input and output signal number, respectively.

The CCI can be a good indication to find strong correlated measurements of various locations as inputs of the ARX model.

2.3 Validation Methodology of System Dynamic Response

Event and ambient data are used as datasets for training the model. Event data are much easier to train the ARX model than ambient data because event data change obviously. However, ambient data, which are collected before an event, can also provide effective information for estimating event responses. Measurement data always have noise. Therefore, one critical thing in the procedure of data preparation is to extract and clean ambient or event signals from raw data before train the model.

2.3.1 De-Trending Method

An important preprocessing procedure to build out the measurement-based model for the dynamic response estimation is to remove direct component (DC) trends within measurement data. Normally, this operation is known as de-trending, and keeps the result from being overwhelmed by the nonzero mean and the trend.

The first step of implementing the de-trending method is to get the mean value of the original signal and then raw data can be deducted by the mean value to remove the DC offset:

$$\boldsymbol{y}(\boldsymbol{k}) = \boldsymbol{x}(\boldsymbol{k}) - \overline{\boldsymbol{x}} \tag{2–17}$$

where k is the sample number of the original signal and $\bar{x}$ is the average value of the signal over the period. y is the data without the DC offset.

The next step is to de-trend the angle signal $y(k)$ by removing the trend of the angle reference point, $y_f(k)$ is the reference data that its mean value is removed.

$$\boldsymbol{r}(\boldsymbol{k}) = \boldsymbol{y}(\boldsymbol{k}) - \boldsymbol{y}_{\boldsymbol{f}}(\boldsymbol{k}) \tag{2–18}$$

where k is the sample number of the original signal and r is the data without the DC offset and reference value.

For analysis using measurement data, this method may highlight any major oscillations and transient changes through either event data or ambient data while slow drift and steady-steady responses are removed.

2.3.2 Implementation of Dynamic Response Estimation

Optimal input signals are selected by the CCI for the ARX method to estimate dynamic responses of events. However, the CCI may be not effective in some sense for choosing the input signals to estimate responses using ambient data. The methodology is described by the flowchart below in Figure 2–1.

Therefore, if the CCI cannot obtain the good inputs for the ARX model, the optimal input signals can be selected by the measurement units' geographic proximity to each other as an alternative approach. To estimate a dynamic response, two sets of data are needed. One set of data is considered as the training data of the model. Another set of data will be applied to estimate the dynamic response and evaluate the result.

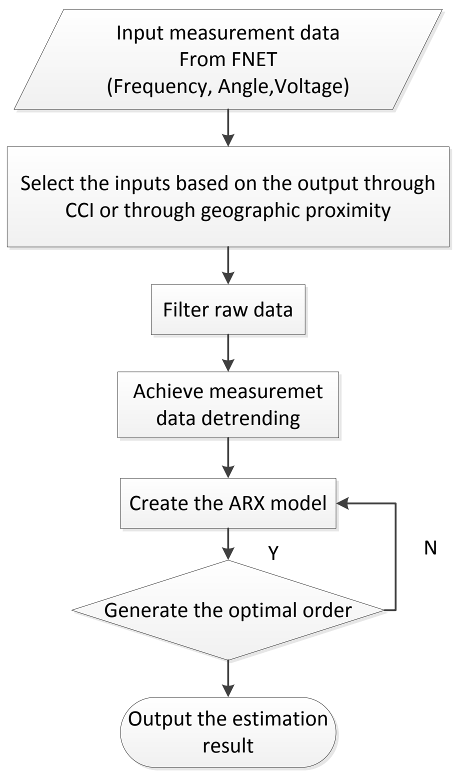

Figure 2–1 Flowchart of the system dynamic response estimation

To train and verify the ARX model, the most critical thing is to determine the order of the model since it is associated with the structure and dimension of the model. Some pre-defined models can be the candidate models. The model with the best estimation from pre-defined models would have the optimal order. According to empirical data, the model with accuracy index equal or greater than 85 may be acceptable. Otherwise, the ARX model should be re-trained.

2.4 Case Study

Case studies are based on data collected by FNET/GridEye in the EI system. The validation is performed with two types of data: event data and ambient data. For each case, the dynamic responses of frequency, voltage phase angle and voltage magnitude are estimated by corresponding ARX models.

2.4.1 Event Dynamic Response Estimated by Event Data

In this part, there are four combinations, including the response estimation of a generation trip using the model trained by a load shedding (Case 1), the response estimation of a load shedding using the model trained by a generation trip (Case 2), the response estimation of a load shedding using the model trained by a load shedding (Case 3) and the response estimation of a generation trip using the model trained by a generation trip (Case 4). In each case, four inputs, one output and one reference point that is the angle reference for the angle dynamic response estimation are selected and marked in the map where the FDRs are deployed. Furthermore, the comparisons between estimated voltage, angle and frequency responses and their actual responses from the output point are given in Figure 2–2, Figure 2–3, Figure 2–4 and Figure 2–5, respectively.

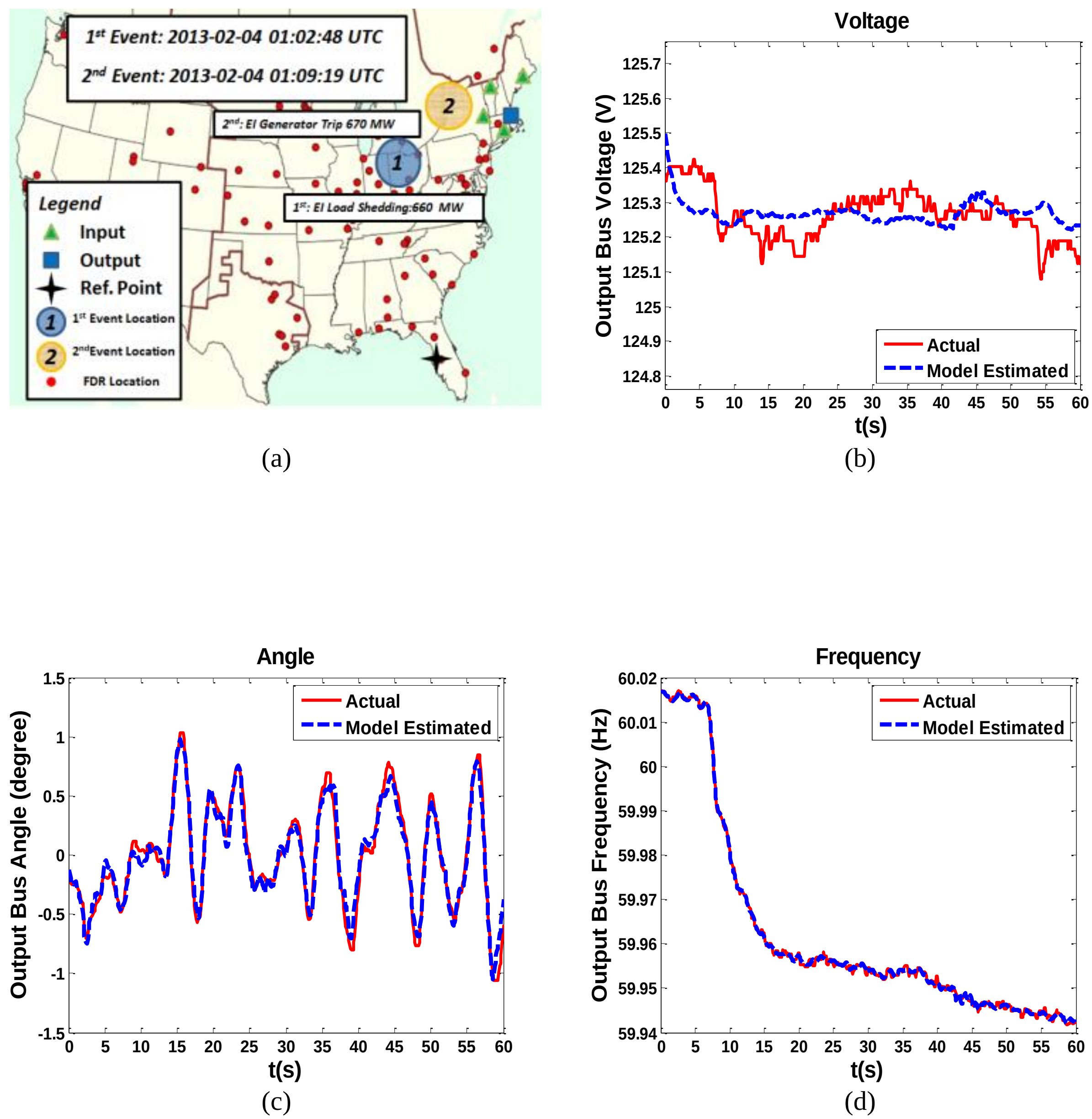

Figure 2–2 Comparison between the actual measurement and estimation in case 1

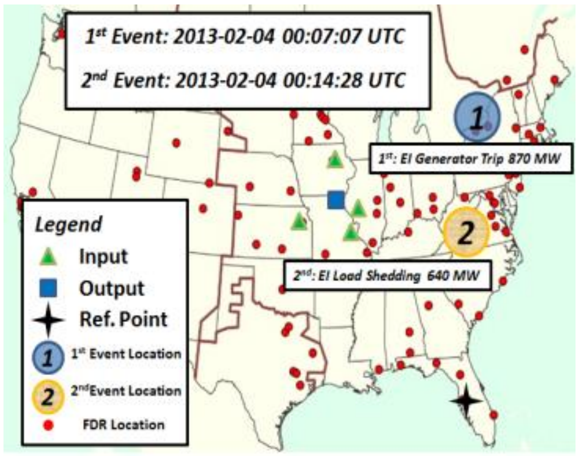

(a)

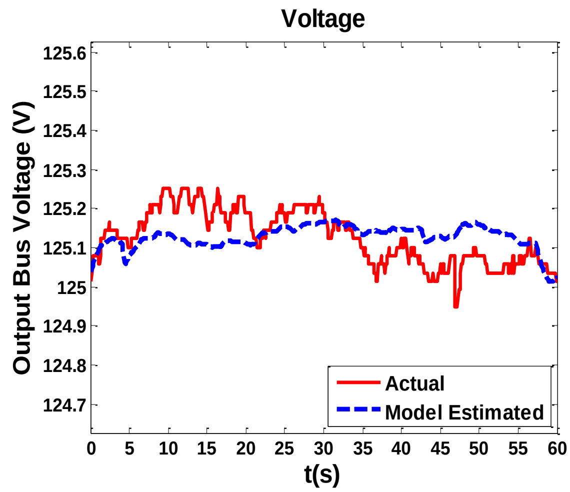

(b)

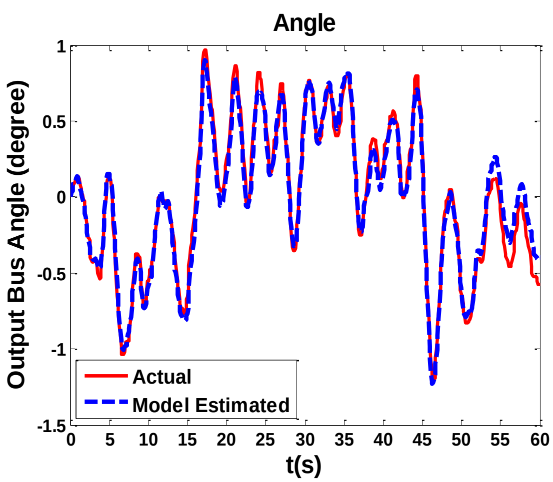

(c)

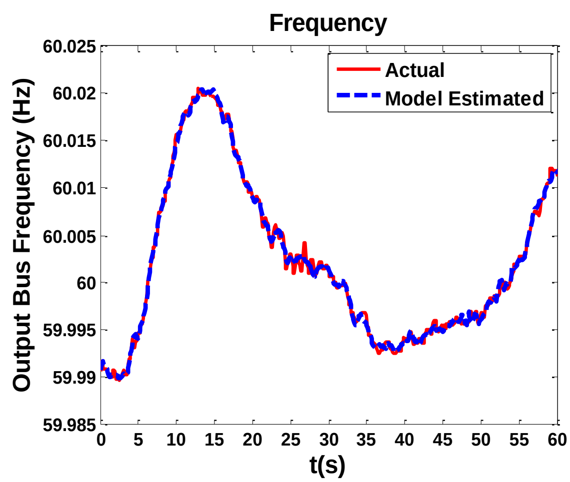

(d)

Figure 2–3 Comparison between the actual measurement and estimation in case 2

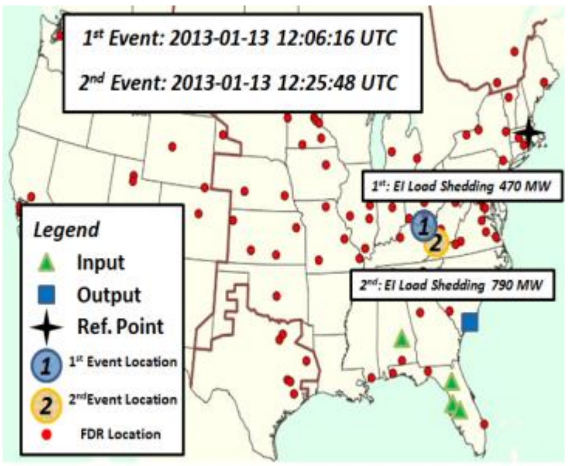

(a)

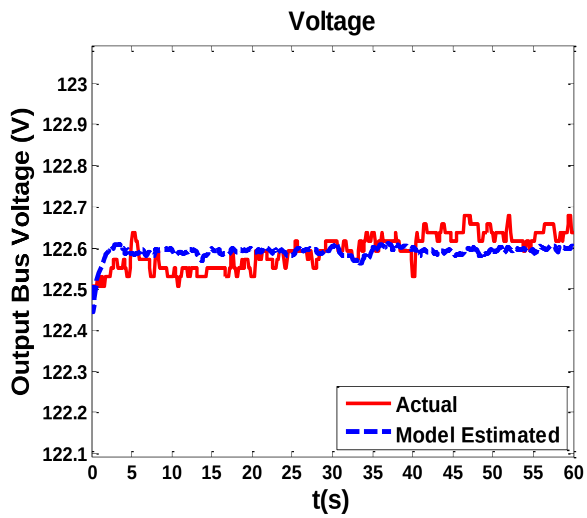

(b)

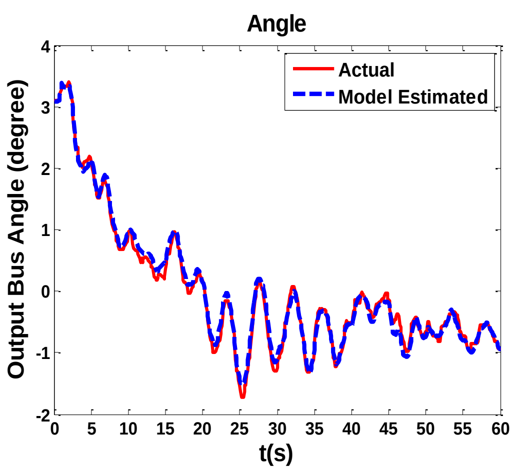

(c)

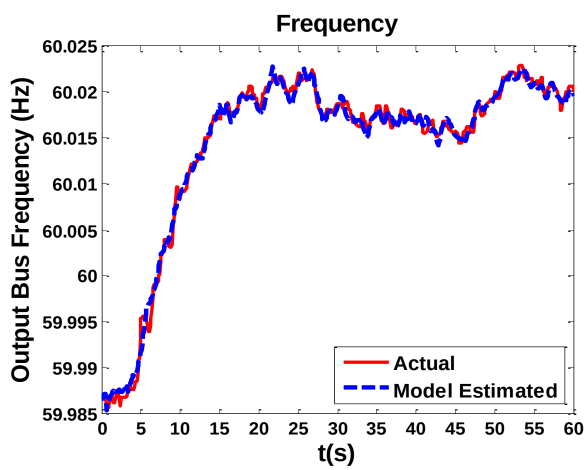

(d)

Figure 2–4 Comparison between the actual measurement and estimation in case 3

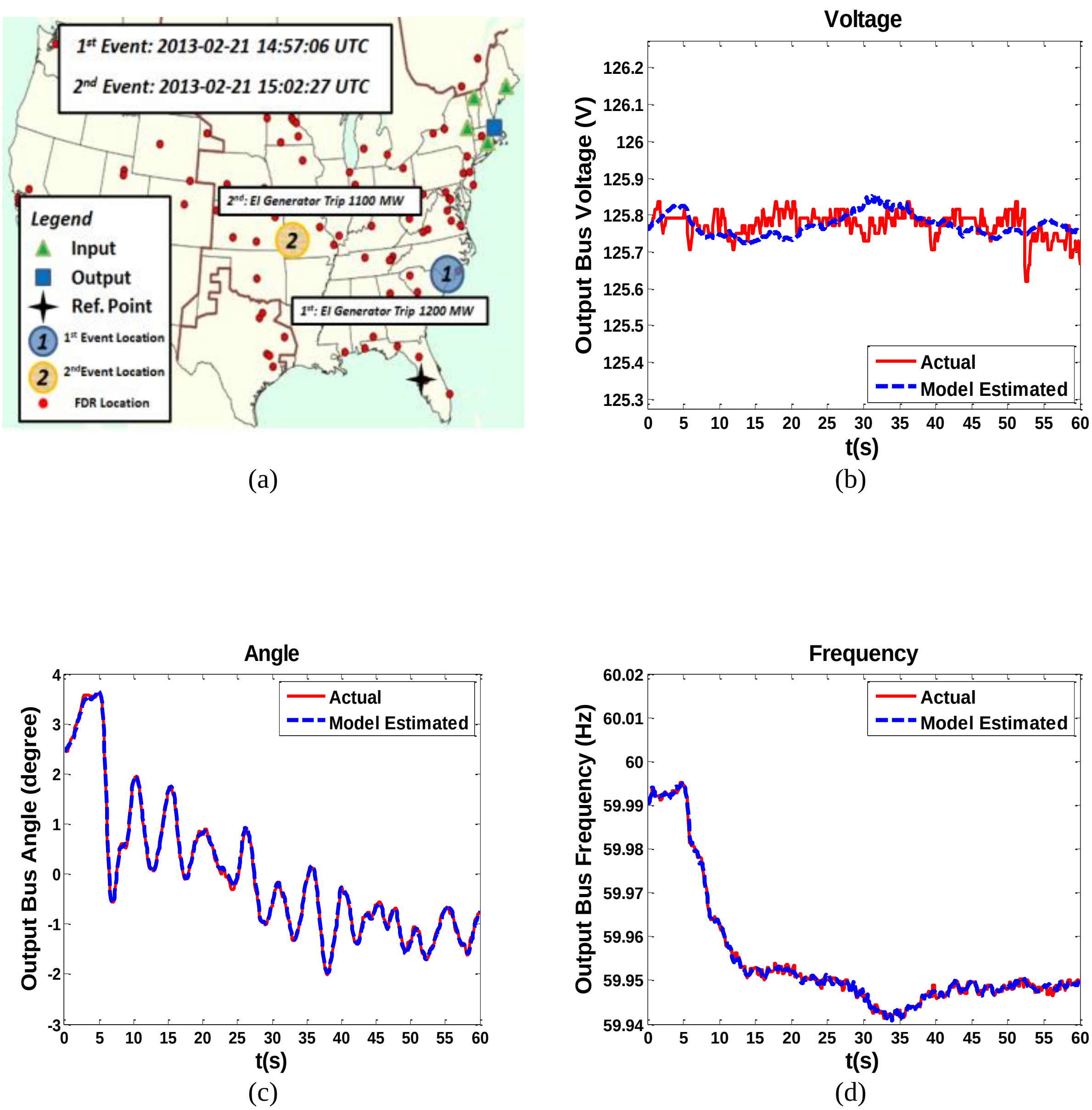

Figure 2–5 Comparison between the actual measurement and estimation in case 4

In Table 2-1, the estimated dynamic responses of angle and frequency match the actual response well since these quantities are relatively correlated in the wide area. Although the frequency accuracy index is much higher than the angle accuracy index in the same case, the estimation results are all satisfactory. Therefore, regardless of the event type for training the ARX model, the ARX model can achieve the good estimation of the angle and frequency dynamic response consistently. However, the voltage response estimation is not good generally. The rooted reason is the voltage magnitude is very local and regional in the distribution level. Thus, in terms of the voltage magnitude, it is difficult to select proper inputs based on the specific output from the distribution network for training the ARX model. In the following tests, the estimation of angle/frequency dynamic responses is included only.

Table 2-1 Voltage/Angle/Frequency accuracy index from case 1 to case 4

	Voltage accuracy index	Angle accuracy index	Frequency accuracy index
Case 1	30.21	93.71	95.02
Case 2	36.86	94.11	96.55
Case 2	65.34	91.06	92.63
Case 4	52.73	88.49	94.31

2.4.2 Event Dynamic Response Estimated by Ambient Data

The ARX models for the cases in the previous part are trained by event data from FNET/GridEye. However, the number of events is limited and the information provided by the events is not adequate. Ambient data can be obtained continuously and sufficiently through the data collection. Moreover, they can provide operating information and be alternative data for event data. The following tests utilize ambient data to estimate event responses.

In this part, there are also four combinations, including the response estimation of generation trips (Case 5 and Case 6) and the response estimation of load sheddings (Case 7 and Case 8) from the ARX models trained by ambient data, respectively.

To compare the results from the ARX models trained by event data and ambient data, event data are replaced with ambient data to train the ARX models in four cases from the previous part. Ambient data are collected before events happen. The results from Case 5 to Case 8 are presented in Figure 2–6, Figure 2–7, Figure 2–8 and Figure 2–9, respectively.

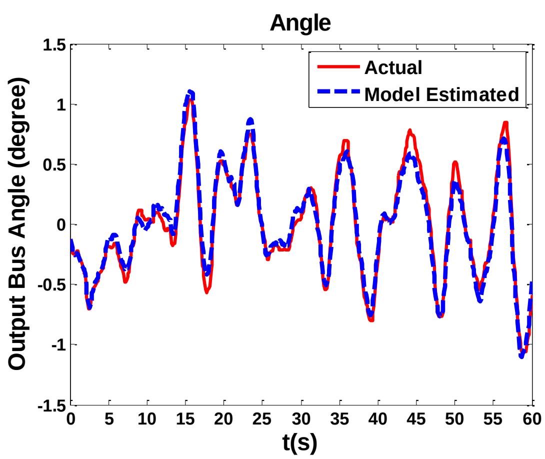

(a)

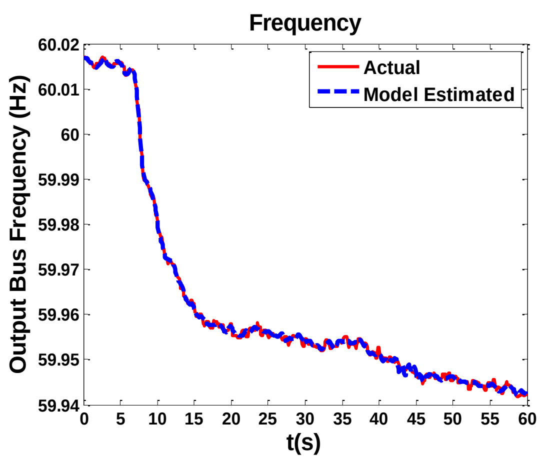

(b)

Figure 2–6 Comparison between the actual measurement and estimation in case 5

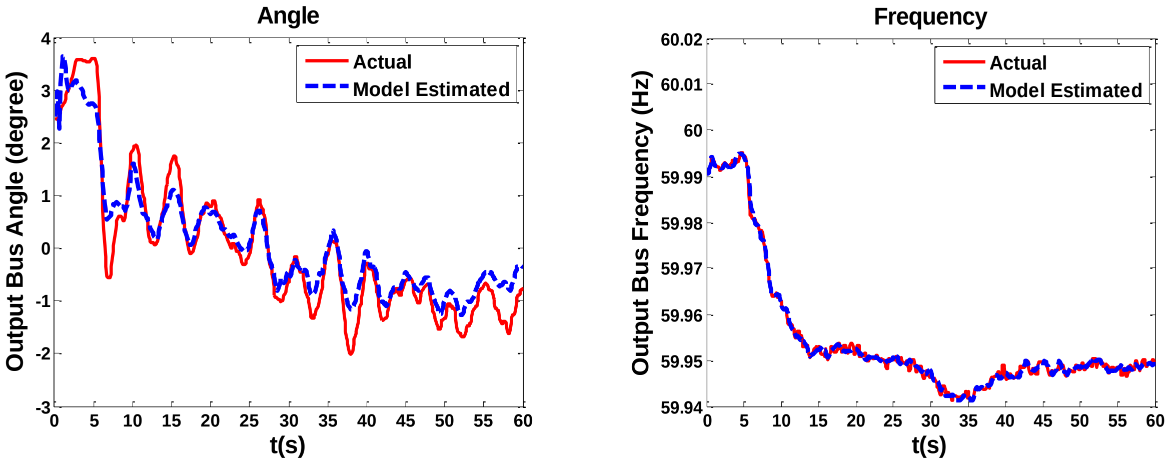

(a) (b)

Figure 2–7 Comparison between the actual measurement and estimation in case 6

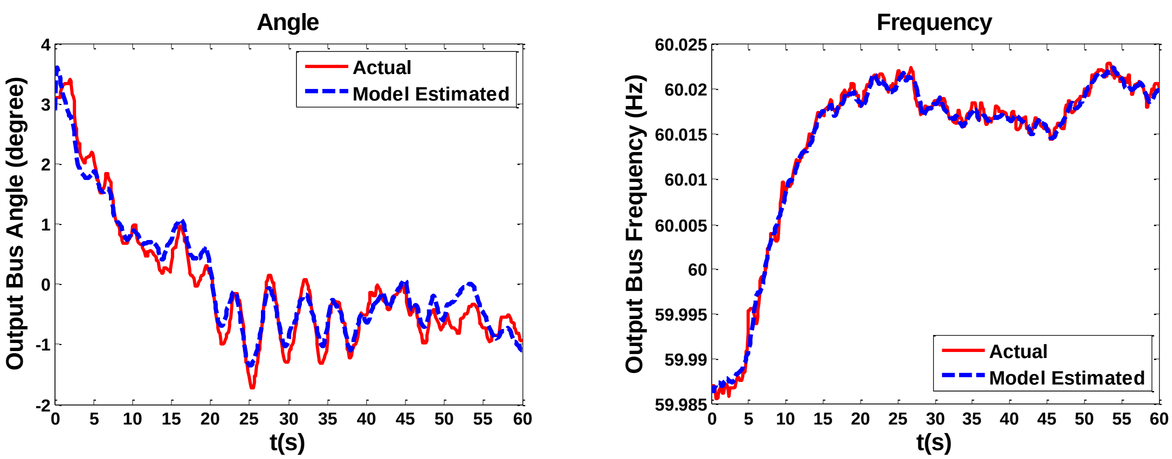

(a) (b)

Figure 2–8 Comparison between the actual measurement and estimation in case 7

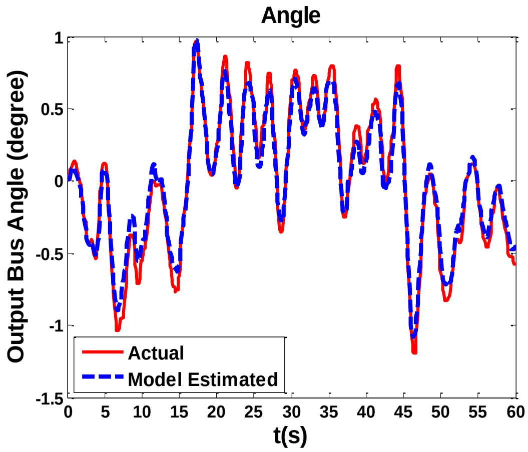

(a)

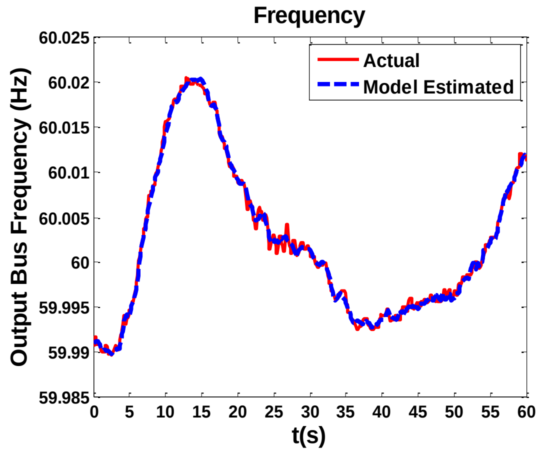

(b)

Figure 2–9 Comparison between the actual measurement and estimation in case 8

Based on the estimated results with ambient data in Table 2-2, the angle/frequency accuracy index is not as good as the results derived by event data, but the results are reliable to present correct trends. Since ambient data contain the information about the operating condition and the dynamic response before the event happens, the ARX model can be trained by ambient data when triggered events are insufficient.

Table 2-2 Angle/Frequency accuracy index from case 5 to case 8

	Angle accuracy index	Frequency accuracy index
Case 5	88.44	94.78
Case 6	87.03	91.69
Case 7	77.49	90.81
Case 8	68.13	90.35

2.4.3 Ambient Dynamic Response Estimated by Ambient Data

The event response estimation is acceptable while the ARX model is trained by either event data or ambient data. For a potential online application, the ARX model can estimate ambient responses as well.

Case 9 and Case 10 demonstrate the ambient response estimation through the ARX model trained by ambient data. The time interval between the training dataset and the estimated dataset is about 10 minutes in both cases. The results of Case 9 and Case 10 are presented in Figure 2–10 and Figure 2–11, respectively.

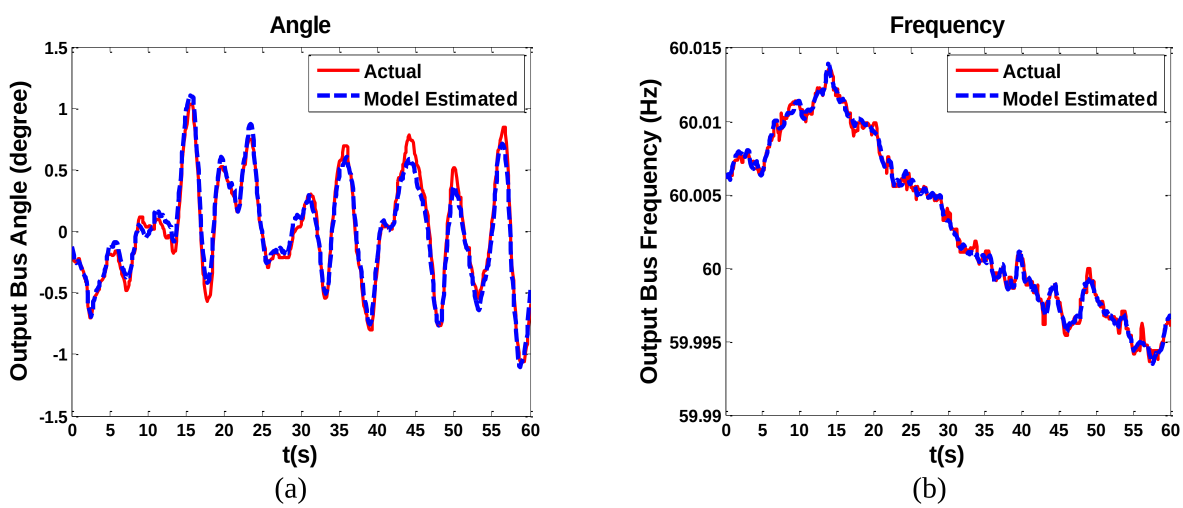

Figure 2–10 Comparison between the actual measurement and estimation in case 9

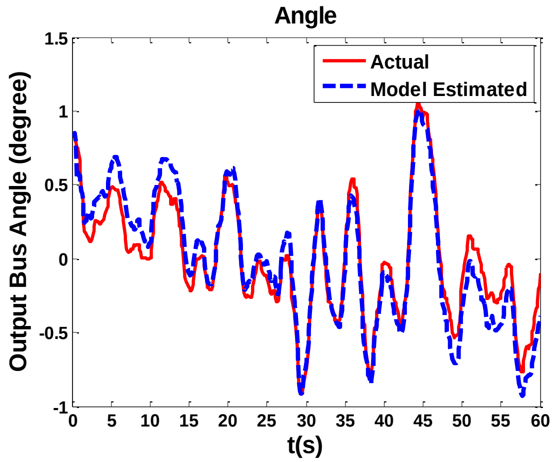

(a)

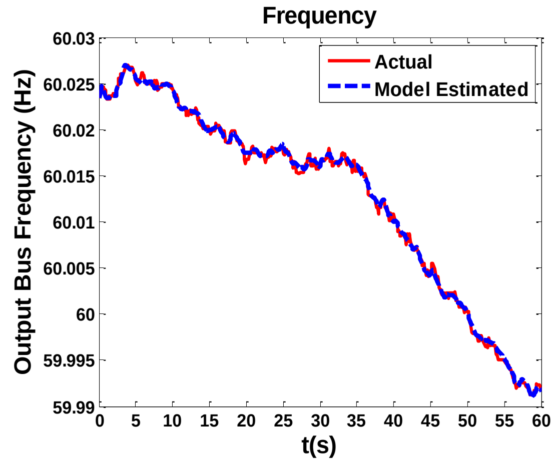

(b)

Figure 2–11 Comparison between the actual measurement and estimation in case 10

From the results in Table 2-3, either the angle accuracy index or the frequency accuracy index turns to be worse, but they are still acceptable. The estimated results exhibit that the ARX models trained by ambient data may still reserve and carry ambient responses correctly

Table 2-3 Angle/Frequency accuracy index from case 9 to case 10

	Angle accuracy index	Frequency accuracy index
Case 9	79.66	88.21
Case 10	71.89	89.48

2.5 Conclusions

Through validation using measurement data, it is shown that the ARX model can estimate frequency and angle responses correctly. Both event data and ambient data can be used to train the ARX model. In terms of the angle or frequency accuracy index, the ARX model trained by event data is better. However, the ARX model trained by either event data or ambient data can obtain acceptable results. In addition, the validation tests indicate that the proposed approach has good generalization capability.

CHAPTER 3 TRANSFER FUNCTION MODEL IDENTIFICATION USING WIDE-AREA MEASUREMENT

3.1 Introduction

In today's interconnected power grids [18]–[21], low-frequency oscillation is a significant issue limiting the power transfer capability and even deteriorating the power system security [22]. In order to suppress low-frequency oscillations, local and wide-area power system stabilizers (PSSs) are installed or proposed to provide supplementary damping control through generator excitation systems [23], flexible alternating current transmission systems (FACTS) devices [24], and high-voltage direct current (HVDC) links [25].

However, since these oscillation damping controllers are usually tuned based on several typical operating conditions, their performances may degrade if the actual operating condition is significantly different from the typical operating conditions considered in the offline design procedure. One typical example is from the design of PSS. Conventional design tunes the time constants and gain of the PSS, which are lead-lag compensators using modal frequency approaches. Thus, many designs are mainly specific for a given operating condition. In some extreme cases, they even provide negative damping. Limited adaptivity is considered one of the main drawbacks of these controllers.

A robust control scheme can be utilized to improve adaptivity. In general, a robust oscillation damping controller is designed based on a detailed system model under a selected dominant operating condition with bounded model uncertainty [26], [27]. The variations of operating condition are reflected in the additive and/or multiplicative uncertainty of the system model. Nevertheless, it is not easy to determine the uncertainty boundary of the system model. Additionally, the controller performance may not be optimal when the actual operating condition deviates from the dominant one.

An adaptive control scheme is another approach to improve adaptivity, which can update the controller parameters online to track the continuous variations in operating conditions. Recently, with the increasing application of the WAMS [28], [29] and the rapid development of system identification techniques [30], the adaptive control approach has drawn increasing attention. For instance, a self-tuning adaptive PSS based on artificial neural networks is proposed in [31]. In [32], the parameters of phase lead-lag compensators are updated based on the online modal analysis. However, most of the research focuses on the adaptivity of the individual damping controller, while the coordination among different controllers has not been fully addressed. If the system model depicting all the dominant oscillation modes is identified online, it is feasible to optimize the controllers' parameters at the control center, and remotely configure the parameters of dispersed damping controllers. In this way, the adaptivity of the individual controller and the coordination among different oscillation modes can be achieved simultaneously [33].

Fast online identification of the system model to capture all oscillation modes (not a single mode) of the power system is the prerequisite of the adaptive and coordinated oscillation damping control. Two categories of measurement-based models can be used for system identification: the subspace state space model, and the auto-regressive moving average exogenous inputs (ARMAX) model. The subspace state space model is usually identified by numerical algorithms for the subspace state-space system identification (N4SID) method [34]–

[36] or the stochastic subspace identification method [37], [38]. However, the main drawback of these two approaches is slow computation speed due to singular value decomposition (SVD) of a large-dimensional matrix, which is a factorization of a real or complex matrix. Since the slow calculation speed is one of the barriers to apply the subspace state space model for oscillation damping control in the online environment, a recursive adaptive stochastic subspace identification method is presented in [38] to reduce the computation time.

The ARMAX model identification can be an alternative to overcome the drawback of high computational burden [39], [40]. The family of "auto-regressive" models has already been used to represent system dynamics for oscillation damping control [41], [42]. However, the identified ARMAX model is generally a single-input single-output model, which may reflect only one oscillation mode because the model is used to control single oscillation mode.

This chapter proposes a methodology to identify a multi-input multi-output (MIMO) ARMAX-based transfer function model using measurement data to capture all the dominant oscillation modes. Both the ambient data and the ring-down data are used for system identification. The proposed approach is demonstrated by a case study in the 16-machine 68-bus Northeast Power Coordinating Council (NPCC) system. Results show that the identified model using ARMAX may accurately represent the power system dominant oscillatory behaviors. Compared with the subspace state space model, the ARMAX model has equivalent accuracy but lower order and improved computational efficiency.

The remaining content of this chapter is organized as follows. The second part of the chapter describes the relationship between the full-order system model and the measurement-based models. In addition, the methodology and the flowchart of system identification for oscillation damping control are presented. The methodology is also validated by the case study in the NPCC system in the fourth part. Then, the oscillation damping control using the proposed approach is exhibited in the fifth part. The implementation on the large testbed is described in the sixth part. The last part concludes this chapter.

3.2 Relationship between Full-Order System Models and Measurement-Based Models

The full-order system model for the small signal analysis is usually represented by the state space method which is a set of first order differential equations based on the linearization around a certain operation point, as shown in the following equations.

$$\Delta\dot{\boldsymbol{x}} = \boldsymbol{A}\Delta\boldsymbol{x} + \boldsymbol{B}\Delta\boldsymbol{u} \tag{3–1}$$

$$\Delta\boldsymbol{y} = \boldsymbol{C}\Delta\boldsymbol{x} + \boldsymbol{D}\Delta\boldsymbol{u} \tag{3–2}$$

where, Δx is the state vector, Δy is the output vector, and Δu is the input vector; A is the state matrix, B is the input matrix, C is the output matrix, and D is the feedforward matrix.

Obviously, the subspace state space model is indeed a kth order reduced model of the full-order system model. The only parameter that needs to be determined before A, B, C and D matrix estimation is the reduced model order, which requires SVD of a large-dimensional matrix. On the other hand, the MIMO ARMAX model is the equivalent discrete transfer function model of the original system. Based on (3–1) and (3–2), the continuous transfer function between inputs and outputs is represented as

$$\boldsymbol{G}(\boldsymbol{s}) = \boldsymbol{C}(\boldsymbol{sI} - \boldsymbol{A})^{-\mathbf{1}}\boldsymbol{B} + \boldsymbol{D} \tag{3–3}$$

If the inputs and outputs of the system are determined, the system model can be represented as:

$$\begin{bmatrix} \boldsymbol{G_{11}(s)} & \cdots & \boldsymbol{G_{1n}(s)} \\ \boldsymbol{G_{21}(s)} & \cdots & \boldsymbol{G_{2n}(s)} \\ \vdots & \cdots & \vdots \\ \boldsymbol{G_{m1}(s)} & \cdots & \boldsymbol{G_{mn}(s)} \end{bmatrix} \begin{bmatrix} \Delta\boldsymbol{u_1(s)} \\ \Delta\boldsymbol{u_2(s)} \\ \vdots \\ \Delta\boldsymbol{u_n(s)} \end{bmatrix} = \begin{bmatrix} \Delta\boldsymbol{y_1(s)} \\ \Delta\boldsymbol{y_2(s)} \\ \vdots \\ \Delta\boldsymbol{y_m(s)} \end{bmatrix} \tag{3–4}$$

where $\Delta u_i(s)$ and $\Delta y_j(s)$ are the ith and jth elements of the input vector and the output vector, respectively. G_{ij} is the element of the G matrix at position (i, j). m and n are the number of system outputs and the number of system inputs, respectively.

Since the denominator of each element G_{ij} of G contains the common eigenvalues of the system [43], (3–3) can be expressed as:

$$\boldsymbol{G(s)} = \frac{\boldsymbol{1}}{\prod_{\boldsymbol{i=1}}^{r}(\boldsymbol{s}-\boldsymbol{\lambda_i})}\boldsymbol{\overline{G}(s)} \tag{3–5}$$

where λ_i is ith mode in the system. In the model, the characteristic polynomial has inter-area modes which are observable to most of the system and local modes which are observable to the certain part of the system. The common denominator can reduce the model order substantially since the transfer function derived here is a reduced order model of the full power system model.

Equation (3–4) shows that the certain output may be regarded as the aggregated result from the contribution of all inputs. Therefore, in the discrete-time domain, the contribution of the input signals to the outputs at the sampling time t can be exhibited as [30]

$$\boldsymbol{\alpha}(\boldsymbol{z})\boldsymbol{y}(\boldsymbol{t}) = \boldsymbol{\beta}(\boldsymbol{z})\boldsymbol{u}(\boldsymbol{t}) + \boldsymbol{\gamma}(\boldsymbol{z})\boldsymbol{e}(\boldsymbol{t}) \tag{3–6}$$

where $y(t)$ is the vector of m outputs, $u(t)$ is the exogenous part which is the vector containing the known p excitations, and $e(t)$ is the moving average part which is the vector with q unknown noise. $p + q = n.$ $\alpha(z)$, $\beta(z)$ and $\gamma(z)$ are the autoregressive polynomial matrix, the exogenous polynomial matrix, and the moving average polynomial matrix, respectively. z is the shift operator.

$$\boldsymbol{\alpha}(\boldsymbol{z}) = \boldsymbol{I} + \boldsymbol{\alpha}^{\boldsymbol{1}}\times\boldsymbol{z}^{-\boldsymbol{1}} + \cdots + \boldsymbol{\alpha}^{\boldsymbol{n_\alpha}}\times\boldsymbol{z}^{-\boldsymbol{n_\alpha}} \tag{3–7}$$
$$\boldsymbol{\beta}(\boldsymbol{z}) = \boldsymbol{\beta}^{\boldsymbol{0}} + \boldsymbol{\beta}^{\boldsymbol{1}}\times\boldsymbol{z}^{-\boldsymbol{1}} + \cdots + \boldsymbol{\beta}^{\boldsymbol{n_\beta}}\times\boldsymbol{z}^{-\boldsymbol{n_\beta}} \tag{3–8}$$
$$\boldsymbol{\gamma}(\boldsymbol{z}) = \boldsymbol{I} + \boldsymbol{\gamma}^{\boldsymbol{1}}\times\boldsymbol{z}^{-\boldsymbol{1}} + \cdots + \boldsymbol{\gamma}^{\boldsymbol{n_\gamma}}\times\boldsymbol{z}^{-\boldsymbol{n_\gamma}} \tag{3–9}$$

The matrices $\boldsymbol{\alpha}$(z), $\boldsymbol{\beta}$(z) and γ(z) in (3–7)-(3–9) can be expanded as (3–10)-(3–12).

$$\boldsymbol{\alpha(z)} = \begin{bmatrix} \mathbf{1} & \cdots & \mathbf{0} \\ \vdots & \ddots & \vdots \\ \mathbf{0} & \cdots & \mathbf{1} \end{bmatrix} + \begin{bmatrix} \boldsymbol{\alpha_{11}}^{(\mathbf{1})} & \cdots & \boldsymbol{\alpha_{1m}}^{(\mathbf{1})} \\ \vdots & \ddots & \vdots \\ \boldsymbol{\alpha_{m1}}^{(\mathbf{1})} & \cdots & \boldsymbol{\alpha_{mm}}^{(\mathbf{1})} \end{bmatrix} \times \boldsymbol{z^{-1}} + \cdots + \begin{bmatrix} \boldsymbol{\alpha_{11}}^{(\boldsymbol{n_\alpha})} & \cdots & \boldsymbol{\alpha_{1m}}^{(\boldsymbol{n_\alpha})} \\ \vdots & \ddots & \vdots \\ \boldsymbol{\alpha_{m1}}^{(\boldsymbol{n_\alpha})} & \cdots & \boldsymbol{\alpha_{mm}}^{(\boldsymbol{n_\alpha})} \end{bmatrix} \times \boldsymbol{z^{-n_\alpha}} \tag{3–10}$$

$$\boldsymbol{\beta(z)} = \begin{bmatrix} \boldsymbol{\beta_{11}}^{(\mathbf{0})} & \cdots & \boldsymbol{\beta_{1p}}^{(\mathbf{0})} \\ \vdots & \ddots & \vdots \\ \boldsymbol{\beta_{m1}}^{(\mathbf{0})} & \cdots & \boldsymbol{\beta_{mp}}^{(\mathbf{0})} \end{bmatrix} + \begin{bmatrix} \boldsymbol{\beta_{11}}^{(\mathbf{1})} & \cdots & \boldsymbol{\beta_{1p}}^{(\mathbf{1})} \\ \vdots & \ddots & \vdots \\ \boldsymbol{\beta_{m1}}^{(\mathbf{1})} & \cdots & \boldsymbol{\beta_{mp}}^{(\mathbf{1})} \end{bmatrix} \times \boldsymbol{z^{-1}} + \cdots + \begin{bmatrix} \boldsymbol{\beta_{11}}^{(\boldsymbol{n_\beta})} & \cdots & \boldsymbol{\beta_{1p}}^{(\boldsymbol{n_\beta})} \\ \vdots & \ddots & \vdots \\ \boldsymbol{\beta_{\mathbf{m1}}}^{(\boldsymbol{n_\beta})} & \cdots & \boldsymbol{\beta_{mp}}^{(\boldsymbol{n_\beta})} \end{bmatrix} \times \boldsymbol{z^{-n_\beta}} \tag{3–11}$$

$$\boldsymbol{\gamma(z)} = \begin{bmatrix} \mathbf{1} & \cdots & \mathbf{0} \\ \vdots & \ddots & \vdots \\ \mathbf{0} & \cdots & \mathbf{1} \end{bmatrix} + \begin{bmatrix} \boldsymbol{\gamma_{11}}^{(\mathbf{1})} & \cdots & \boldsymbol{\gamma_{1q}}^{(\mathbf{1})} \\ \vdots & \ddots & \vdots \\ \boldsymbol{\gamma_{m1}}^{(\mathbf{1})} & \cdots & \boldsymbol{\gamma_{mq}}^{(\mathbf{1})} \end{bmatrix} \times \boldsymbol{z^{-1}} + \cdots + \begin{bmatrix} \boldsymbol{\gamma_{11}}^{(\boldsymbol{n_\gamma})} & \cdots & \boldsymbol{\gamma_{1q}}^{(\boldsymbol{n_\gamma})} \\ \vdots & \ddots & \vdots \\ \boldsymbol{\gamma_{m1}}^{(\boldsymbol{n_\gamma})} & \cdots & \boldsymbol{\gamma_{mq}}^{(\boldsymbol{n_\gamma})} \end{bmatrix} \times \boldsymbol{z^{-n_\gamma}} \tag{3–12}$$

where n_α, n_β and n_γ are the orders of the outputs, exogenous inputs, and noise, respectively. $\alpha(z)$ is an $m\times m$ matrix, $\beta(z)$ is an $m\times p$ matrix, and $\gamma(z)$ is an $m\times q$ matrix.

To calculate the coefficient matrix, the two-stage least squares algorithm is detailed as follows. The two-stage least squares approach is provided in [30] for the SISO ARMAX algorithm, and is extended to the MIMO ARMAX case in (3–6). The least squares algorithm may be applied twice in two stages. The first stage is to estimate the unknown random inputs for the MIMO ARMAX model through the MIMO ARX model

$$\boldsymbol{\alpha^F(z)y(t)} = \boldsymbol{\beta^F(z)u(t)} + \boldsymbol{e(t)} \tag{3–13}$$

where F is the order of autoregressive and input parts of the model, and F is higher than any of the orders in the MIMO ARMAX model but is not more than double of the highest order in the MIMO ARMAX.

The linear regression vector in [30] can be presented as:

$$\boldsymbol{\varphi^F(t) = [-y^T(t-1)\ \cdots - y^T(t-F)\ u^T(t-1)\ \cdots u^T(t-F)]^T} \tag{3–14}$$

In addition, Θ^{F} is the coefficient matrix.

$$\boldsymbol{\Theta^F = [\alpha_1^F \cdots \alpha_F^F \ \ \beta_1^F \cdots \beta_F^F]^T} \tag{3–15}$$

where α_i^F is ith autoregressive coefficient matrix, and β_i^F is ith known input matrix. The first least squares estimation from N samples of measurement is:

$$\boldsymbol{\widehat{\Theta}^F = \left[\frac{1}{N}\sum_{t=1}^{N} \varphi^F(t)[\varphi^F(t)]^T\right]^{-1} \left[\frac{1}{N}\sum_{t=1}^{N} \varphi^F(t) y^T(t)\right]} \tag{3–16}$$

The estimated unknown inputs are:

$$\boldsymbol{\hat{e}(t) = \widehat{\alpha}^F(z) y(t) - \widehat{\beta}^F(z) u(t)} \tag{3–17}$$

Therefore, (3–6) can be modified as (3–18), which is the pseudo-ARMAX model since it contains the estimation results.

$$\boldsymbol{\alpha}(\boldsymbol{z})\boldsymbol{y}(\boldsymbol{t}) = \boldsymbol{\beta}(\boldsymbol{z})\boldsymbol{u}(\boldsymbol{t}) + \boldsymbol{\gamma}(\boldsymbol{z})\hat{\boldsymbol{e}}(\boldsymbol{t}) \tag{3–18}$$

Similarly, the linear regression is pseudo-linear regression:

$$\begin{gathered}\hat{\boldsymbol{\varphi}}(\boldsymbol{t}) = [-\boldsymbol{y}^{\boldsymbol{T}}(\boldsymbol{t}-\mathbf{1}) \cdots - \boldsymbol{y}^{\boldsymbol{T}}(\boldsymbol{t}-\boldsymbol{n_a}) \ \ \boldsymbol{u}^{\boldsymbol{T}}(\boldsymbol{t}-\mathbf{1}) \ \cdots \boldsymbol{u}^{\boldsymbol{T}}(\boldsymbol{t}-\boldsymbol{n_b})^{\boldsymbol{T}} \\ \hat{\boldsymbol{e}}^{\boldsymbol{T}}(\boldsymbol{t}-\mathbf{1}) \ \cdots \ \hat{\boldsymbol{e}}^{\boldsymbol{T}}(\boldsymbol{t}-\boldsymbol{n_c})]\end{gathered} \tag{3–19}$$

Thus, the coefficient matrix is:

$$\boldsymbol{\Theta} = [\boldsymbol{\alpha}^{\mathbf{1}} \cdots \boldsymbol{\alpha}^{\boldsymbol{n_a}} \ \ \boldsymbol{\beta}^{\mathbf{1}} \cdots \boldsymbol{\beta}^{\boldsymbol{n_b}} \ \boldsymbol{\gamma}^{\mathbf{1}} \cdots \boldsymbol{\gamma}^{\boldsymbol{n_c}}]^{\boldsymbol{T}} \tag{3–20}$$

The estimated coefficients of the MIMO ARMAX model can be obtained from the second stage of the least squares algorithm.

$$\widehat{\boldsymbol{\Theta}} = \left[\frac{\mathbf{1}}{\boldsymbol{N}}\sum_{\boldsymbol{t}=\mathbf{1}}^{\boldsymbol{N}} \hat{\boldsymbol{\varphi}}(\boldsymbol{t})\hat{\boldsymbol{\varphi}}^{\boldsymbol{T}}(\boldsymbol{t})\right]^{-\mathbf{1}} \left[\frac{\mathbf{1}}{\boldsymbol{N}}\sum_{\boldsymbol{t}=\mathbf{1}}^{\boldsymbol{N}} \hat{\boldsymbol{\varphi}}(\boldsymbol{t})\boldsymbol{y}^{\boldsymbol{T}}(\boldsymbol{t})\right] \tag{3–21}$$

where $\hat{\Theta}$ is the matrix coefficients which can be calculated by two-stage least squares.

The MIMO ARMAX model is identified in the discrete-time domain. If converted into the continuous-time domain, the system transfer function can be represented by a polynomial function as

$$\boldsymbol{G}(\boldsymbol{s}) = \boldsymbol{y}(\boldsymbol{s}) \times \begin{bmatrix} \boldsymbol{u}(\boldsymbol{s}) \\ \boldsymbol{e}(\boldsymbol{s}) \end{bmatrix}^{-1} = [\boldsymbol{\alpha}^{-1}(\boldsymbol{z})\boldsymbol{\beta}(\boldsymbol{z}) \;\; \boldsymbol{\alpha}^{-1}(\boldsymbol{z})\boldsymbol{\gamma}(\boldsymbol{z})]_{\boldsymbol{z}=\boldsymbol{e}^{\boldsymbol{s}\boldsymbol{T}_{\boldsymbol{s}}}} \tag{3–22}$$

where $\boldsymbol{T}_{\boldsymbol{s}}$ is the sampling period.

$$\boldsymbol{G}(\boldsymbol{s}) = \frac{\boldsymbol{\alpha}^{*}(\boldsymbol{z})}{|\boldsymbol{\alpha}(\boldsymbol{z})|}[\boldsymbol{\beta}(\boldsymbol{z}) \;\; \boldsymbol{\gamma}(\boldsymbol{z})]_{\boldsymbol{z}=\boldsymbol{e}^{\boldsymbol{s}\boldsymbol{T}_{\boldsymbol{s}}}} \tag{3–23}$$

where $\boldsymbol{\alpha}^{*}(\boldsymbol{z})$ is the adjugate matrix of $\boldsymbol{\alpha}(\boldsymbol{z})$ and $|\boldsymbol{\alpha}(\boldsymbol{z})|$ can be rewritten as (3–24).

$$\prod_{\boldsymbol{i}=\boldsymbol{1}}^{\boldsymbol{r}}(\boldsymbol{s} - \boldsymbol{\lambda}_{\boldsymbol{i}}) = |\boldsymbol{\alpha}(\boldsymbol{z})|_{\boldsymbol{z}=\boldsymbol{e}^{\boldsymbol{s}\boldsymbol{T}_{\boldsymbol{s}}}} \tag{3–24}$$

Since the identification procedure may introduce the unexpected modes which are numerical artifacts and weaker modes, these modes need to be filtered out from the dominant low-frequency modes which range from 0.2 Hz to 2.5 Hz. In [44], a feasible method which can finish selecting the modes through pseudo-energy from the MIMO ARMAX model has been employed in the proposed method. The modes with the highest energy may be the true system modes, and ones with low energy would be fake modes.

Based on above analysis, both the MIMO subspace state space model and the MIMO ARMAX model are equivalent transfer function models of the original system. The subspace state space model is represented by a set of differential equations in continuous-time domain, while the MIMO ARMAX model is represented by a set of difference equations in discrete-time domain.

3.3 Methodology for ARMAX Model Identification

This section introduces the methodology to build out the MIMO ARMAX model using measurement data to capture dominant inter-area modes of the power system for oscillation damping control. The block diagram of the presented methodology is shown in Figure 3–1, which consists of five steps: input selection, output selection, identification trigger, model estimation, and model validation. In addition, the concept of the adaptive and coordinated control design based on the validated MIMO ARMAX model is discussed in this part.

3.3.1 ARMAX Model Input Selection

The first step is to choose the input signals [45]. If applying the MIMO ARMAX model for an oscillation mode meter, any measurable signal can be selected as the input of the MIMO ARMAX model. However, since the purpose of the MIMO ARMAX model in this research is oscillation damping control, actual controllable signals in the power system should be selected as the inputs of the MIMO ARMAX model, e.g., the controllable setpoint signals of PSS, FACTs devices, and HVDC links. In other words, the input signals of the MIMO ARMAX model can be controlled and modulated to suppress the target oscillation modes. Furthermore, to reduce the number of the MIMO ARMAX inputs, the conventional residue method can be used to pre-select the signal with high sensitivity of dominant oscillation modes.

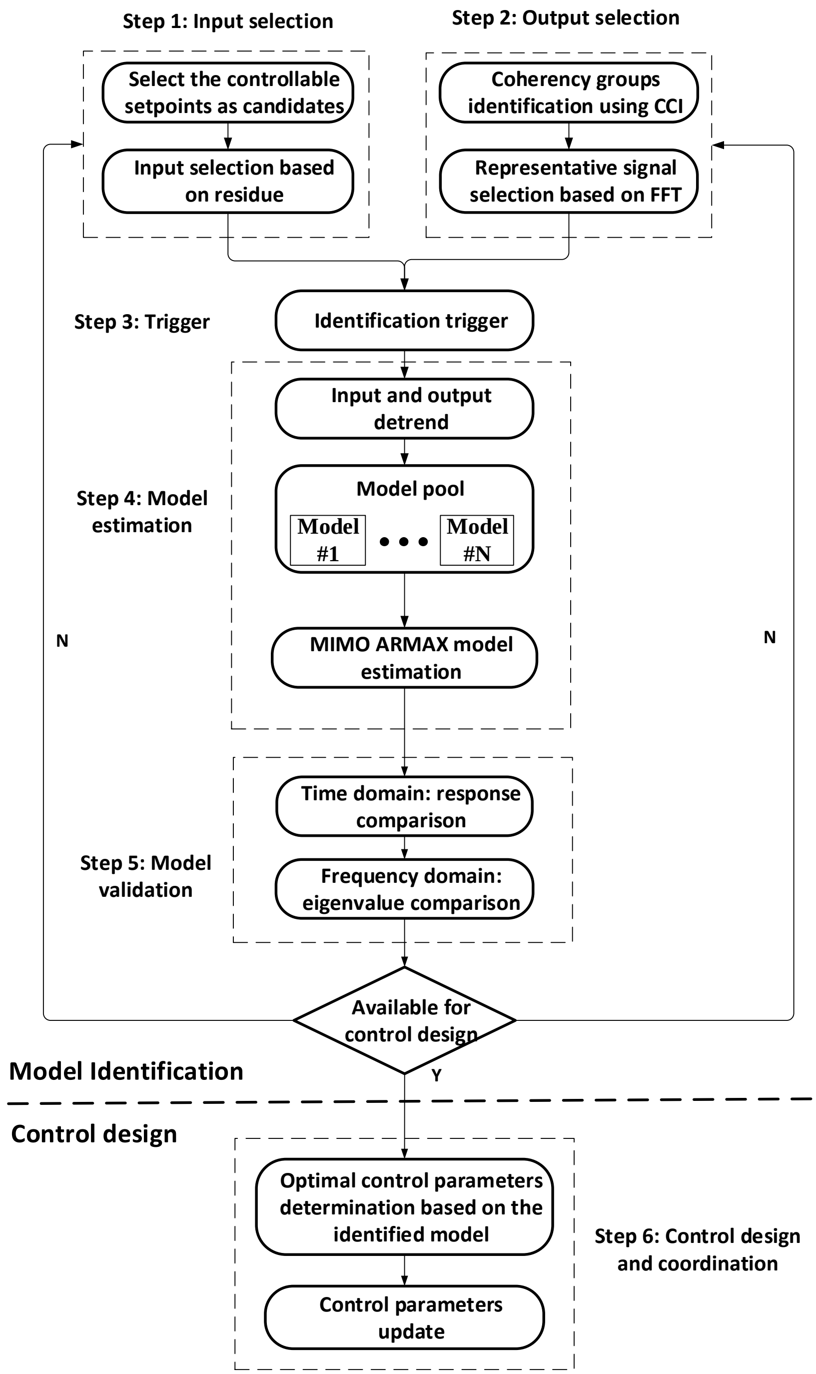

Figure 3–1 Flowchart of the proposed model identification methodology

Taking PSS as an example, the selected input signal is illustrated in Figure 3–2. The voltage reference of the excitation system (V_{ref}) is usually a given constant value to maintain the generator terminal voltage around its rating value. For a local PSS, its output (V_{pss}) is added to the V_{ref} to provide damping to suppress local oscillation modes. If using probing data for the MIMO ARMAX model identification, the sum of V_{ref} and the probing signal can be selected as the input. Nevertheless, when using ambient data or ring-down data, since there is no variant signal added to V_{ref}, the summation of the voltage reference, terminal voltage (V_t), and the output of PSS, is selected as the input signal of the MIMO ARMAX model.

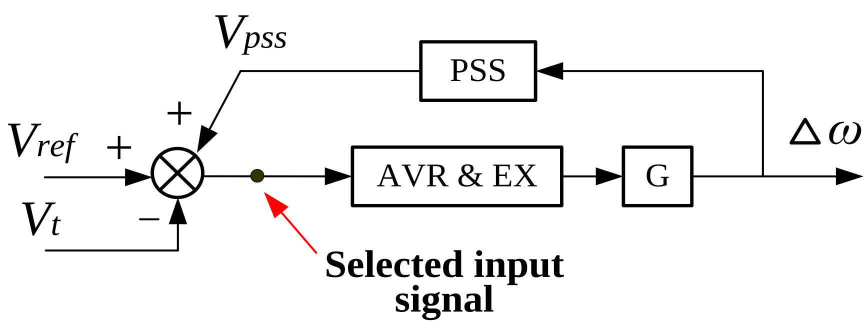

AVR: automatic voltage regulator	*Vpss*: output of PSS
EX: exciter	*Vref*: voltage reference
G: generator	*Vt*: generator terminal voltage
PSS: power system stabilizer	Δω: rotor angular speed deviation

Figure 3–2 Illustration of the input signal of the ARMAX model

3.3.2 ARMAX Model Output Selection

The outputs of the MIMO ARMAX model should reflect the dominant modes in the power system. Rotor angular speed, tie-line active power, and generator bus frequency are the most commonly used observation signals to reflect oscillations. These types of signals can be selected as the outputs of the MIMO ARMAX model.

For a large power system, it is unnecessary to select too many signals as the outputs of the MIMO ARMAX model. Instead, it is feasible to select one representative signal for each coherent group to reduce the output number of the MIMO ARMAX model. Traditionally, coherency analysis is conducted by using a classical two-order generator model in the offline environment [46]. This research utilizes the CCI to identify the coherency groups online using pure measurement data in the online environment.

The process of identifying coherent machines does not necessarily guarantee that inter-area modes can be observed in the measurements. Therefore, the Fast Fourier Transform (FFT) algorithm is adopted to select the optimal output of the MIMO ARMAX model in each coherent group after the coherency analysis. The candidate measurement signals are ranked from high to low according to the normalized magnitude at the frequency point of the dominant modes, and then the highest one in each coherent group will be selected as the outputs of the MIMO ARMAX model. Summarily, the criterion for the representative outputs in each of coherency groups is that they have the best observability for all target inter-area oscillation modes through the FFT computation. Furthermore, in order to retain the characteristics for the full system, each coherency group may keep a measurement at least.

3.3.3 Identification Trigger

Three types of measurement data (probing data, ambient data, and ring-down data) can be utilized to build the ARMAX model [47]–[49]. For a large power grid, probing data are theoretically ideal to build the model because system response usually contains most of the modes when a probing signal is injected into the system. However, probing data require consistent excitations, which is not practical during system operations. Compared with probing data, ambient data and ring-down data are much easier to be collected in the online environment because they can be measured when load variation/generation regulation is within a small range or with large system disturbances (e.g., line trips, generation trips, and load sheddings) during system operations. Hence, both ambient data and ring-down data are considered in this chapter.

The online model identification is triggered by system events including generation trips, load sheddings, and topology changes due to line trips, etc. these system events can be detected by the existing situational awareness functions based on wide-area measurement. If there are events, the model will be update immediately when the data collection is ready. In addition, the identification procedure can be triggered by predefined timer (periodical trigger). If there are no system events, the model will be updated using collected ambient data in every 5 minutes.

3.3.4 ARMAX Model Estimation

Before using the ambient data and ring-down data, it is necessary to remove direct current trends within the measurement data. Normally, this operation is known as de-trending, and keeps the result from being overwhelmed by the nonzero mean and the trend terms.

There are several candidate models in the model pool, which is expected to avoid revising models several times in one update cycle so that the identification process can keep the computational efficiency. In the model pool, the orders of the MIMO ARMAX models have been adopted depending on the priori knowledge. The highest order of the MIMO ARMAX model in the model pool is 50. When the identification is triggered, these MIMO ARMAX models with different orders in the model pool will be identified simultaneously. The model coefficients in (3–10) - (3–12) can be computed by using the two-stage least squares algorithm which is given in the previous part of the chapter. The model with highest accuracy in both time domain and frequency domain specified in the next subsection is selected as the identified model. If the identification results from all MIMO ARMAX models cannot fulfill the accuracy requirements, the current identification would be abandoned. The parameters of the adaptive controllers would not be model updated in this cycle.

3.3.5 ARMAX Model Validation

In time domain, the response of the identified model is compared with actual response. To determine if the response of the model matches with the actual one, the fitting accuracy index is defined as (2–5).

In the frequency domain, the eigenvalues calculated by the denominator polynomial of the MIMO ARMAX model are compared with results of Matrix Pencil (MP) analysis of the measurement data. MP is a modal extraction technique (similar to Prony method), which effectively estimates the dominant modes' information in a response [50]. Meanwhile, it can be also viewed as a benchmark to examine the outputs from the MIMO ARMAX model. In (3–24), the modes of the system can be derived from the denominator of the polynomial function. Based on the sampling period T_s, a mode with real part σ and imaginary part ω can be written as

$$\boldsymbol{\sigma} + \boldsymbol{j\omega} = \frac{\mathbf{1}}{\boldsymbol{T_s}} \times \ln(\boldsymbol{\xi}) \tag{3–25}$$

where ξ is a vector of poles in the z–domain.

The criterion, which determines the model is good or not, is that the accuracy index is over 85%, and the deviations of real parts and imaginary parts of eigenvalues in frequency domain are less than 0.05, compared with the results of MP.

Supposing the inputs and outputs are temporarily unavailable due to the topology changes, the selection of inputs and outputs needs to be redone manually.

3.3.6 Concept of Control Design

The use of the MIMO ARMAX model has many obvious and potential benefits. The simplest but most important one is that the model is a measurement-based model, which requires very little prior information about the system. Since the MIMO ARMAX model selects actual controllable signals in a power system as the inputs, it is a causal model which can capture all the dominant oscillation modes and represent the entire power system for oscillation damping control. More importantly, the MIMO ARMAX model has equivalent accuracy with the MIMO subspace state space model, but requires lower order and less computation time. Hence, it is more suitable to improve adaptivity and coordination of the oscillation damping control system in the online environment. Moreover, the case study shows the circumstance where only the setpoints of PSS are selected as the input of the MIMO ARMAX model. If FACTS devices and HVDC links are employed by a power system, the proposed methodology still applies for the circumstances where the setpoints of FACTS devices and HVDC links are selecting as the inputs signals.

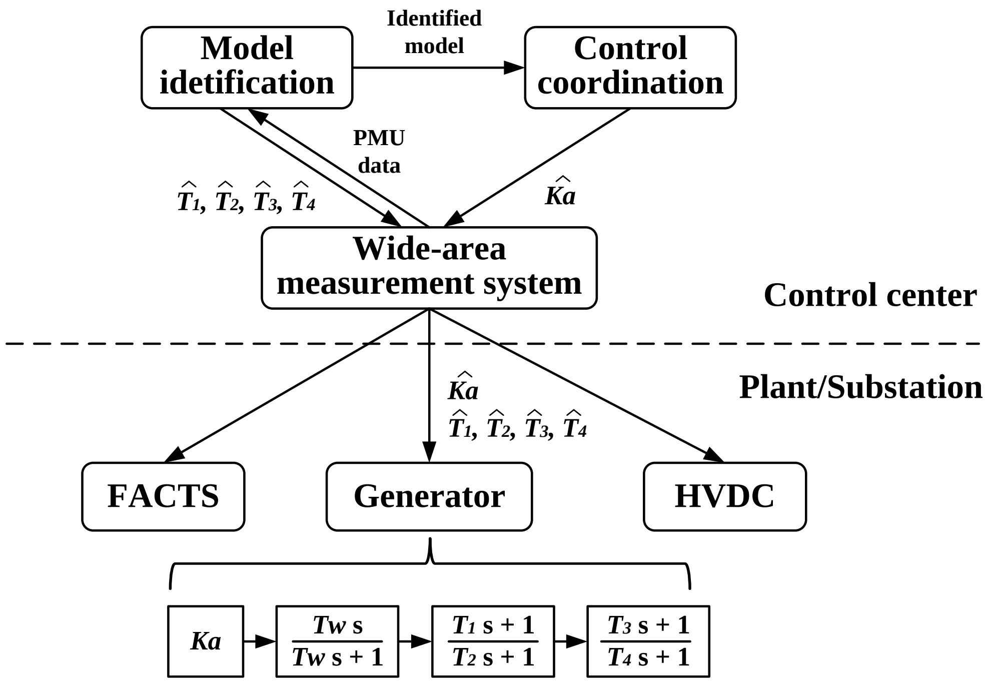

Figure 3–3 Architecture of the adaptive and coordinated oscillation damping control system

The general architecture of the adaptive and coordinated oscillation damping control system is shown in Figure 3–3. Taking one wide-area oscillation damping controller at a generation based on lead-lag compensation for instance, the MIMO ARMAX model is identified using ambient data or ring-down data from WAMS. In normal operating conditions, the model will be updated using ambient data. The model updating rate could be once per 5 minutes. If an event (e.g., line trip, generation trip, or load shedding) occurs, the model is updated using the latest ring-down data. The model could be updated within 11-12 seconds (including data window and computation time). The starting point of the ring-down data can be determined by event detection function in WAMS. It is noted that the identified model is a closed-loop system model, which includes the controller requiring parameter update. However, since the parameters of the controller are already known, it is not difficult to derive the open-loop system model which excludes the controller.

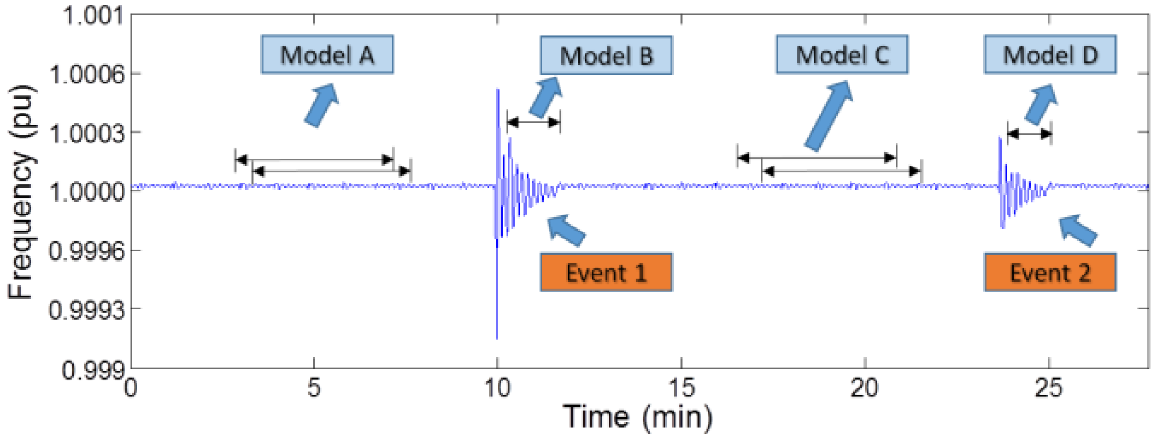

Figure 3–4 Time sequence of the adaptive approach

Based on the identified model, the residue phase can be estimated under the latest operating condition, and is used to update the parameters of the lead-lag compensator (T_1, T_2, T_3, and T_4). Moreover, the optimal gain (K_a) is determined by optimization to maximize the overall damping improvement of all oscillation modes in consideration. The updated control parameters are remotely configured to dispersed controllers in different power plants and substations.

Figure 3–4 shows the time sequence of the adaptive approach. Model A is identified using the ambient data, and then the oscillation damping controllers are tuned based on Mode A for the next disturbance. If there is no event, Model A and controller parameters are updated using the ambient data in the next data window. When an event (Event 1) occurs, the controllers will perform with tuned parameters based on the latest Model A. After Event 1 occurred, Model B is identified using the ring-down data, and the controller parameters can be updated based on Model B. Although the controllers perform with the parameters tuned based on Model A (not Model B) during Event 1, the oscillation damping control system may track the continuous variation of operating conditions and ready to experience the next disturbance. Similarly, Model C can be identified by the ambient data after Event 1, while Model D will be identified using the ring-down data in Event 2 to tune controllers for the subsequent disturbance.

3.4 Case Study

3.4.1 Brief Introduction of the NPCC System

The proposed method is validated in the 16-machine 68-bus NPCC system, which is a reduced order model of the New England test system (NETS)/New York power system (NYPS) interconnected system. As shown in Figure 3–5, NETS and NYPS are represented by two groups of generators (G1 to G9 and G10 to G13), respectively. Three other neighboring areas are approximated by equivalent generator models (G14 to G16). Generators G1 to G8 and G10 to G13 have direct current excitation systems, while G9 has fast static excitation. The rest of the generators have manual excitation. To create multiple oscillation modes with poor damping ratios, only G1 to G3 and G8 to G9 are equipped with local PSSs. The system parameters can be seen in [51].

The study system has four dominant inter-area oscillation modes. Their oscillation frequencies and damping ratios are given in Table 3-1. There are three modes with poor damping ratio. It is noted that the 0.63 Hz mode has the smallest damping ratio, in which the generators in NETS oscillate against the generators in NYPS.

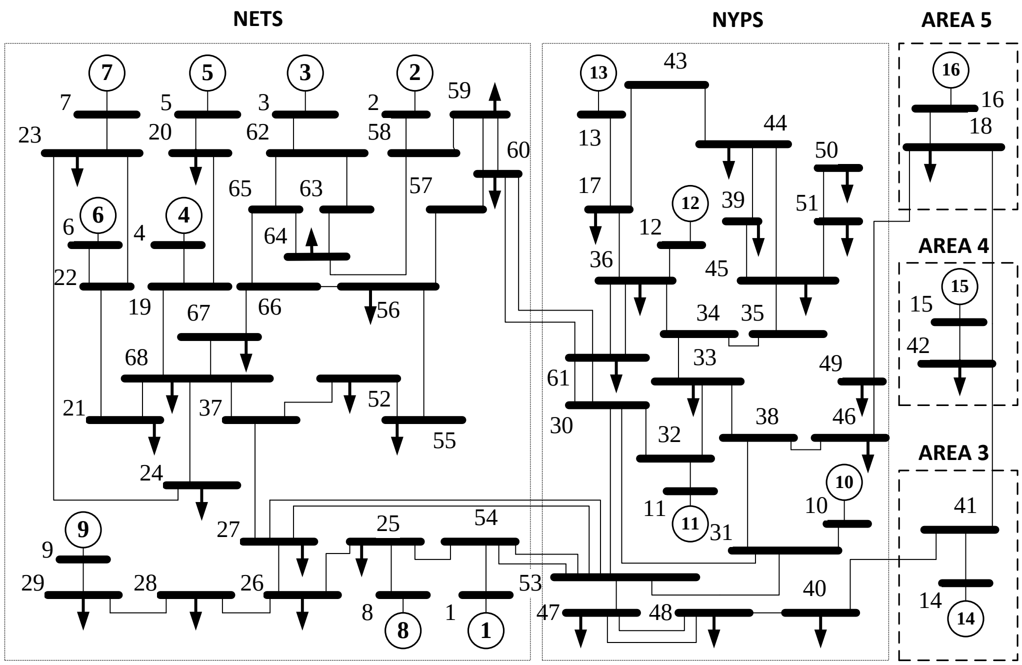

Figure 3–5 Single line diagram of the 16-machine 68-bus NPCC system

Table 3-1 Modal analysis of the NPCC system

	Type	Frequency (Hz)	Damping ratio (%)	Participated generators
1	Inter-area	0.38	15.90	G1~G13 vs. G14, G15
2	Inter-area	0.41	6.38	G1~G14 vs. G15, G16
3	Inter-area	0.63	3.57	G1~G9 vs. G10~G13
4	Inter-area	0.83	5.28	G14, G16 vs. G15

It is assumed that PMU devices are installed at all the buses to measure bus frequency and generator variables, like voltage reference of excitation system, PSS output, and generator terminal voltage. In this chapter, measurement data are generated by dynamic simulation in MATLAB/Simulink. According to the PMU measurement accuracy specified in the standard IEEE C37.118-1, a randomized time-variant measurement error within 5 mHz is added to the simulation data [52]. The simulation data and the measurement error together are considered to be real measurement data collected by field PMUs.

3.4.2 Input and Output Selection

As mentioned in section 3.3.1, the controllable setpoint signals of a power system should be selected as the input signals. Since there are five generators equipped with local PSSs, and ambient data and ring-down data are utilized for the model identification, the sum of voltage reference, terminal voltage, and output of PSS at each of these five generators is selected as an input signal of the ARMAX model.

The output selection is based on coherency analysis and FFT analysis. The results of CCI-based coherency analysis are given in Figure 3–6.

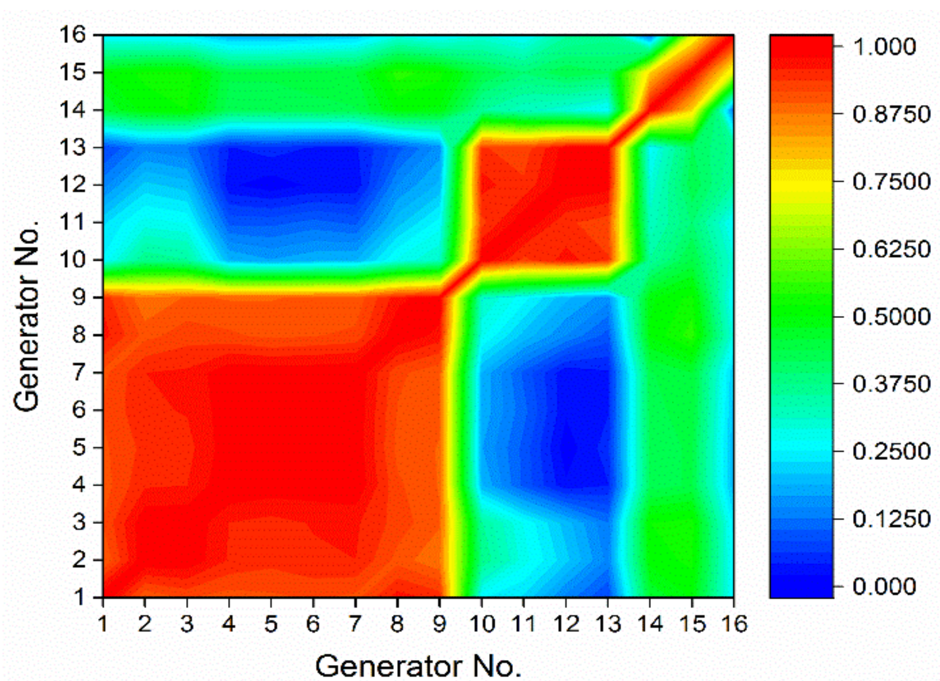

Figure 3–6 Coherency analysis based on CCI

The red part, green part, and blue part represent high, intermediate, and low coherency between different generators, respectively. The results illustrate that the study system can be divided into five coherency groups: G1 to G9, G10 to G13, G14, G15 and G16. The coherency analysis results are consistent with those of the conventional method [22]. In this chapter, frequency signals at each generator bus are the candidate output signals. Since G14, G15, and G16 are the equivalent generators in coherency group 3, 4, and 5, respectively, bus frequency f14, f15, and f16 are selected as the representative signal of each coherency groups.

To select one representative signal for group 1 and 2, all the generator bus frequency signals in group 1 and 2 are analyzed by using FFT analysis in several separate tests. The normalized results of FFT analysis are shown in the radar chart in Figure 3–7. Bus frequency at Bus 5 and Bus 13 always have the highest amplitudes for four dominant inter-area modes under these different operating conditions. The above result can be compared and verified by the results derived from the residue method based on the full-order system model.

Figure 3–8 shows the magnitude of different generator buses in the residue analysis. Thus, the analysis result based on measurement match with the result from the circuit-based model. Finally, bus frequencies f5, f13, f14, f15, and f16 are the selected observation signals for coherency groups 1, 2, 3, 4, and 5, respectively.

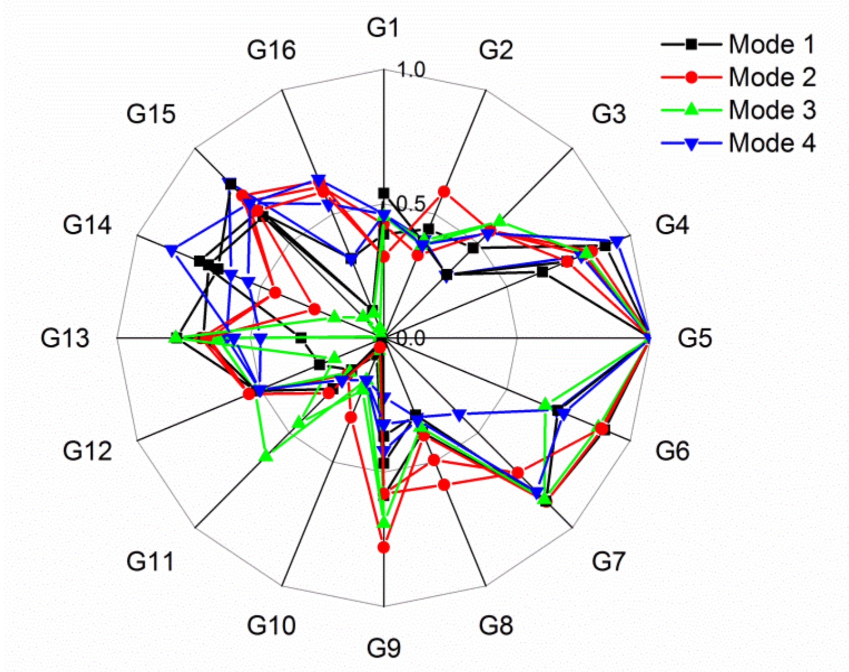

Figure 3–7 Observation signal selection results using FFT analysis of three tests

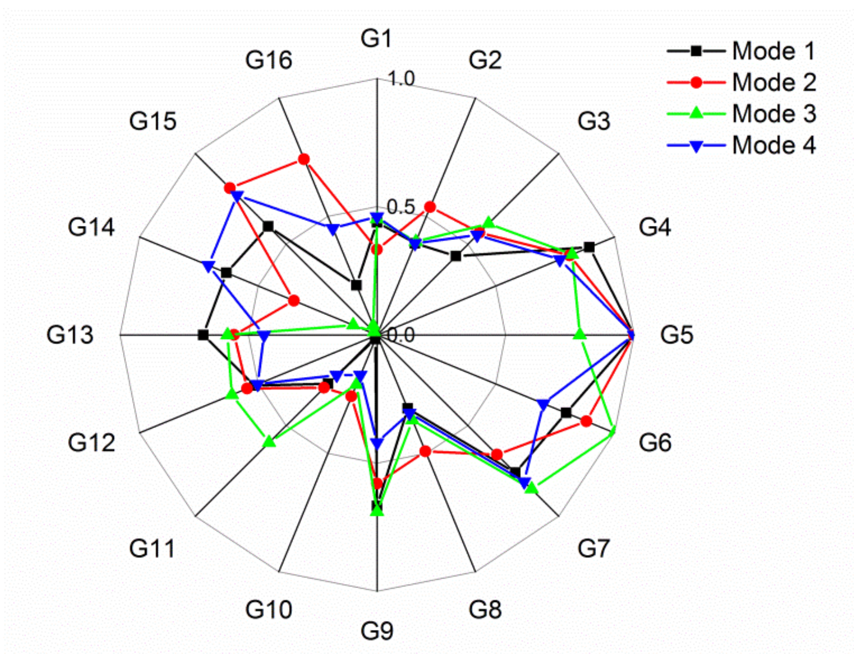

Figure 3–8 Observation signal selection results using residue method

3.4.3 Performance of the MIMO ARMAX Model

Both ambient data and ring-down data are applied to build the MIMO ARMAX model. As mentioned in 3.3.4, the fitting accuracy index is used for time domain validation, while the results from the MP algorithm are selected as the benchmark in frequency domain validation. Additionally, the MIMO ARMAX model is compared with the MIMO N4SID model in estimation accuracy and computation time. Base on numerous offline experiments, the structures of models in the model pool can be determined. The best four different orders of the MIMO ARMAX models for identification using ambient data and ring-down data are (6, 4, 3), (8, 5, 3), (12, 8, 5) and (15, 9, 5), while the best four different orders of the MIMO N4SID models are 30, 40, 50 and 60.

Ambient Data: The ambient data are created by modulating generation (or load) within a narrow range ($\pm$2%) at each generator bus (or load bus). These 50 (16 generator buses and 34 load buses) independent sets of ambient data are used to build the MIMO ARMAX model and the MIMO N4SID model. In addition, the measurement error within 5 mHz is injected into the output signals to emulate the noise in the measurement data. The data is downsampled to a rate of 5 samples per second and 5-minute window size length is chosen in the ambient data analysis.

Taking the independent sets of ambient data by generation modulation at Bus 3 and load modulation at Bus 10 for instance, Figure 3–9 and Figure 3–10 show the time domain response comparison of the actual system, the MIMO ARMAX model and the MIMO N4SID model in these two cases, respectively.

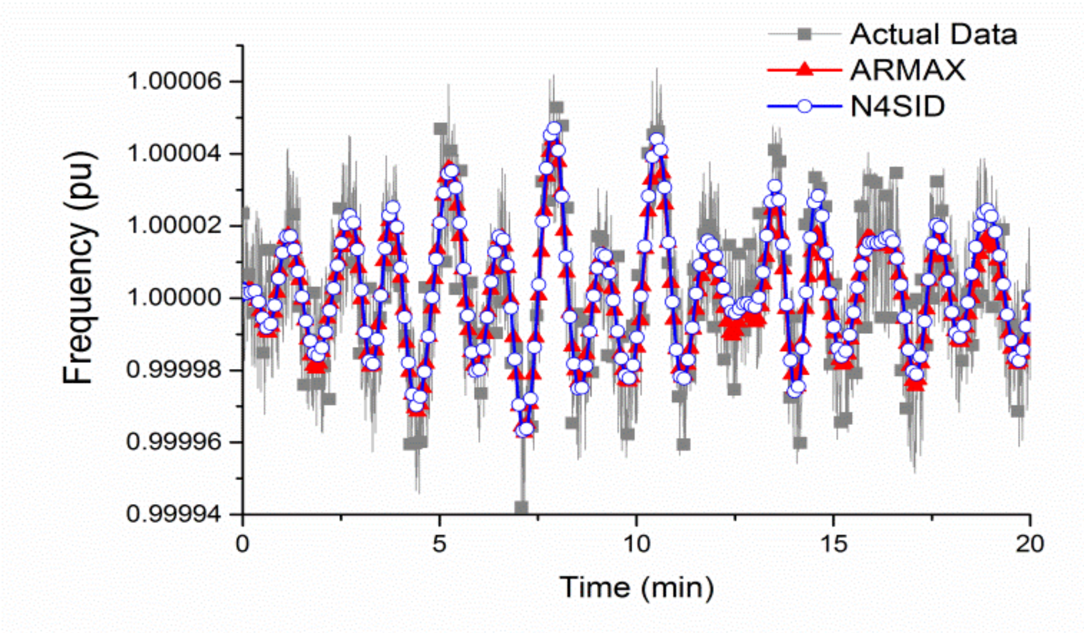

Figure 3–9 Comparison of bus frequency response at Bus 5

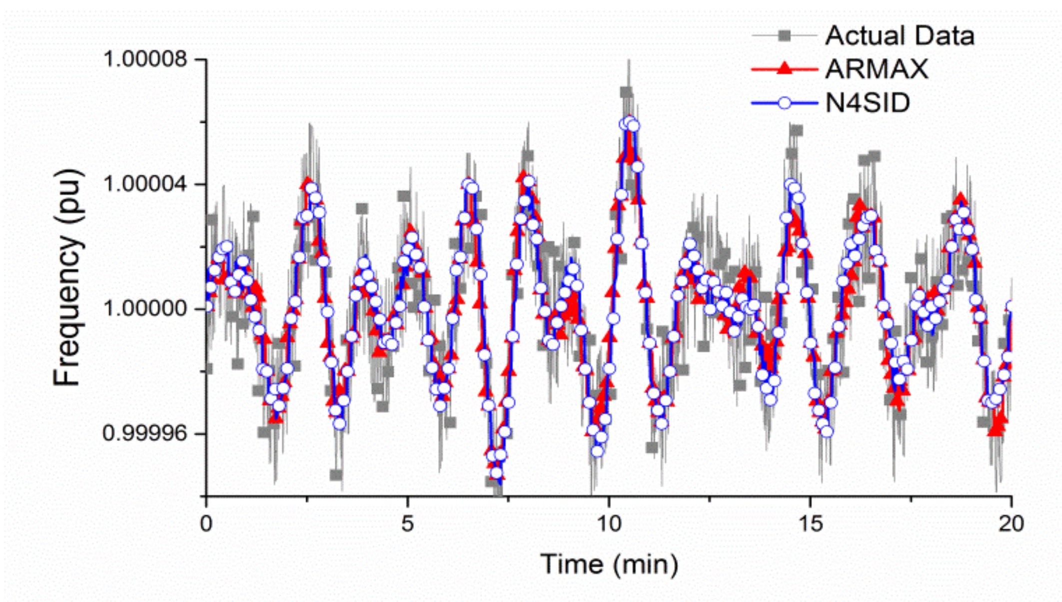

Figure 3–10 Comparison of bus frequency response at Bus 5

The optimal order of the MIMO ARMAX model for maximum fitting accuracy is $(n_\alpha, n_\beta\ , n_\gamma) = (8, 5, 3)$, while the optimal order of the MIMO N4SID model is 40. Both the MIMO ARMAX model and the MIMO N4SID model have similar time domain response with the actual system even if measurement error is present. Due to page limitation, other four outputs of the measurement-based models (frequency of Bus13, Bus14, Bus15, and Bus16) are not given (similarly hereinafter).

In frequency domain, the eigenvalues of all the four dominant inter-area modes are also estimated by using the MP algorithm, the MIMO ARMAX model, and the MIMO N4SID model using the 50 independent sets of ambient data. For the optimal orders in two models, the eigenvalues comparison and the error of modes identification comparing with MP are shown in Figure 3–11 and Table 3-2 which contains absolute values of maximum bias (Max.) and standard deviation (Std.), respectively. Both MIMO ARMAX model and the MIMO N4SID model can capture all the inter-area oscillation modes. Nevertheless, the estimation results of the MIMO ARMAX model are slightly closer to the benchmark than the MIMO N4SID model.

Ring-down Data: Generation trip, load shedding, and line trip events are generated to demonstrate how the proposed methodology behaves with the ring-down data. The sampling rate is 30 samples per second, and the data window is 10 seconds. To eliminate the impact of system transient, the first swing data is removed for the model identification. Also, 5-mHz measurement error is included.

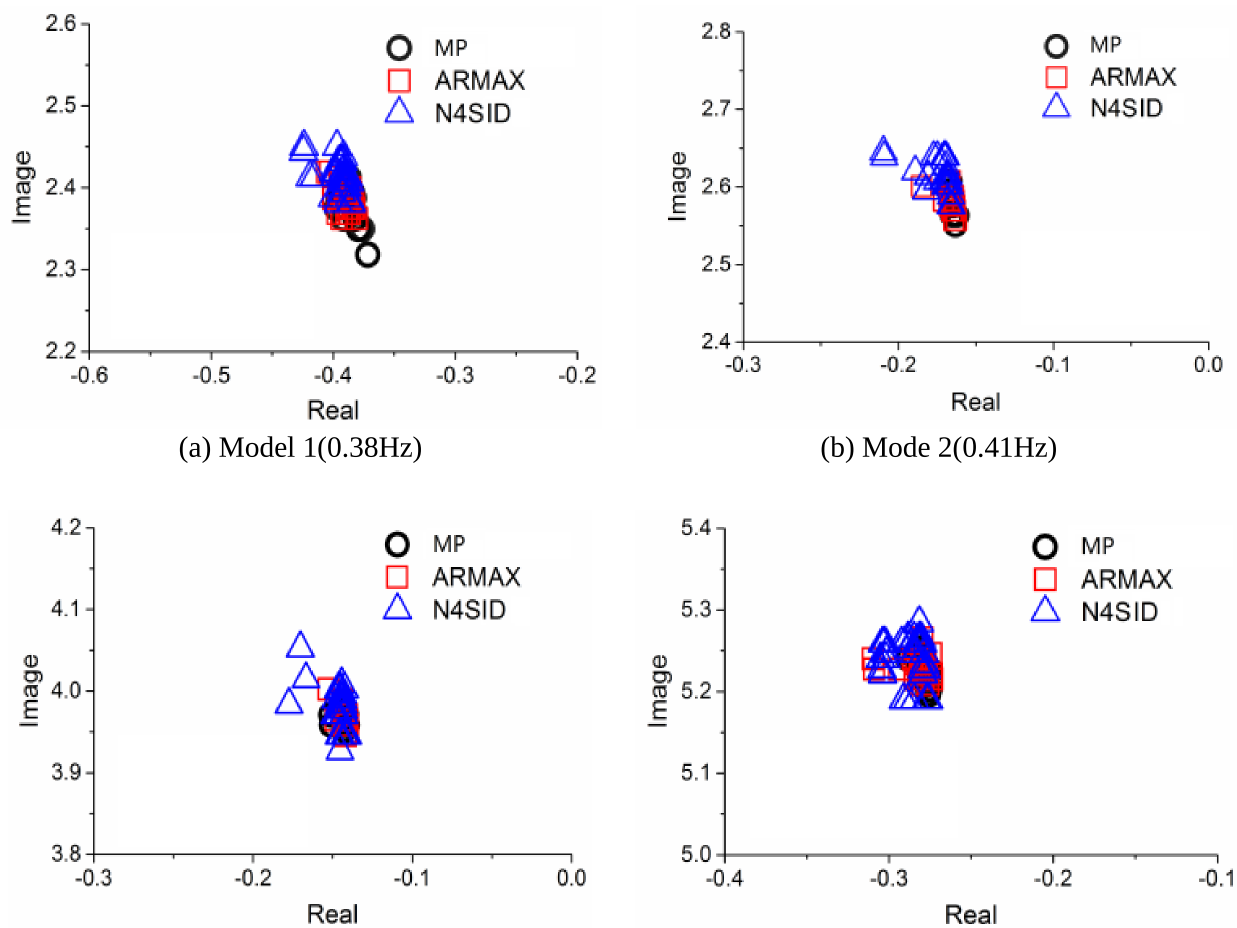

(a) Model 1(0.38Hz)

(b) Mode 2(0.41Hz)

(c) Mode 3(0.63Hz)

(d) Mode 4(0.83Hz)

Figure 3–11 Eigenvalue comparison

Table 3-2 Accuracy of modes for ARMAX and N4SID using ambient data

		Bias	Mode1	Mode2	Mode3	Mode4
MIMO ARMAX	Real	Max.	0.04	0.03	0.02	0.05
		Std.	0.01	0.02	0.01	0.01
	Imag.	Max.	0.05	0.03	0.03	0.02
		Std.	0.00	0.01	0.02	0.01
MIMO N4SID	Real	Max.	0.08	0.07	0.05	0.08
		Std.	0.02	0.02	0.03	0.04
	Imag.	Max.	0.10	0.11	0.14	0.05
		Std.	0.02	0.01	0.05	0.02

Figure 3–12 and Figure 3–13 are two cases of validation using the 53 (16 generations, 34 loads and 3 tie-lines) independent sets of ring-down data. Figure 3–12 shows the bus frequency response at Bus 5 in case of 20% generation trip of G3 at time $t = 1$ second. Figure 3–13 shows the bus frequency response at Bus 5 in case of 20% load shedding at Bus 39 at time $t = 1$ second. In the two cases, the optimal order the MIMO ARMAX model is $(n_\alpha, n_\beta, n_\gamma) = (12, 8, 5)$, and the optimal order the MIMO N4SID model is 60.

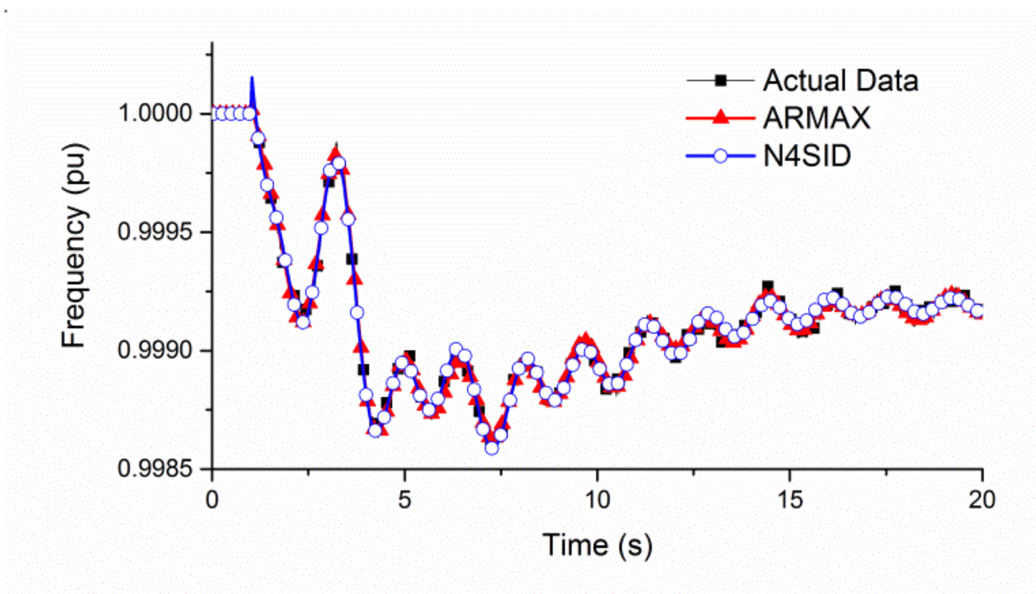

Figure 3–12 Comparison of bus frequency response at Bus 5

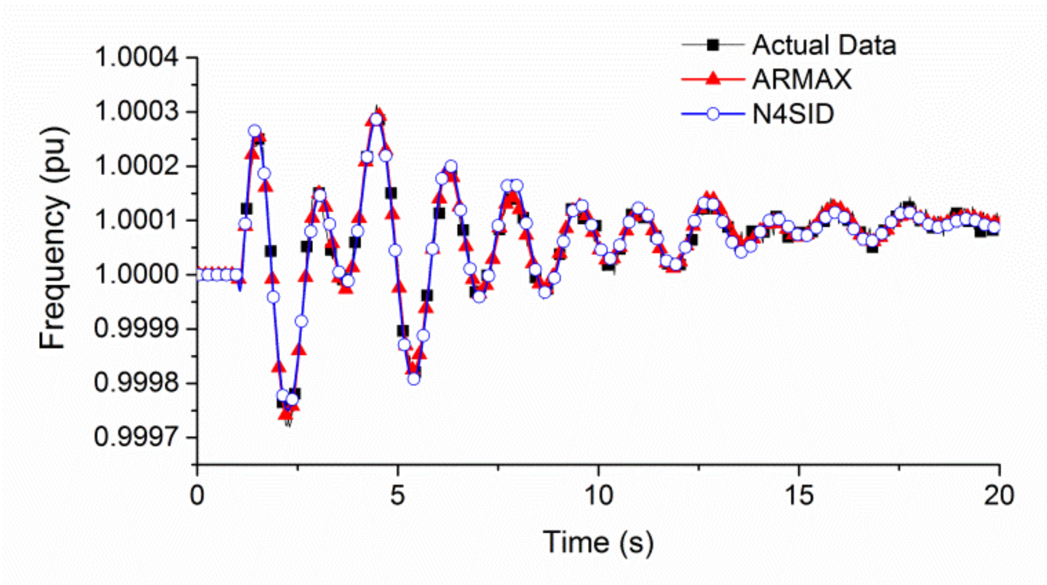

Figure 3–13 Comparison of bus frequency response at Bus 5

For the optimal orders in two models from all sets of ring-down data, the comparison of the estimated eigenvalues using each independent set of ring-down data and the error of modes identification comparing with MP are given in Figure 3–14 and Table 3-3, which contains absolute values of maximum bias (Max.) and standard deviation (Std.), respectively.

Similarly, both the MIMO ARMAX model and the MIMO N4SID model can capture all the dominant oscillation modes of the study system. The event data at the first swing are removed for the identification since the strong non-linearity may corrupt the model identification.

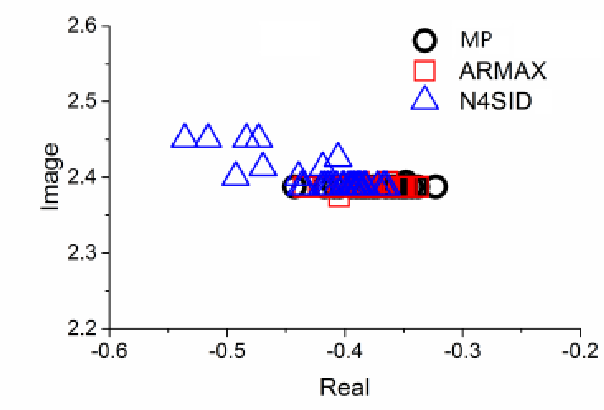

(a) Model 1(0.38Hz)

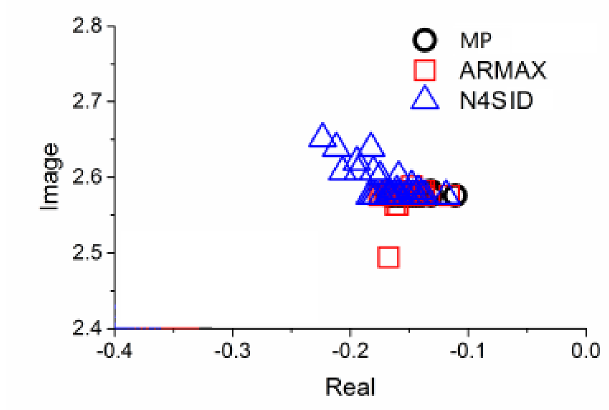

(b) Mode 2(0.41Hz)

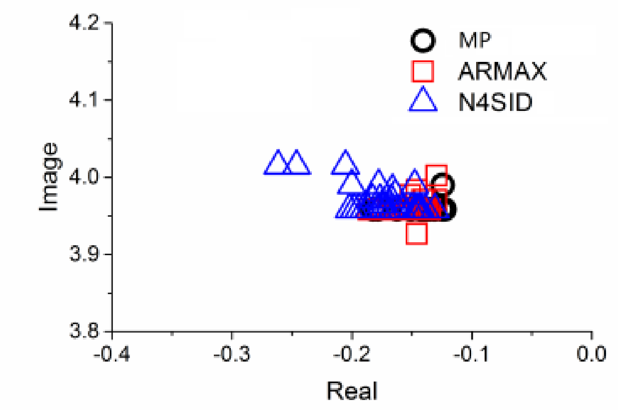

(c) Mode 3(0.63Hz)

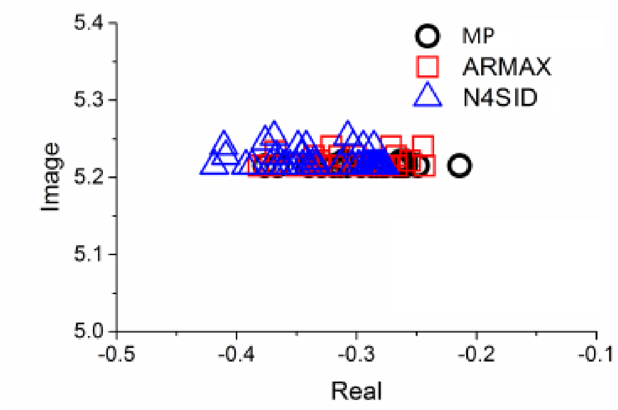

(d) Mode 4(0.83Hz)

Figure 3–14 Eigenvalue comparison

Table 3-3 Accuracy of modes for ARMAX and N4SID using ring-down data

		Bias	Mode1	Mode2	Mode3	Mode4
MIMO ARMAX	Real	Max.	0.11	0.05	0.05	0.10
		Std.	0.02	0.01	0.02	0.03
	Imag.	Max.	0.03	0.07	0.05	0.04
		Std.	0.02	0.01	0.01	0.02
MIMO N4SID	Real	Max.	0.20	0.10	0.13	0.10
		Std.	0.05	0.04	0.06	0.09
	Imag.	Max.	0.10	0.07	0.07	0.05
		Std.	0.03	0.02	0.03	0.03

The estimation accuracy and computation time comparison of the two models are shown in Table 3-4. The cases "generation modulation at Bus 3" and "20% load shedding at Bus 39" are selected as examples. To have equivalent fitting accuracy and mode estimation results with the MIMO ARMAX model, it is necessary to increase the order of the MIMO N4SID model. For instance, when using ring-down data, the MIMO N4SID models with low order are not capable of exhibiting the dynamic behavior under the contingencies in the system unless the order is increased to 60. If the order of the MIMO N4SID model is 40 (or 50), the fitting accuracy index is 65.3% (or 74.1%). However, the order of the MIMO ARMAX model is $(n_\alpha, n_\beta, n_\gamma) = (12, 8, 5)$, which is much less.

Table 3-4 Performance comparison of the two models in model pool

Data type	Model type	Model order	Accuracy Index (%)	Time (sec)
Ambient	ARMAX	(6, 4, 3)	81.2	0.85
	ARMAX	(8, 5, 3)	91.4	0.93
	ARMAX	(12, 8, 5)	86.1	1.14
	ARMAX	(15, 9, 5)	82.5	2.17
	N4SID	30	78.2	6.40
	N4SID	40	86.5	7.71
	N4SID	50	84.3	8.23
	N4SID	60	74.7	8.44
Ring-down	ARMAX	(6, 4, 3)	78.1	0.88
	ARMAX	(8, 5, 3)	83.6	1.02
	ARMAX	(12, 8, 5)	91.8	1.26
	ARMAX	(15, 9, 5)	89.2	2.10
	N4SID	30	61.7	4.67
	N4SID	40	65.3	6.27
	N4SID	50	74.1	7.35
	N4SID	60	85.4	8.61

More importantly, if two models need to achieve similar results, the MIMO N4SID model identification requires about 7-8 seconds, while the MIMO ARMAX model requires about 1 second. The computation time of the MIMO ARMAX model is much less than that of the MIMO N4SID model. It is noted that although the order of the MIMO ARMAX for identifying the ring-down data is higher than the order for identifying the ambient data, the computational speed does not increase significantly.

3.5 Oscillation Damping Control Using Measurement-Based Approach

In this part, the measurement-driven model is computed and updated online using synchronized measurements obtained from selected locations in the system. In addition, the effectiveness of the proposed measurement-driven adaptive wide-area damping controller (WADC) has been demonstrated in a two-area four-machine system on the hardware test-bed under various disturbance scenarios [53].

3.5.1 Controller Parameters Determination

Based on the identified model, the residue angle can be estimated under the latest operating condition, and is used to update the parameters of the lead-lag compensator [54]. For the state matrix:

$$\boldsymbol{AM} = \boldsymbol{M\Lambda} \tag{3–26}$$

$$\boldsymbol{NA} = \boldsymbol{N\Lambda} \tag{3–27}$$

where Λ is a diagonal matrix, and M and N are right and left model matrices, respectively, defined in following equations:

$$\boldsymbol{\Lambda} = \boldsymbol{diag}(\boldsymbol{\lambda_1}, \boldsymbol{\lambda_2}, \cdots, \boldsymbol{\lambda_n}) \tag{3–28}$$

$$\boldsymbol{M} = [\boldsymbol{m_1}, \boldsymbol{m_2}, \cdots, \boldsymbol{m_n}] \tag{3–29}$$

$$\boldsymbol{N} = [\boldsymbol{n_1}, \boldsymbol{n_2}, \cdots, \boldsymbol{n_n}] \tag{3–30}$$

To provide sufficient damping, the oscillation damping controller should move the eigenvalues of the target oscillation mode to the left side of the complex plane. The phase to be compensated (ϕ_i) is determined by the residue angle ($\angle R_i$) of the ith mode (λ_i).

$$\boldsymbol{\phi_i} = \boldsymbol{180^{\circ}} - \angle \boldsymbol{R_i} \tag{3–31}$$

where

$$\boldsymbol{R_i} = \boldsymbol{C m_i n_i^T B} \tag{3–32}$$

Hence, the transfer function of a WADC employing the lead-lag structure is

$$\boldsymbol{H_{WADC}(s)} = \boldsymbol{K_{WADC}} \frac{\boldsymbol{T_w s}}{\boldsymbol{1 + T_w s}} \left(\frac{\boldsymbol{1 + sT_1}}{\boldsymbol{1 + sT_2}}\right)^{\boldsymbol{2}} \tag{3–33}$$

where T_1 and T_2 are the lead and lag time constants, respectively. T_w is the washout constant (5-20s), and K_{WADC} is the gain of the WADC, which can be determined by the root locus. T_1 and T_2 can be determined by the following equations.

$$\boldsymbol{T_1} = \frac{\boldsymbol{1}}{\boldsymbol{\omega\sqrt{\alpha}}}, \boldsymbol{T_2} = \boldsymbol{\alpha T_1}, \boldsymbol{\alpha} = \frac{\boldsymbol{1 - sin(\frac{\phi_i}{2})}}{\boldsymbol{1 + sin(\frac{\phi_i}{2})}} \tag{3–34}$$

where ω is the oscillation frequency of the ith mode, ϕ_i is the compensation angle of the ith mode.

Since the identified measurement-driven model is in the form of state space, the oscillation frequency can be determined by identified A matrix, and the lead and lag time constants can be determined accordingly with (3–33) and (3–34).

3.5.2 Controller Parameters Remote Configuration

The updated control parameters are remotely configured to dispersed controllers in different power plants and substations. For the security of parameter configuration, the controller has separate zones to store operating parameters and backup parameters. The updated parameters are configured in the backup zone, and are switched as operating parameters when the output of the controller is steady so that no interferences would interrupt the system operation.

3.6 Implementation on the Large Testbed

The hardware testbed, which is located in the National Science Foundation (NSF) and Department of Energy (DOE) funded engineering research center—the Center for Ultra-wide-area Resilient Electric Energy Transmission Networks (CURENT), is a platform built for power grid control methodology testing and demonstration [55]. The configuration of the hardware testbed is shown in Figure 3–15.

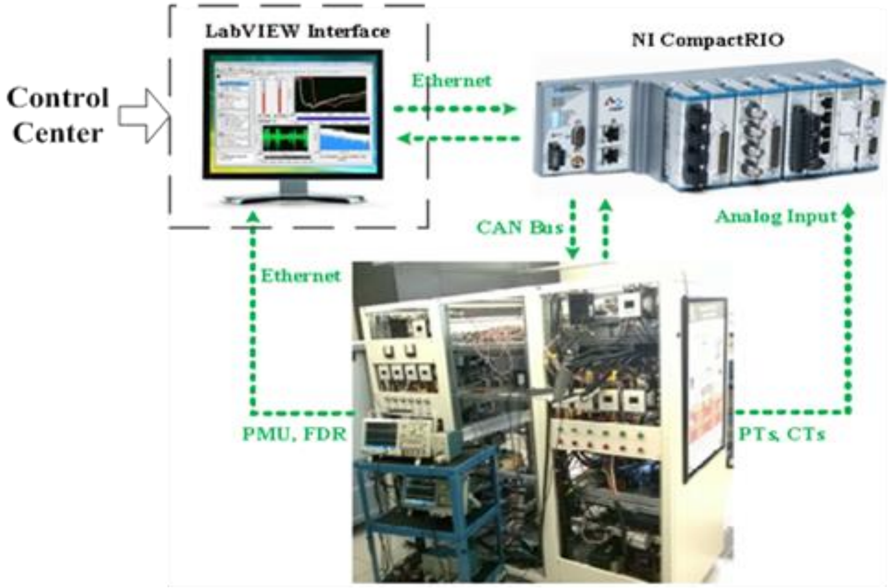

Figure 3–15 CURENT hardware testbed

The two-area four-machine system as shown in Figure 3–16 is now emulated on the hardware testbed, which provides a perfect environment for WADC implementation, testing, and demonstration. All the generators are represented using sub-transient models. Governors and excitation systems are also included. G1 and G3 are equipped with local PSS devices, whose actuation signals are utilized to mitigate the local oscillation modes using their own rotor angular speed as the observation signals. In addition, the loads are represented by constant impedance models.

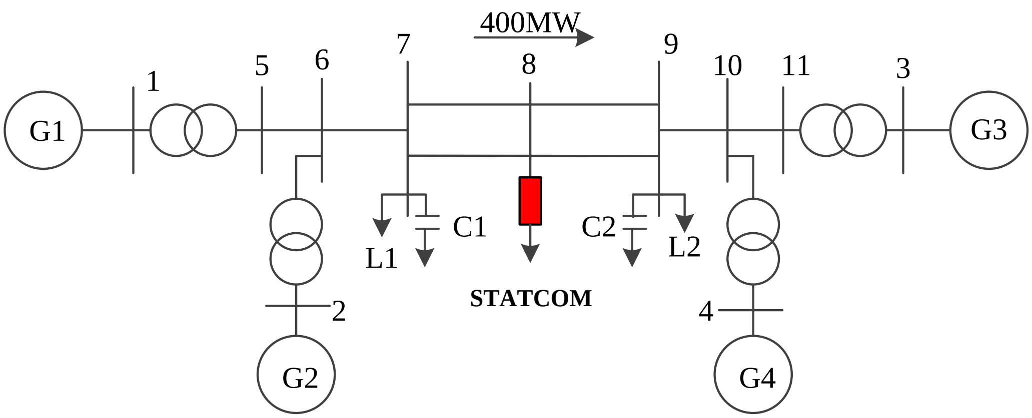

Figure 3–16 Two-area four-machine system

3.6.1 Simulation Results

To compare the performances of the fixed WADC and the adaptive WADC, different operating conditions are created by (1) changing length of transmission line 7-8 and 8-9 from 50% and 220% of original length; (2) Increasing load at Bus 9 from 1,276 MW to 2,076MW. Changing the length of transmission lines is used to change the line impedance and emulate transmission line trip or reclosing event. Figure 3–17 shows the variations of the lead-lag time constants and compensation angles in different operating conditions. It is noted that the compensation angle varies more than 140° (20° to 160°) in Figure 3–17 (b).

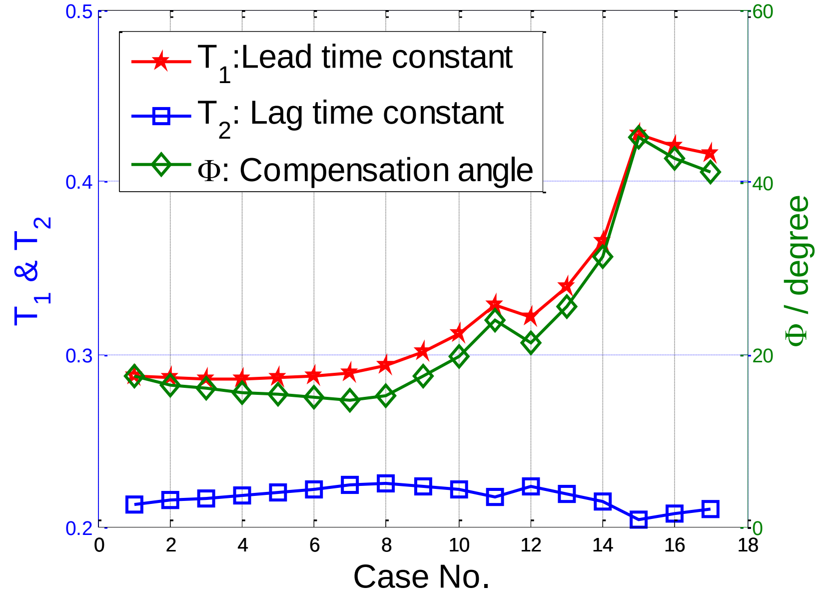

(a) Transmission line 7-8 and 8-9 impedance variation

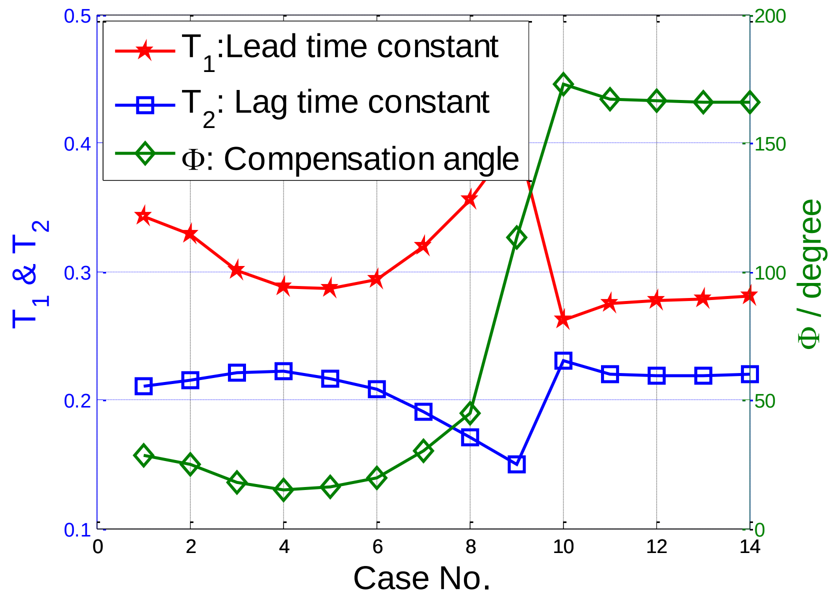

(b) Load variation at Bus 9

Figure 3–17 Variations of lead and lag time constants and compensation angle with changes of operating condition

Specifically, two operating conditions (scenarios) are selected for further comparison. In Scenario 1, based on the base scenario, two consecutive events occur, (1) line trip (the length of transmission line 7-8 is 150% of original length), and (2) load increase (load at Bus 9 is increased by 300 MW). After the line trip event, the Model B in Figure 3–4) will be identified using the ring-down data, and the controller parameters are updated accordingly. Also, after the load increase event, both the model (Model D in Figure 3–4) and controller parameters are updated once again. After these two consecutive events, the updated controller parameters are given in Table 3-5. Similarly, in Scenario 2, two consecutive events occur (line trip, the length of transmission line 7-8 is 200% of original length, and load shedding, load at Bus 9 is shut down by 200 MW), and the model and controller parameters are updated twice.

Table 3-5 Comparison of fixed WADC and adaptive WADC

Scenario No.	Fixed WADC			Adaptive WADC		
	T_1	T_2	K_{WADC}	T_1	T_2	K_{WADC}
1	0.2855	0.2209	4.89	0.4308	0.1627	5.35
2	0.2855	0.2209	4.89	0.4517	0.1538	5.17

Assuming the time delay in the control loop varies from 100 ms to 300 ms, the adaptive delay compensator can measure the time delay in each control cycle, and update its parameters to eliminate the impact the time delay. To reduce the computational burden, a lookup table is designed, as shown in Table 3-6.

Table 3-6 Lookup table for time delay compensator

	d (ms)	T_{C1} (s)	T_{C2} (s)	K_C
1	100	0.2984	0.1970	0.2899
2	125	0.3147	0.1868	0.2875
3	150	0.3320	0.1771	0.2850
4	175	0.3507	0.1677	0.2826
5	200	0.3707	0.1586	0.2802
6	225	0.3925	0.1498	0.2778
7	250	0.4161	0.1413	0.2754
8	275	0.4419	0.1330	0.2731
9	300	0.4702	0.1250	0.2708

Table 3-7 Comparison of damping ratios in different operating conditions

Scenario No.	No control	Fixed WADC	Adaptive WADC
1	2.53%	6.31%	9.18%
2	2.44%	3.69%	8.21%

The parameters of the adaptive WADC are given in Table 3-5, and the comparison of fixed WADC and adaptive WADC is given in Table 3-7. Since there is only one inter-area mode in the study system, the optimal control gain of the adaptive WADC can be easily determined by increasing the gain value by one step in each step until the damping ration does not increase. The control effects of no additional control, fixed WADC and adaptive WADC are compared by time-domain simulation. After two consecutive events, the parameters of fixed WADC do not change, while the adaptive WADC updates its parameters based on the identified measurement-driven model. If another line trip event (one line between Bus 8 to Bus 9) occurs, the damping performances during this event are given in Figure 3–18 and Figure 3–19 for two selected scenarios. It can be found that the adaptive WADC can provide better damping than fixed WADC.

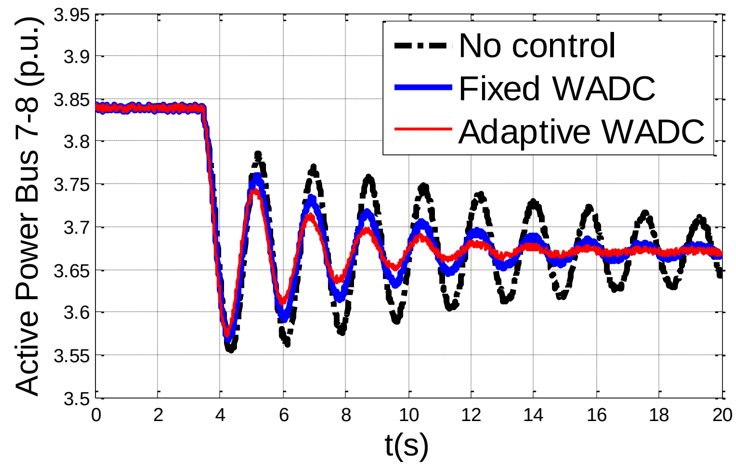

Figure 3–18 Control effect comparison of fixed WADC and adaptive WADC in scenario 1

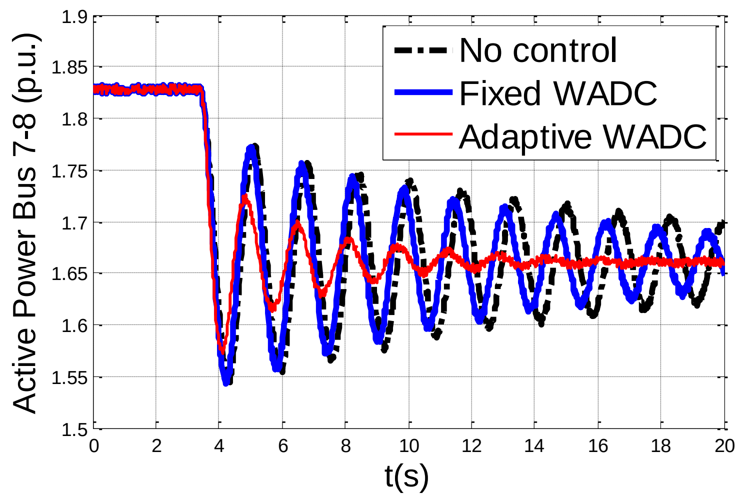

Figure 3–19 Control effect comparison of fixed WADC and adaptive WADC in scenario 2

3.7 Conclusion

Aiming for the adaptive and coordinated oscillation damping control, the methodology to identify the MIMO ARMAX-based transfer function model using pure measurement is proposed in this chapter. The case study in the NPCC system demonstrates that the identified MIMO ARMAX model using ambient data or ring-down data may accurately capture all the dominant oscillation modes.

The time domain response of the MIMO ARMAX model reflects that of the actual system, and the estimated eigenvalues are very close to the results of MP analysis. Compared with the MIMO subspace state model, the MIMO ARMAX model has equivalent accuracy but lower order and less computation time. Meanwhile, the implementation on the hardware testbed demonstrates the feasibility of practical implementation of a measurement derived model-based WADC for small and large disturbances over a wide range of operating conditions. The future work includes achieving coordinated and adaptive damping control among inter-area modes using the measurement-driven model. The further demonstration of the proposed adaptive WADC on the CURENT hardware testbed would be also exhibited.

CHAPTER 4 COMPARISON OF MIMO SYSTEM IDENTIFICATION METHODS FOR ELECTROMECHANICAL OSCILLATION DAMPING ESTIMATION

4.1 Introduction

In interconnected systems, damping of inter-area oscillations is one of the main concerns for improving power system stability and power transmission [56]. Traditionally, the electromechanical oscillation damping estimation is mainly based on the offline circuit-based model which is not feasible to update frequently and promptly. If proper online monitoring tools are available, this can help operators determine the security margin of the system, therefore allowing them to take proper actions in real time. Since PMUs are deployed throughout American continent, it is practical to estimate oscillation modes through the data-driven methods with wide-area measurement data [57].

As known, various identification methods can be applied to estimate the oscillation modes using measurement data, such as wavelet transform, spectral analysis, state space identification, transfer function identification and so on [58].

Theoretically, all algorithms can serve as mode meters with the SISO structure. Some earlier studies have compared the performance of above approaches. However, few studies discuss the performances of MIMO models.

Compared to SISO models, MIMO models have significant advantages:

- Linear systems may be built by MIMO models based on inputs and outputs.
- MIMO models can estimate system modes as accurate as SISO models. Meanwhile, they can be applied to design the damping controller.
- It is feasible for MIMO models to calculate mode shapes which are hard through SISO models.

However, it is quite difficult or impossible for some algorithms to convert SISO models into MIMO models. In this chapter, two categories of algorithms, which are the subspace state-space identification and the transfer function identification, are selected to compare in terms of the performance of MIMO identification approaches.

For subspace state space methods, MIMO N4SID identification, MIMO MOESP identification and MIMO stochastic subspace identification are selected. In the transfer function group, it has MIMO ARMAX with two-stage least squares (2LS) and MIMO ARMAX with recursive least squares (RLS).

The remaining content of the chapter is organized as follows. The next part describes two families of identification methods. Then, the performance is compared by case studies in the NPCC system. The final part gives the conclusion.

4.2 MIMO System Identification Algorithms

The power system model for the small signal analysis is usually represented by the state space method, which is a set of first order differential equations based on the linearization around a certain operation point, as shown in the equations (3–1) and (3–2), respectively.

4.2.1 MIMO Subspace State-Space Identification

According to (3–1) and (3–2), the linear system can be presented by the subspace state-space algorithm. A system with m inputs and p outputs has the state-space equations as follow:

$$\boldsymbol{x}(\dot{\boldsymbol{t}}) = \boldsymbol{A}\boldsymbol{x}(\boldsymbol{t}) + \boldsymbol{B}\boldsymbol{u}(\boldsymbol{t}) + \boldsymbol{K}\boldsymbol{e}(\boldsymbol{t}) \tag{4–1}$$

$$\boldsymbol{y}(\boldsymbol{t}) = \boldsymbol{C}\boldsymbol{x}(\boldsymbol{t}) + \boldsymbol{D}\boldsymbol{u}(\boldsymbol{t}) + \boldsymbol{e}(\boldsymbol{t}) \tag{4–2}$$

where $x(t)$ is the state variable vector with n elements. A , B , C , D and K are system identification matrices, respectively. $u(t)$, $e(t)$ and $y(t)$ are the observable input signal vector, unobservable measurement vector and output signal vector.

Essentially, to get the whole system identification model, two subsystems, which are deterministic model and stochastic model, may need to estimate respectively, then combine them into a consolidated model. When the MIMO subspace state space approach is applied to estimate the system model, the deterministic model needs to be mainly considered.

Meanwhile, the stochastic model can be computed by the ambient signal analysis. The major steps for system identification are described below in terms of the MIMO state space model [34], [35], [40]:

- Estimation of the state, which includes order estimation.
- Estimation of the matrix A and C.
- Estimation of the noise model.
- Estimation of the matrix B and D.

In [59], the stochastic subspace method avoids forming the covariance matrix and using semi-infinite block Hankel matrices. Hence, the stochastic subspace identification may compute more rapidly than the subspace state space identification.

4.2.2 MIMO Transfer Function Identification

From 3.2, the MIMO transfer function between inputs and outputs is represented as (3–3) and (3–4). (3–4) shows that the certain output may be regarded as the aggregated result from the contribution of all inputs. Therefore, in the discrete-time domain, the contribution of the input signals to the outputs at the sampling time t can be exhibited as (3–6).

4.3 Case Study

The five methods, which are MIMO ARMAX-2LS, MIMO ARMAX-RLS, MIMO N4SID, MIMO MOESP and MIMO stochastic subspace, are tested in the 16-machine 68-bus NPCC system, which is a reduced order model of the New England test system (NETS)/New York power system (NYPS) interconnected system. The detailed information and topology is provided by Figure 3–5.

Both ambient data and ring-down data are applied to build the MIMO ARMAX model. Total 50 ambient data tests and 50 ring-down data tests are created to evaluate the performance of five methods.

To demonstrate the performance of five methods, accuracy index is still used for time domain validation, while the estimated results are compared to modes from the model-based algorithm, which is selected as the benchmark in frequency domain validation. To evaluate the computation speed associated with model order, the maximum order for all models is 50.

Meanwhile, the model structure is also depended on the number of inputs and outputs. Thus, the number of inputs is 5 and the number of outputs is 16 which means to use generator buses as measurement points.

4.3.1 Results of System Identification using Ambient Data

The ambient data are generated by tuning generation or load within a narrow range. The 50 independent datasets of ambient data are utilized in the test. In ambient data, the measurement error within 5 mHz is added in the output data. The data is downsampled to a rate of 5 samples per second and the calculation window is 5 minutes.

Figure 4–1 shows the result identified from Bus 5 using ambient data which is generated by load changing at Bus 10. Compared to the actual data, the identification results from five methods with the best order can obtain the high fitting accuracy index which is over 85%.

Fitting accuracy indices of MIMO AMARX-2LS, MIMO AMARX-RLS, MIMO N4SID, MIMO MOESP and MIMO Stochastic Subspace are 93%, 89%, 91%, 86% and 87%, respectively. Even though the top identification results belong to MIMO ARMAX-2LS and MIMO N4SID, the results from other methods are acceptable. However, the computation costs are varied in terms of the structures and orders of five models.

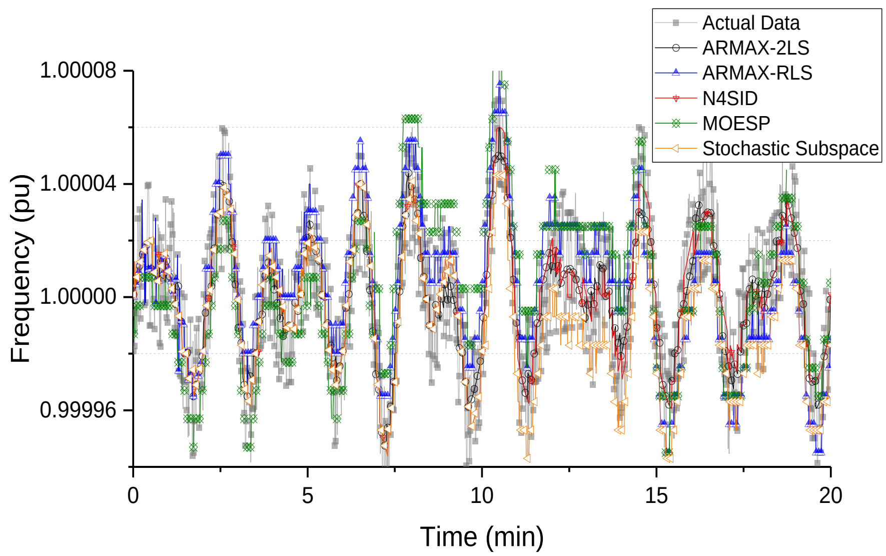

Figure 4–1 Identification results and comparison using ambient data

In frequency domain, four dominant low-frequency oscillation modes can be identified by five methods using 50 independent datasets. According to the optimal orders in five methods, the oscillation mode comparison is presented in Figure 4–2.

The errors of mode identifications are Figure 4–3 and Figure 4–4 which have absolute values of maximum bias (Max.) and standard deviation (Std.).

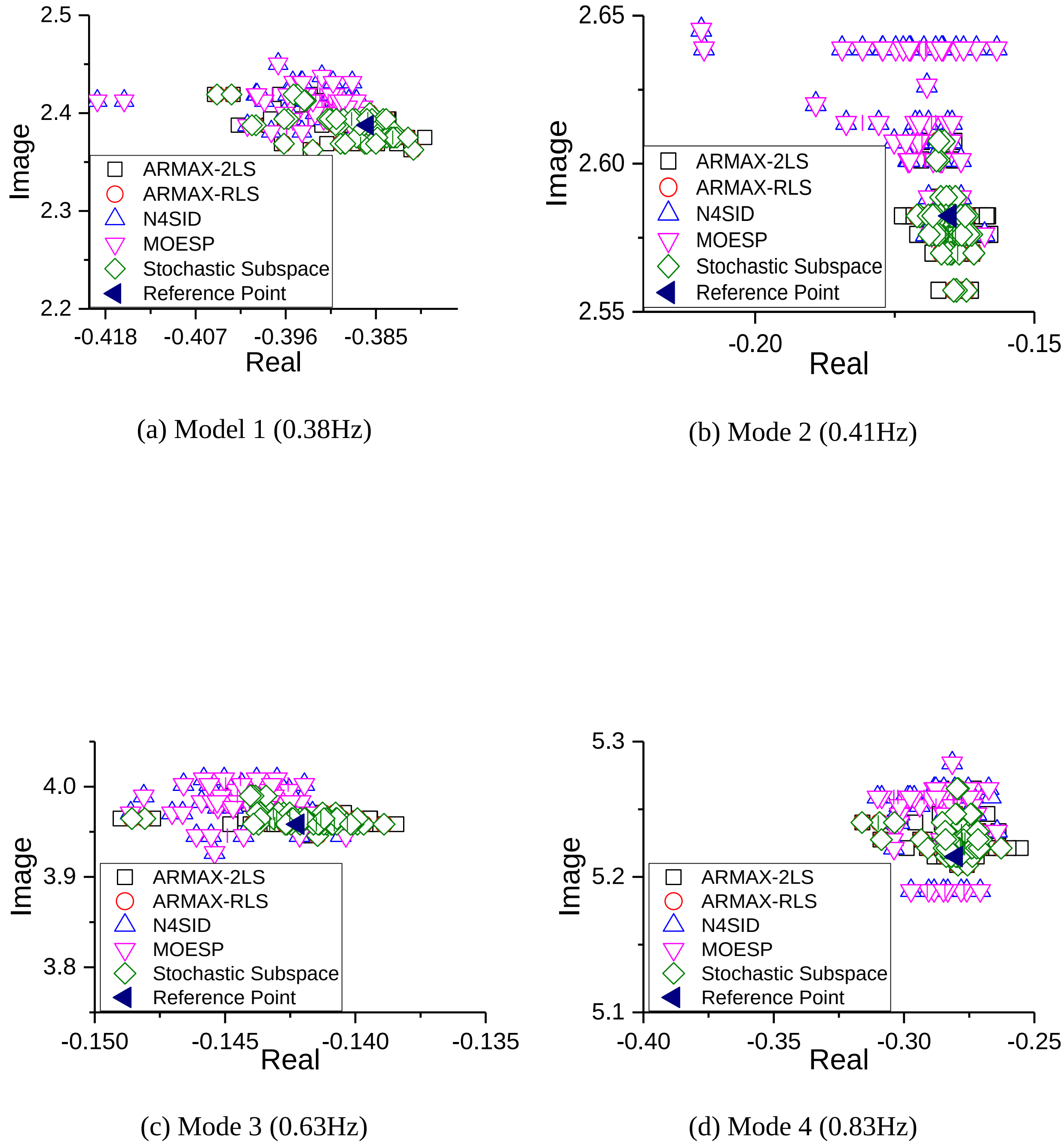

Figure 4–2 Eigenvalue comparison

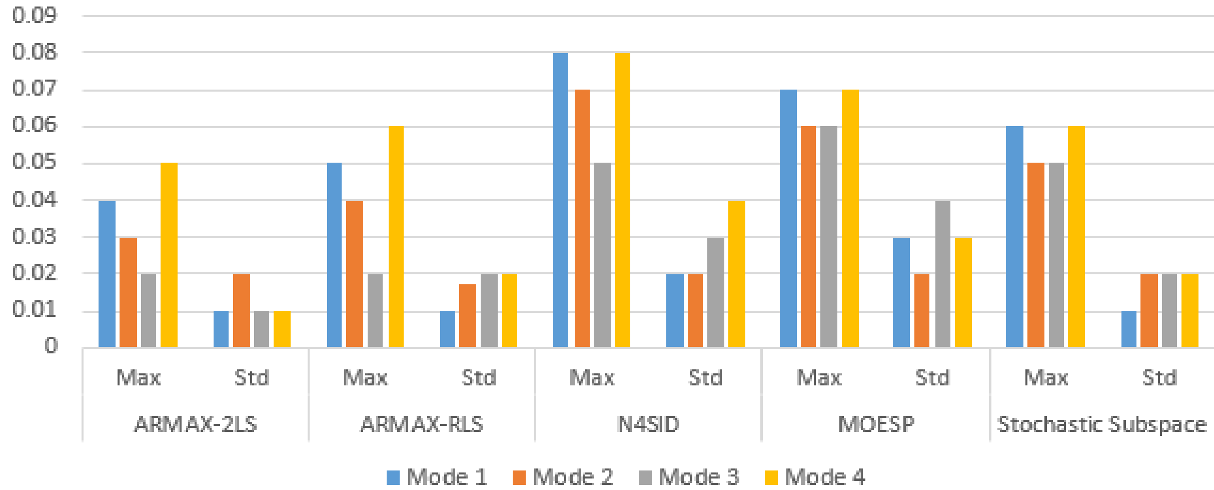

Figure 4–3 Accuracy comparison of real part of modes for five methods

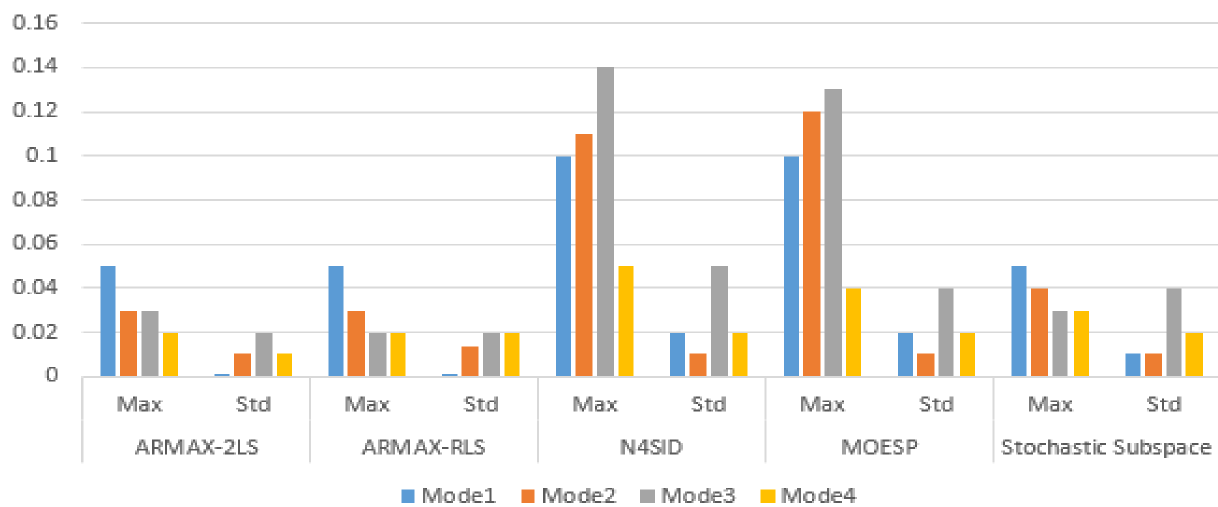

Figure 4–4 Accuracy comparison of image part of modes for five methods

4.3.2 Results of System Identification using Ring-Down Data

The ring-down data are generated by events happened in the system which include generation trip, load shedding and line trip. Similarly, the 50 independent datasets of ring-down data are utilized in the test. The measurement error within 5 mHz is added in the output data. The data is downsampled to a rate of 30 samples per second and the calculation window is 10 seconds. Since power systems present strong non-linear features during events happen, the identification methods may avoid the first swing from the ring-down data to estimate the oscillation modes. the number of inputs is 5 and the number of outputs is 16 which means to use generator buses as measurement points. Figure 4–5 demonstrates that one event from 50 independent datasets is 20% generation trip happened at G3. The frequency domain comparison for four dominant oscillation modes is shown in Figure 4–6.

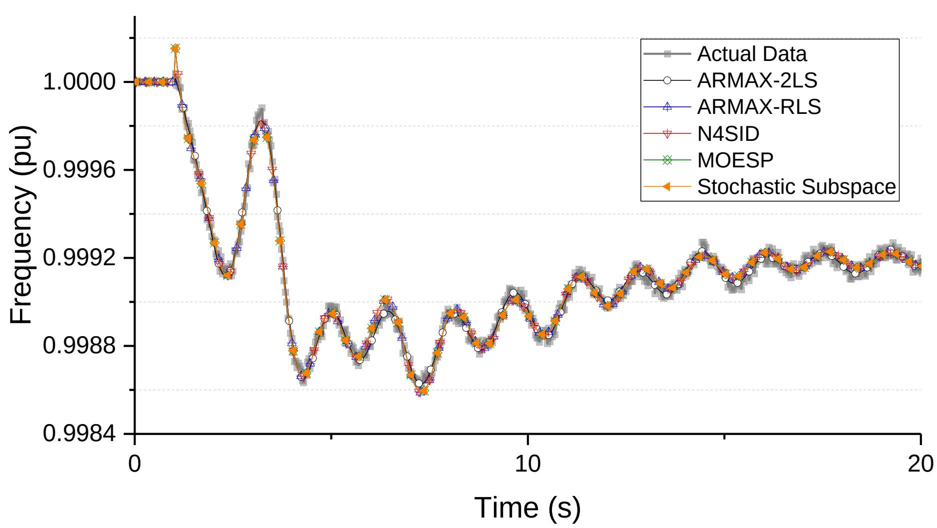

Figure 4–5 Identification results and comparison using ring-down data

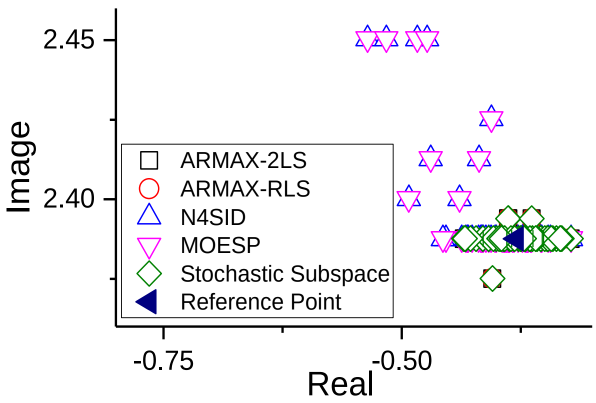

(a) Model 1 (0.38Hz)

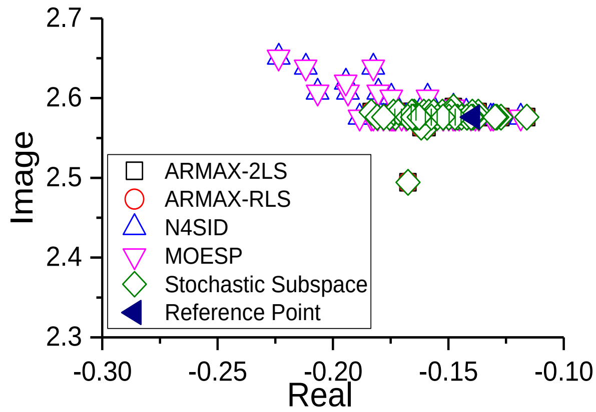

(b) Mode 2 (0.41Hz)

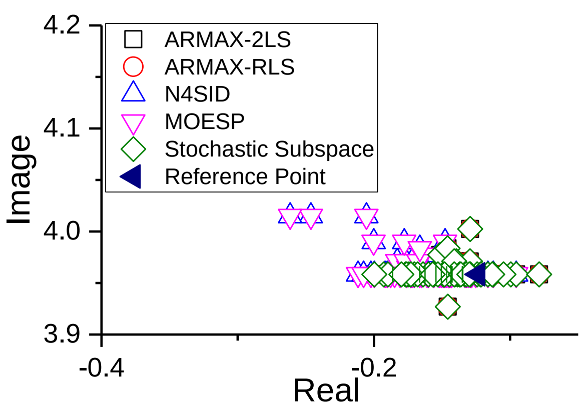

(c) Mode 3 (0.63Hz)

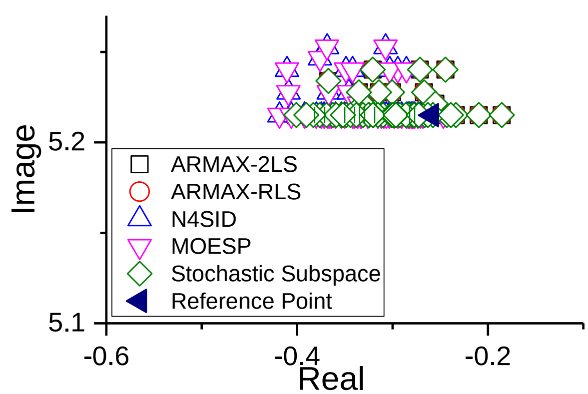

(d) Mode 4 (0.83Hz)

Figure 4–6 Eigenvalue comparison

Similarly, compared to the actual data, the optimal identification results from five methods are also presented in Figure 4–5. Fitting accuracy indices of MIMO ARMAX-2LS, MIMO ARMAX-RLS, MIMO N4SID, MIMO MOESP and Stochastic Subspace are 92%, 90%, 89%, 88% and 90%, respectively. All identification results in time domain are over 85%. It implies that the identification results are quite good when ring-down data are used to derive models.

Compared to the estimated results from ambient data, the estimated results from ring-down data are slightly worse because the particular disturbance makes the capture of oscillation modes more difficult. Similarly, Figure 4–7 and Figure 4–8 exhibit the error of modes identification.

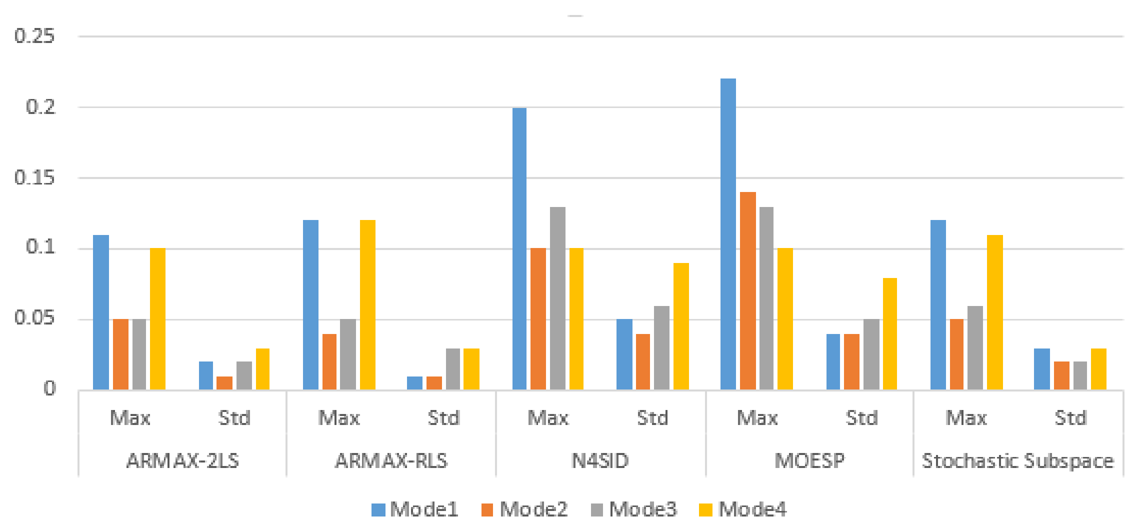

Figure 4–7 Accuracy comparison of real part of modes for five methods

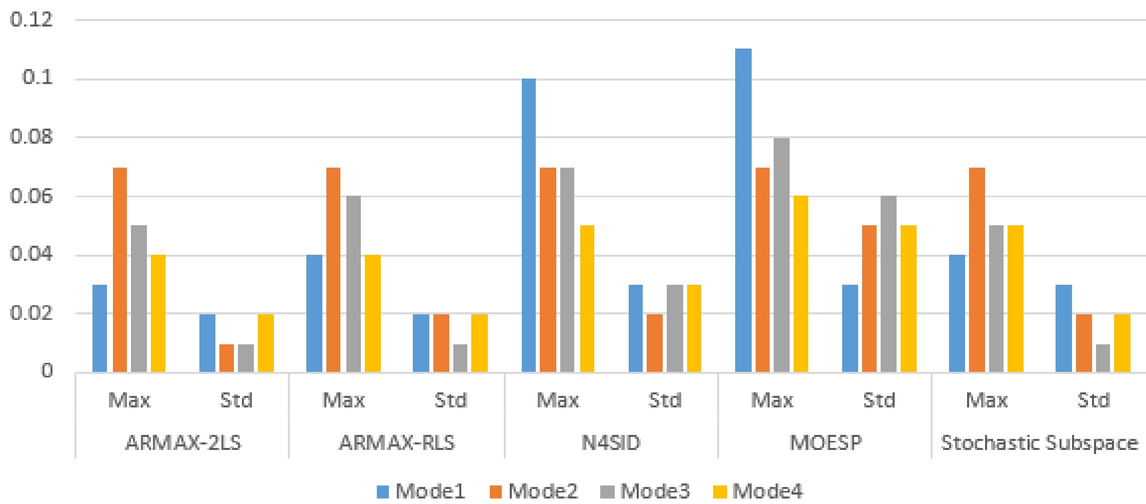

Figure 4–8 Accuracy comparison of image part of modes for five methods

4.3.3 Performance Analysis

All testing data and five methods are implemented on a computer with Intel i5-3230M 2.6 GHz CPU, 2GB RAM. In order to observe the computation time of five methods, the order of models increase while fix the number of inputs and the number of outputs, which are 16 inputs and 16 outputs. The computation time of the five methods is shown in Figure 4–9.

However, the performance of the five models not only depends on the computation time but it also is determined by the structures of five models which mean the order of models. In Figure 4–9, the time consumption would be high while the order of the identification model increases.

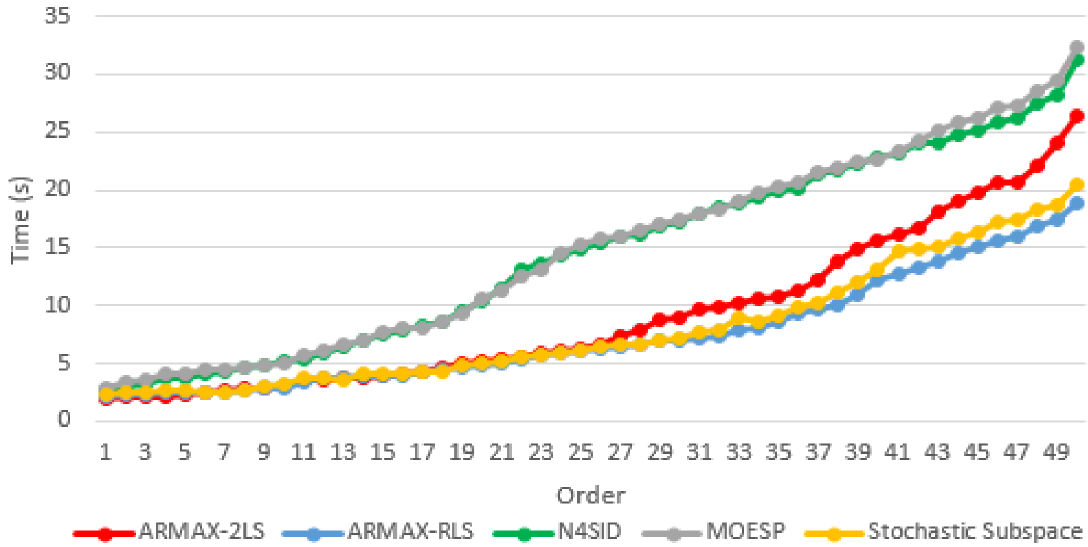

Figure 4–9 Computation time of five methods

Essentially, each method has an optimal model from the candidate models with different orders. In independent tests using the ambient and ring-down data, the optimal order is referred to as the order which derives the best identification results.

Thus, the optimal order of the model needs to be examined. Based on the test system, Figure 4–10 (a) and Figure 4–10 (b) presents the optimal models of five methods which the accuracy index is over 80% and can obtain the quite accurate mode estimation using ambient data and ring-down data, respectively.

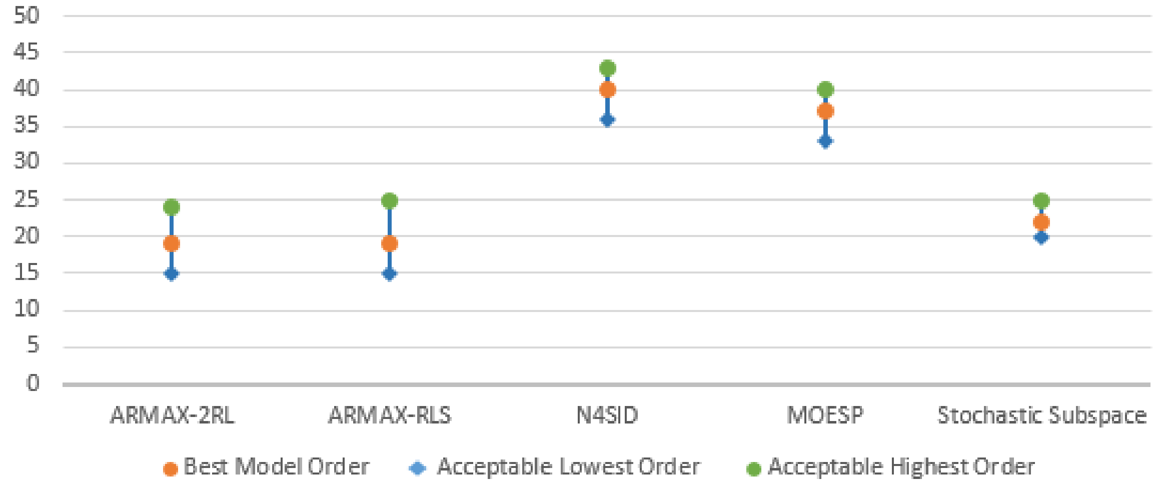

(a)

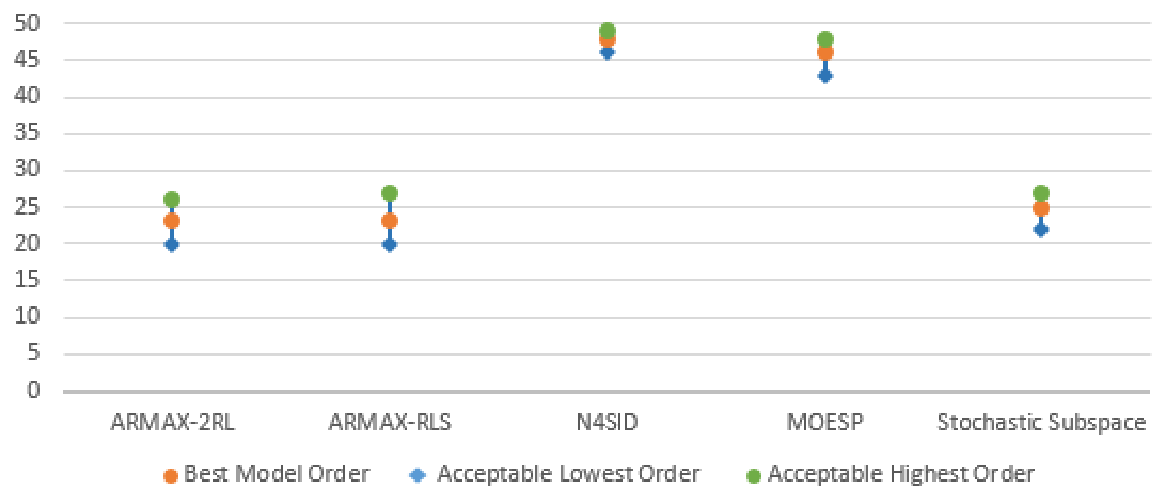

(b)

Figure 4–10 Orders of five methods with acceptable estimation

4.4 Conclusion

According to the above analysis and comparison, the MIMO ARMAX with 2RL, MIMO ARMAX with RLS and MIMO stochastic subspace model may have better performance using the ambient data and ring-down data. The accuracy of modes estimation from five methods is adequate with slight differences. From computation speed aspect, the MIMO ARMAX methods may have low-order model structures that reduce the computation burden. In the family of transfer function, the recursive calculation method is fairly rapid during optimizing the coefficients of the MIMO ARMAX model. Thus, the MIMO ARMAX with RLS may have better performance. Meanwhile, since the stochastic subspace avoid effectively forming the covariance matrix and using semi-infinite block Hankel matrices. The computation speed is close to the MIMO ARMAX with RLS.

The most significant feature of MIMO models for oscillation damping estimation is that the model can be further applied to the oscillation damping control or control parameter calibration.

CHAPTER 5 DESIGN AND DEVELOPMENT FOR DATA HISTORIAN PROJECT IN DOMINION VIRGINIA POWER

5.1 Introduction

With the expansion of the scale of power systems and widely used advanced information technologies, the quantities and categories of data and information at various resolutions are increasing dramatically. New phenomena and issues in power systems need to be recognized and analyzed. Therefore, data mining and analytics are critical for the power industry. However, several ubiquitous challenges are many information silos without cross-system integration, the lack of global data description and data models and even insufficient common applications and services. They impede efficient data mining, waste valuable information and obstruct advanced data analytics in electric utilities under the big data environment. Meanwhile, these challenges also have a negative effect on the ever-growing business and delicate management of electric utilities. Dominion Virginia Power (DVP), which is one of the nation's largest producers and transporters of electrical energy, has also suffered these problems for a long time [60].

For the above challenges, academics have suggested some potential solutions [61], [62]. Moreover, some European enterprises have been applying analytic strategies of big data to enhance customer management and operational capability. Meanwhile, in terms of data collection and communication, International Electrotechnical Commission (IEC) has explored, designed and implemented various standard protocols for the power industry. However, most of IEC standards have not gained adequate attentions in American power systems. In addition, IT commercial giants have also proposed enterprise-level integration solutions based on cloud computing in [63]–[65]. However, many of them are conceptual and not easy to practice. In

[66]–[70], electric utilities in China have been developing their information platforms and have had preliminary achievements. But the platforms are mainly for applications and services in control centers rather than the entire enterprise.

Since the existing solutions are not appropriate and adaptive for large electric utilities, the optimal approach is to implement an integrated architecture, an open platform, a flexible and standard method for data sharing, and numerous intelligent functionalities. For the special requirements of DVP, a new system framework based on a time series database is proposed. By adopting advanced information and communication technologies (ICTs), the platform is highly integrated and open, the adapters are standardized, and the system is driven by the data model which is easily shared and can maintain and store entire information and parameters of equipment and devices. Abundant intelligent applications are designed and developed based on the integrated data.

The remaining of this chapter is organized as follows. The second part summarizes the status of technical supporting systems. The third part describes the features of the novel enterprise-level data platform in DVP. The methodology of data integration is introduced in the fourth part. The naming convention which is the basis of the data model is exhibited in the fifth part. The design of the hierarchical data model is presented in the sixth part. In the seventh part, applications and visualizations for the data platform are introduced. The last part concludes this chapter.

5.2 Current Status of Technical Supporting Systems

Because of this ever-growing business and the requirement of delicate management at DVP, advanced information technologies to be widely used internally are promoted. However, since various operation systems are increasing and information barriers appear, the current homegrown data historian cannot fulfill the demand for processing big data and sharing the data on the enterprise level. To solve the problems above, the ultimate goal of the data historian project is to improve the capability of big data management and implement a robust data historian solution for DVP.

In DVP, several challenges impede efficient data mining and obstruct advanced data analytics.

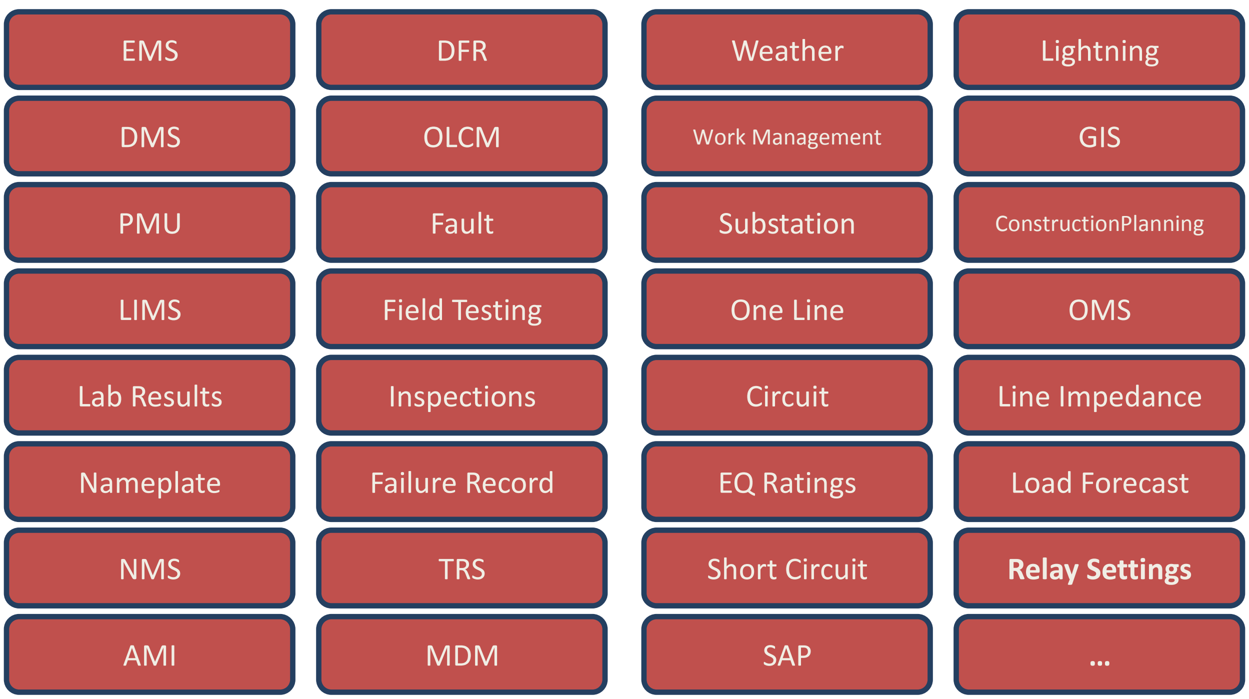

Figure 5–1 Operational systems and applications in DVP

Initially, information silos exist in the technical supporting systems. As Figure 5–1 shows, more than 20 operational systems and applications should be maintained by different departments and groups in DVP. Because of North American Electric Reliability Corporation (NERC) restrictions of cyber security for the different network environments, the systems which are in different networks are incapable of interacting with each other. This is the root cause of information silos. For example, Energy Management System (EMS) is isolated because EMS is in the Process Control Network (PCN) with the highest security. Since the firewall policy does not allow the data stream from the low security network to the high security network, it is not in compliance to send the information of field tests into EMS from Distribution Management System (DMS) which is in the Demilitarized Zone (DMZ) with the lower security. Therefore, if there is not a platform for data collection, the information silos are inevitable.

Furthermore, no semantic layer exists on top of the data. Due to a lack of a global naming convention, it is difficult to identify and describe the same data point among different systems. Therefore, in order to organize and map data in different systems, DVP is in critical need of a semantic layer on top of the data.

In addition, the current Facility Management Recorder (FMRecorder) which collects measurement data and the SAP database which stores the static information have served in DVP for over ten years to provide reports and parameter query services. However, several drawbacks from two standalone and unassociated systems are evident. With this architecture, it is extremely difficult to integrate different data sources, analyze the global information and provide visualizations for individuals because no systems have a powerful integration tool or a centralized processing ability.

Owing to a lack of effective methods to organize data and connect the existing information silos, it is impossible to search and retrieve data and information with convenient approaches.

5.3 Features of Enterprise-Level Data Platform

To manage data and models flexibly and provide applications easily, the innovative platform may have four features:

Scalability: Though the number and the variety of data are increasing continuously, the platform may handle a growing amount of work and to be enlarged to accommodate the growth. For a data repository, the platform can achieve the centralized archive from various sources and upgrade the capacity with very low cost. For third-party applications, the platform would message and share data and models with standards based on the loosely coupling architecture. Moreover, upcoming applications can be integrated into this platform easily and lower the possibility of interferences to the existing business.

Real time: High-resolution real-time data are integrated in the platform. Therefore, the platform uses real-time processing to handle the workload whose state is changing constantly, and has real-time access to historical data and current snapshots. Time series databases can manage high-resolution real-time data much better than traditional relational databases.

Service-oriented architecture: The implementation of encapsulating services for hiding trivial details is critical for users. Meanwhile, the service-oriented architecture (SOA) may guarantee the scalability with the loosely coupling structure. In the platform, the numerous adaptors and interfaces of third party applications or systems become common services in the platform through standard protocols. For users, the platform offers flexible and lightweight tools for data queries, visualizations, and analytics and so on.

High reliability: The platform will be a core part of IT systems within the enterprise and provide services for different departments through networks. Since the system consists of many hardware and software components, partial failures are unavoidable. Therefore, the platform design utilizes cluster servers with load balancers to tackle partial failures gracefully without service interruptions. Furthermore, to prevent network intrusion and survive in a disaster, the platform structure has redundant backup with a disaster recovery system in different sites.

5.4 Methodology of Data Integration

With the rapid growth of both structured and unstructured data from multiple sources, the current IT infrastructure needs to be reorganized to optimize the flow of big data for fulfilling intensive analytic applications. The implementation utilizes the PI system and build a highly reliable and flexible common data repository. The data in the PI system can be fed into applications and analytics based standard adapters. Users can manage and visualize the data through visualization tools in the PI system or data-rich one-line diagrams.

5.4.1 Types of Big Data

Big data sets for the enterprise-level data platform are depicted in Figure 5–2. Most real-time data still depend on the Supervisory Control and Data Acquisition (SCADA) since the deployment of Remote Terminal Units (RTUs) is widely practiced and has provided the operators the ability of monitoring the operation status of the entire system. Meanwhile, the historical data from SCADA contain abundant raw information for Situational Awareness (SA) and system planning. On the other hand, with the increasing number of PMUs, high-resolution

PMU data can provide more adequate dynamic responses and instantaneous values with accurate timestamps.

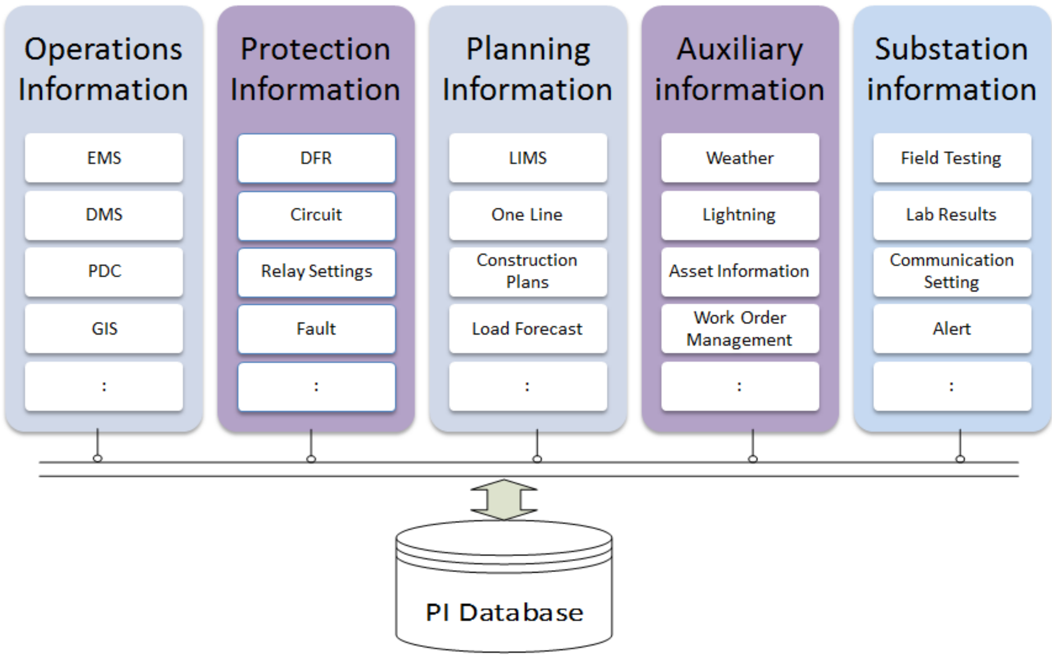

Figure 5–2 Types of big data for the enterprise-level data platform

In the distribution network, with the introduction of intelligent distribution automation equipment and distributed generation into the grid, the need to monitor, analyze, optimize and control the distribution system in real time is greater than ever, and the data from the Distribution Management System (DMS) play an important role to fulfill the above requirements. For protection technicians, comprehensive information from Digital Fault Recorders (DFRs), relay settings and circuit calculation are critical for detecting and analyzing faults. In addition, traditional planning mainly focuses on the off-line limitation calculation, the design of the substation and network topology. If it is easier to involve more statistical information from the data platform, the planning decision should be smarter than ever. Moreover, many electric utilities maintain and collect the auxiliary information and substation information such as asset information, weather information, field test data, and so on. Such information can exert a greater contribution for management and operation in power utilities while it is integrated with data from other sources.

5.4.2Implementation of Big Data Integration

Big data integration (BDI) is fundamental and critical to implement the vision of big data in terms of modeling, application and analytics. The value of data can be exhibited by data mining only when it is possible for disparate data to link and seamlessly interweave with other data to derive a unified and global representation. In [71], the author mentioned that BDI is different from traditional data integration in several dimensions. In Figure 5–3, the IT infrastructure of big data integration is presented.

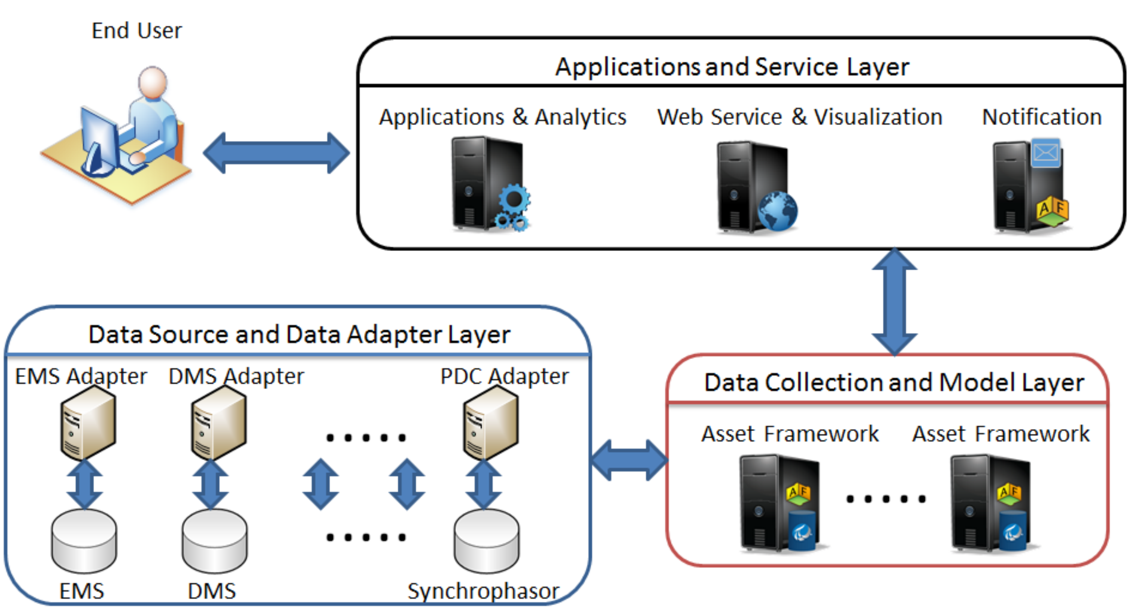

Figure 5–3 High level architecture of big data integration

Meanwhile, several core requirements such as scalability, real time, service-orient service and high reliability are needed to be fulfilled. To tackle the challenges, one practical approach is provided below:

First, the data are integrated through unified interface services. Unified interface services support connecting the platform to disparate data sources. Some interfaces enable history recovery, some simply access the historical data stored in third-party historians. These data sources are seamlessly interwoven into the platform independent of source, protocol or vendor. Interface services can buffer to multiple servers, intelligent data reduction, single tag definition (tags configured on a PI server are synchronized to interface) as well as point by point security. Redundancy and auto point creation are also available on interface services.

Secondly, the data are archived into data collectives and the data-driven model is built. Taking advantage of the exception and compression algorithm, data are instantly stored in archive servers of the platform and available to users in real-time. Meanwhile, the hierarchical data model can create a consistent representation of assets or processes. It can associate data in the proper context. The model may provide the easiest way for users to find the information they need.

Thirdly, the applications are provided to end users. To eliminate barriers to use data and models, the platform provides the popular tools such as Internet browsers, Microsoft Office and mobile phones for end users. It is easy for them to work the data or implement analytics rather than waste time on data collection.

Finally, the backup strategy is required. The platform has redundant design and two groups of systems with same structure serve backup to each other. It can guarantee the reliability during the operation

5.5 Naming Convention for Data Historian

Before the data model is introduced in the next part, naming convention rules for data historian should be presented first. The naming conventions of various systems have been nonexistent or uncoordinated and therefore no overarching naming convention exists within DVP. However, the data model requires unified and consistent rules within the PI system, otherwise data in the data repository cannot be automatically organized as in the hierarchical structure in of PI Asset Framework (AF). AF allows users to search measurements and parameters based on the either device types or data categories rather than data tags and therefore it can improve the users' experience significantly.

The current data semantics in various systems within DVP are not clear. Users are not easy to obtain the device and measurement information based on names of tags. Each system has its own naming conventions that have been inconsistent with time and with other systems. The naming convention of the data historian should follow a standard, systematic methodology that takes into account current and future AF structures, current company standards, and current industry standards. The tag name should include any information that will be necessary to map it to an AF structure, such as location, asset, device of origin, operational identification number, and possibly more. Current company standards should be consulted so that users are familiar with the data naming standard. However, new industry standards, such as IEC 61850, should be consulted as well for insight and conformity on a larger scale.

Since most of existing tag names provide information about which primary equipment the Intelligent Electronic Device (IED) that gathers the tag is installed on and where the primary equipment is located, a functional location oriented naming is one of the objectives of the standard. It is therefore proposed that tag names consist of a Context and a Measurement where the context contains information from the functional location and measurement defines IED specific acquisitions.

Context answers whose information the PI tag is and Measurement explains what information the PI tag is. Figure 5–4 illustrates the standard PI naming frame with Context and Measurement divided into subfields. Context and Measurement are separated by a slash whereas the sub-fields under them are dissected by dots.

Figure 5–4 Standard PI naming structure

The semantics of the proposed Context convention are:

First, Location provides information about the place of the specific device that the PI tag is attached to. Location can be a substation where the PI tag is communicated from or an enterprise-wide software program that generates the PI tag.

Secondly, Device Type provides the type of device, which may be a piece of primary equipment or a specific software program, being referred to by the Location.

Thirdly, DVP has specific identifications associated with a specific internal ID. For that reason, Operation ID in most cases is the operating number of a piece of primary equipment. It can also be the name of an application within a software program, etc.

Finally, Source provides information regarding the source of the information from other systems. An optional extension can also contain additional information such as the standardized name of the IED or a functional relay ID, etc.

The semantics of the proposed Measurement convention are:

Firstly, Function provides information about the standardized smallest entity the application of an IED can be decomposed into. The granularity of the decomposition stops at the smallest parts which act as atomic building blocks for the complex application of an IED. In a nutshell, Function is a group of PI tags that serve a specific function in a Context.

Furthermore, Measurement Type represents specific information and fundamental definition of a PI tag. Measurement Type can be construed to some extent as the data point type of PI tags. Some Measurement Type instances have a Measurement Type attribute field to complete the definition of a Measurement Type.

At last, Variable provides information regarding what property of a Measurement Type PI tags are assigned to. It prescribes the exact quantity a PI tag is associated with. Some Variable instances have a Variable attribute field to complete the definition of a Variable.

5.6 Hierarchical Data Modeling in Data Platform

5.6.1 Common Information Model and Its Extension

The hierarchical structure is used in AF to store and manage data which are mentioned in 5.4. To represent the global data model in AF, the feasible approach is to utilize the hierarchical structure of the Common Information Model (CIM) in AF with customized extensions. It may guarantee the data integration and interoperation from different systems. CIM defines a common vocabulary and basic ontology for various aspects of power industries. Various CIM packages describe basic classes and attributes for the network, energy management, metering, and outage management and so on. However, since CIM would not contain all classes and attributes of a specified application, CIM always needs to be customized and extended based on business requirements.

Here is an example in Figure 5–5 to exhibit the concept of the customized extension. Self-contained equipment containers, which are extensible and have flexible structures, are used to build the hierarchical structure to manage the data in DVP. However, the standard CIM cannot fulfill the demand of building the hierarchical structure to maintain the styles and preferences of the data model in DVP. Existing types of CIM equipment containers, such as Substation, Bay, and VoltageLevel (VL), which are depicted in Figure 5–5, are not self-contained and cannot satisfy the requirement of building a hierarchical structure. Thus, a new class called "FunctionLocation", which is derived from EquipmentContainer (EC), is defined in Figure 5–5. An association is created between FunctionLocation and EquipmentContainer as well, by which a FunctionLocation may have sub-level ECs.

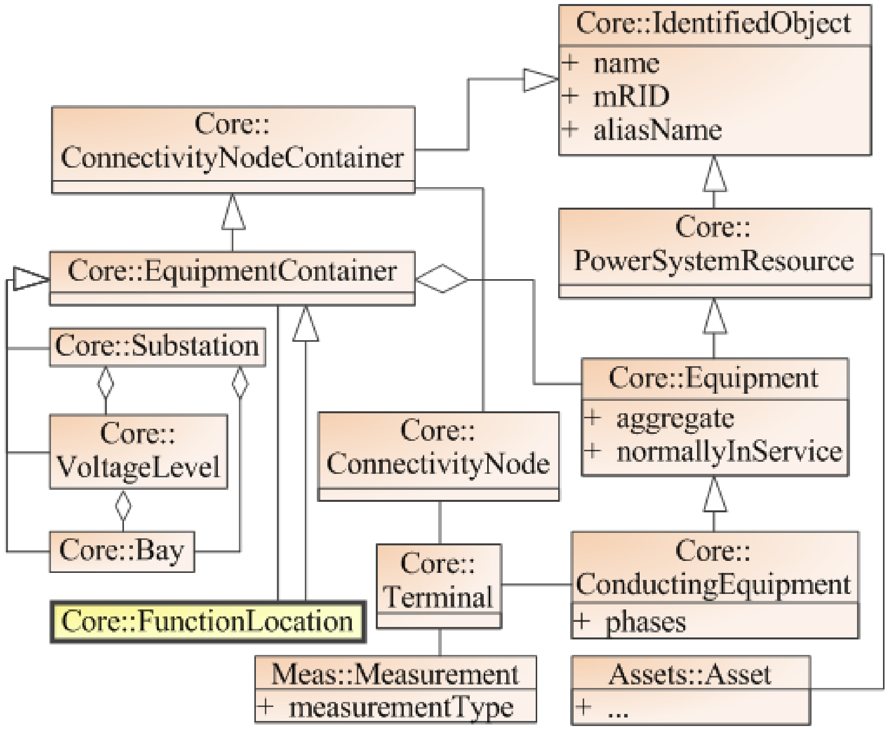

Figure 5–5 Chart for the example of CIM extension

5.6.2 AF Implementation Based on Hierarchical Structure

AF is a single repository for asset-centric models, hierarchies, objects, and equipment (hereafter referred to as elements). It integrates, contextualizes, refines, references, and further analyzes data from multiple sources including one or more PI data archives and non-PI sources such as external relational databases. Together, these metadata and time series data provide a detailed description of equipment or assets.

AF can expose the rich data to components in the PI system such as PI Coresight, PI DataLink, PI Notifications, or PI ProcessBook where they can be used to build displays, run calculations, deliver important information, and so on. AF also can expose these elements and associate data to non-PI systems via a set of data access products. AF also includes many basic and advanced search capabilities to help users obtain static and real-time information.

The AF implementation consists of two steps: the global AF template is created on the ontology layer and the association of data for creating the hierarchical tree is generated.

For the first step, a CIM profile, which is a subset model of CIM, needs to be created for the AF implementation since some of the packages or classes of CIM are needed. Then an AF adaptor is developed to create AF templates according to the CIM profile based on AF SDK, as shown in Figure 5–6.

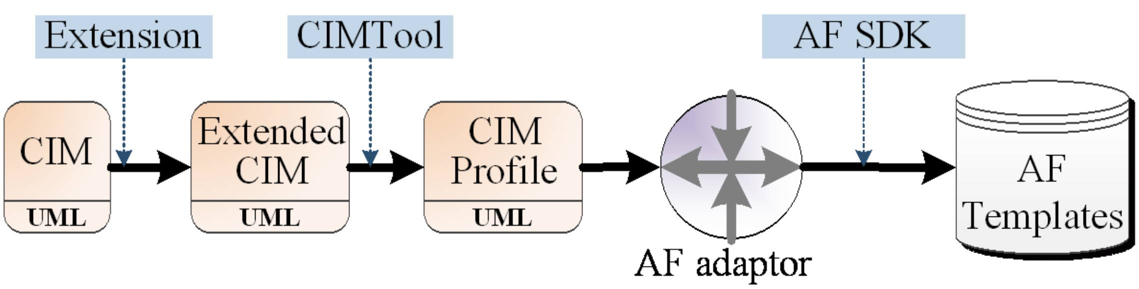

Figure 5–6 Flowchart of generating the AF templates based on CIM

For the second step, links between data objects need to be established. There are two types of links between objects in AF at the data level: Parent-Child and Reference. The ways of creating links in AF based on the CIM model are listed below:

- The aggregation between CIM classes is converted to a Parent-Child link between objects of AF: Figure 5–7 exhibits the aggregation between EC and Equipment. As subclasses of

EC, Substation and VL are aggregate of equipment, and Substation consists of VLs. In AF, equipment, such as buses, breakers, are children of VL, while VL are children of Substation, as shown in the right portion of Figure 5–7.

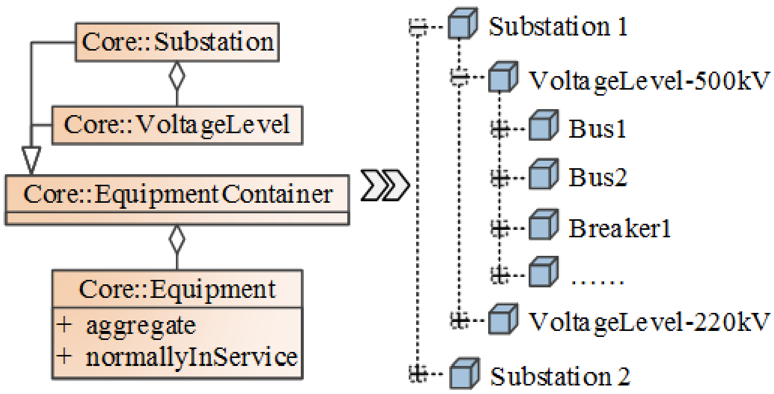

Figure 5–7 Aggregation between Equipment and EquipmentContainer

- The association between CIM classes is converted to a Parent-Child link or a Reference between elements of AF: Here is an example to exhibit how to create links. ConnectivityNode (CN), ConductingEquipment (CE) and a Terminal are used in CIM to describe the topology of the network, as shown in Figure 5–8. Considering most of CEs have two Terminals except for BusbarSection and TransformerWinding which have only one Terminal, the association between CE and the Terminal is converted to Parent-Child link, while the association between CN and Terminal is converted to reference.

The hierarchical structure of AF is shown in Figure 5–9, where represents an element, and indicates a reference link.

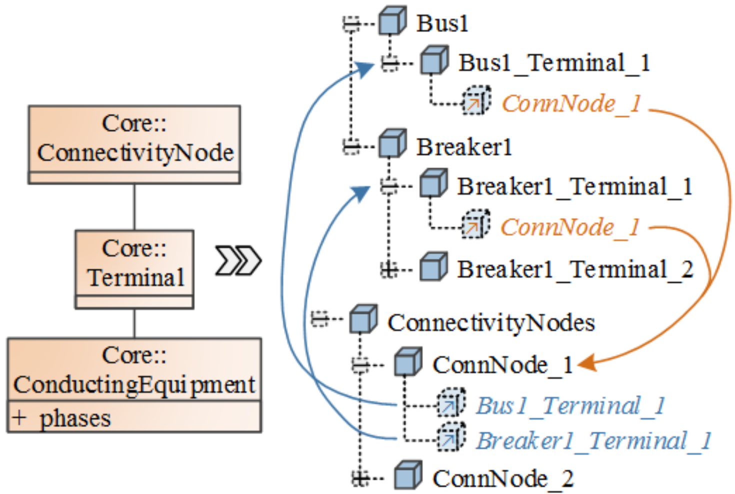

Figure 5–8 Associations between CN, Terminal and CE

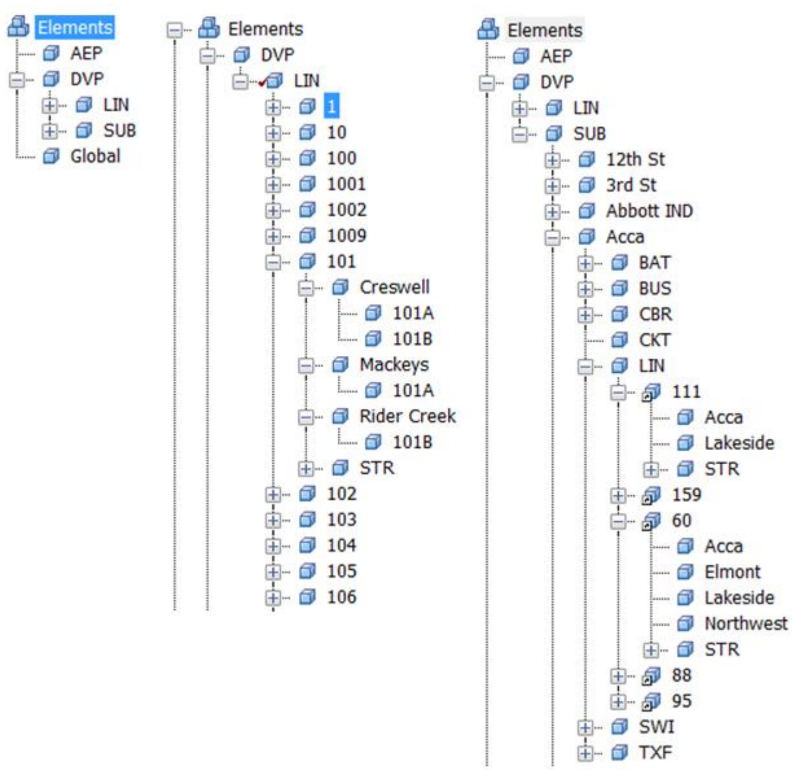

Figure 5–9 Hierarchical structure in AF

For example, Acca substation consists of transformers, transmission lines and other devices, while transmission-line category is an aggregation of different transmission lines. The lines in the “LIN” branch are associated with the lines in the “SUB” branch by reference links.

Once a hierarchical structure is created in AF, applications and visualizations can be built based on AF and achieved data.

5.7 Data-Driven Analytics and Visualizations

5.7.1 Data-Driven Analytics

To improve asset performance, reliability and lifecycle management of assets, it is critical to change the maintenance strategy from calendar-based to conditional-based, in order to reduce the unnecessary maintenance cost. The platform described above can implement the asset monitoring and analytics, and with pre-defined thresholds or conditions, it can generate email notifications and work order automatically.

In terms of asset management in an electric utility, power transformers constitute one of the largest investments, therefore it is a high priority to have an effective diagnostic tool for condition assessment. Dissolved gas analysis (DGA) of insulating oil is considered the single best indicator of a transformer’s overall health condition, with real-time monitoring data streaming, online DGA monitoring is built to visualize the trends of 8 critical gas concentrations for each transformer, as shown in Figure 5–10.

Moreover, the Duval triangle method is utilized to evaluate the current energy level of gas formation, shown in Figure 5–11. This method has proven to be accurate and dependable over many years and is now gaining in popularity

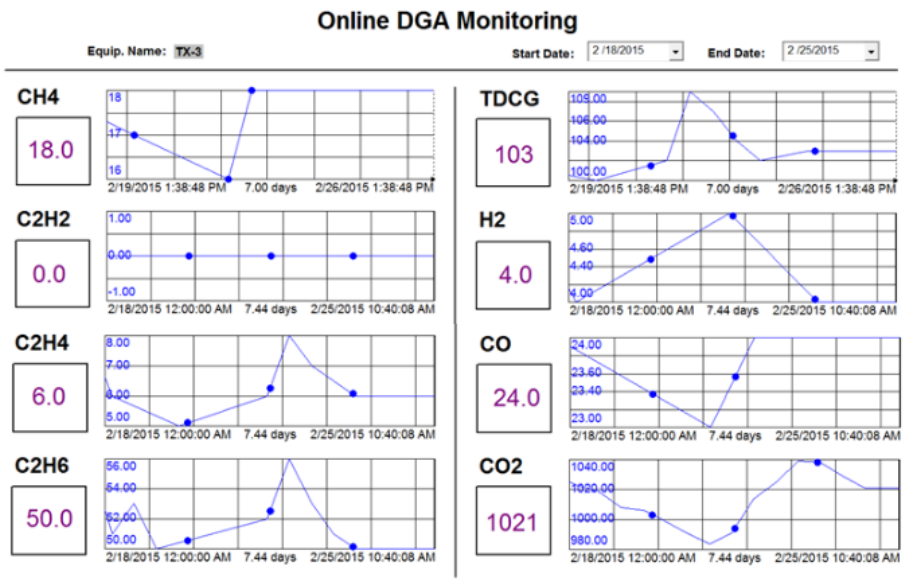

Figure 5–10 DGA visualization dashboard for transformer TX3

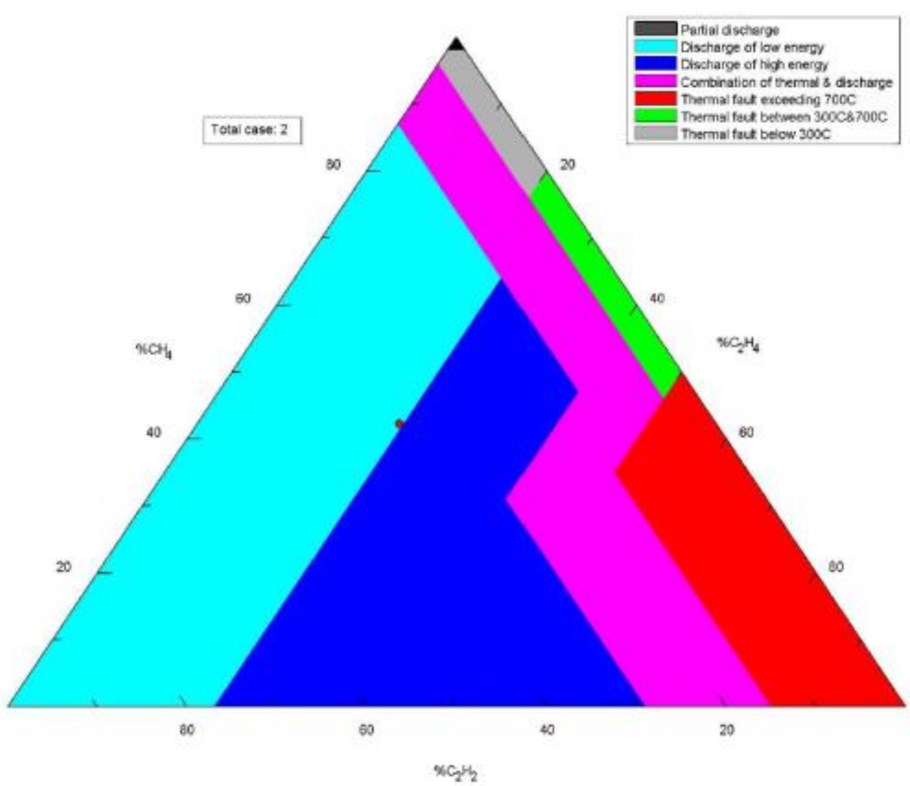

Figure 5–11 Dual triangle method

5.7.2 Data-Driven Approach to Interactive Visualizations

Data and information visualizations appear to be promising and attractive approaches for improving the business practices in the power industry. However, the legacy visualization tools using in power systems restrict users' experiences of visualizations since a limited number of pre-defined patterns and pictures are created by human designers. In order to improve user's experiences, a data-driven approach to interactive visualizations for data historian is proposed and implemented. The powerful data operation and manipulation algorithms are applied to create visualizations and avoid overwhelming duty of human maintains. The case studies present that the data-driven approach can obtain an interactive and data-rich visualization application that improves the understanding and insight of system operating conditions [72].

Traditionally, the visualization tools for power system monitoring, control and analysis are provided by EMS and other specific calculation applications. Thus, product venders provide visualization builders that allow engineers to design and maintain graphical displays that present the real-time information along with estimated data and analysis results to help system operators monitor power system operations. However, a great number of displays are quite intensive-labor to build. They are also difficult to integrate into the data historian since these legacy visualization tools are based on designer-driven methods.

1) Visualizations Based on CIM Model

In today's electric utilities, many applications and tools are designed for specific objectives and discrete business functions. Therefore, the outcome is the diversity of redundant and overlapping information across applications and tools. In order to collect and organize the model in an electric utility environment, a general-purpose model-exploration tool needs to develop with the CIM model, which is an open industry standard, to tackle information integration. To solve the issues of cross-system integration, the IEC has devoted tremendous effort to facilitate the interoperation among various applications and systems. The significant achievement is to publish the CIM standard which is can enhance and implement the information exchange and collaborations.

Since CIM describes all categories and components of a power system, it offers a standard semantic layer for developing a general-purpose model-exploration tool. Taking advantage of the native interoperability in the CIM standard, a visualization tool based on CIM model can be built out and it also can be seamlessly deployed into the current infrastructure of an electric utility. In the real practice, the model-exploration tool can centralize CIM data through consolidating the information from various data sources. Figure 5–12 presents the design of the visualization tool with data fed from various sources.

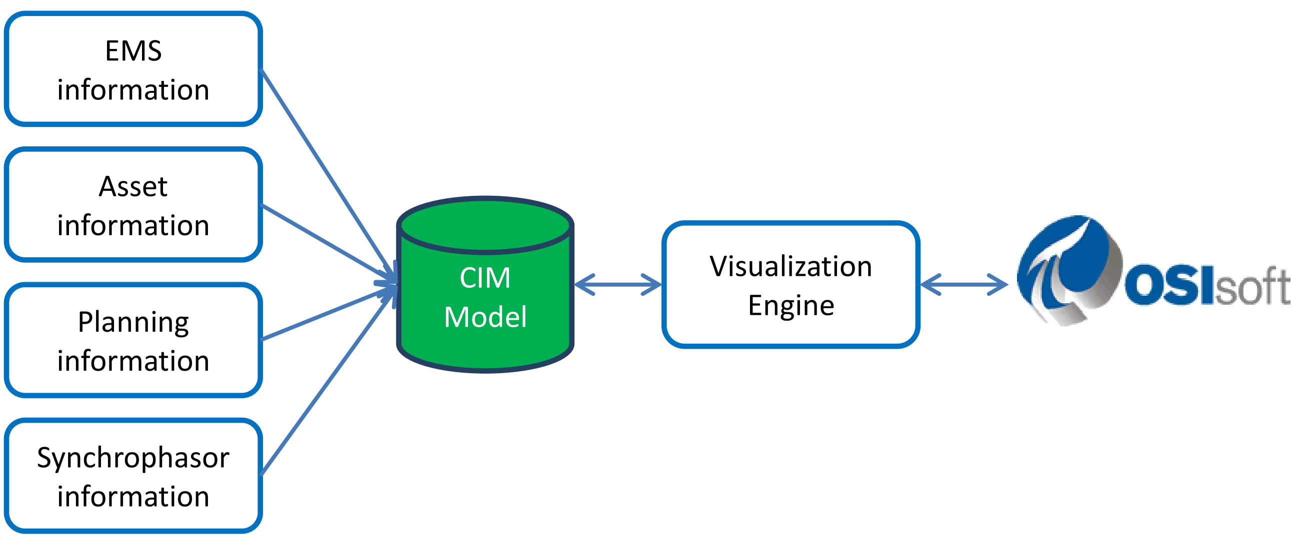

Figure 5–12 Visualization tool based on the CIM model

2) Auto-Generation of One-Line Diagrams

Auto-Generation of a one-line diagram is an attractive topic for electric utilities since this functionality does reduce the labor effort significantly. The objective of auto-generation in the model-exploration tool is to enable users to see accurate and clear one-line diagrams which exhibit the underlying relationship within data.

The implementation of the visualization tool involves presenting data and information through mapping data to graphical components and adapting the graphical elements to present the features of data from various systems. The critical operation for achieving this goal is to discover the mapping and tuning patterns between the data and the graphical components. As long as the discovering operation is completed, various types of one-line diagrams can be created to visualize the substation layout and the system operating condition. Figure 5–13 provides an example of the visualization based on the CIM model which collects and reorganizes the information from EMS. Meanwhile, a substation neighborhood diagram display can be obtained from the CIM model to reflect the topology in Figure 5–14. In Figure 5–14, the highlighted red circle is a selected substation and the display can show the topology connection around this substation intuitively. Theoretically, the entire implementation can be described as: transforming a CIM model to a graphical representation and laying out the auto-generation display to facilitate the interpretation. It can be accomplished through these detailed steps as follows.

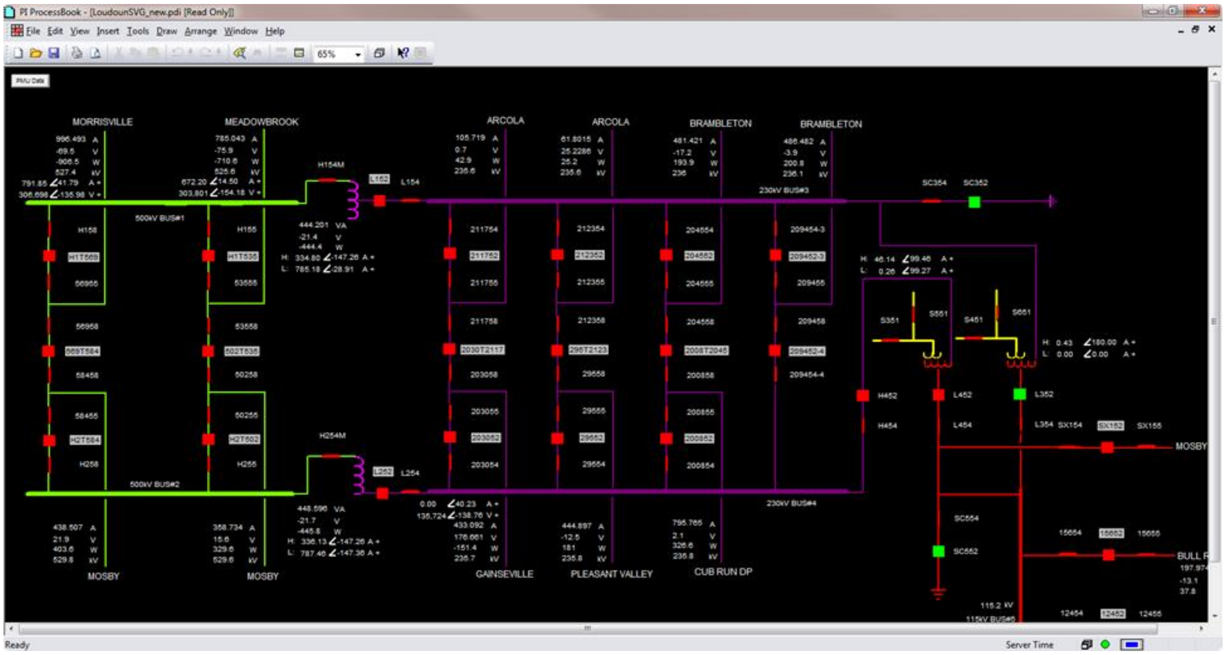

Figure 5–13 Substation layout from auto-generation of one-line diagram

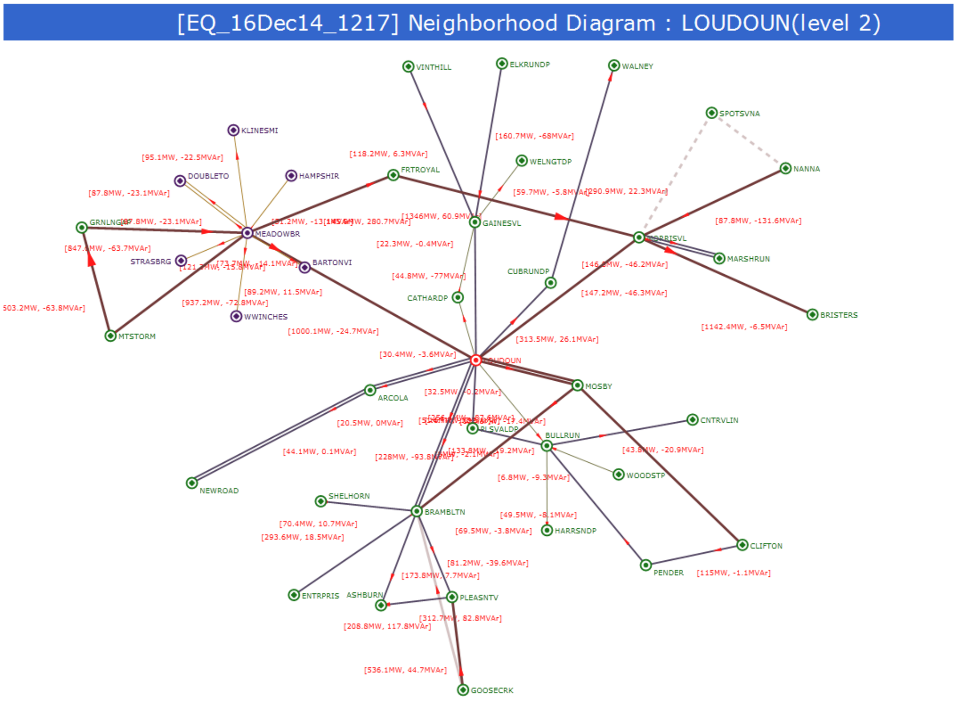

Figure 5–14 Neighborhood diagram

The first step is to convert the CIM model to the query-driven one-line visualization through pre-processing the CIM model. It can create model hierarchical trees and indices to support users to locate the information of interest. In electric utilities, the CIM model is always huge in size. Users expect to browse the data of interest with convenient approaches. Taking advantage of the CIM information which is organized into various hierarchies based on categories of equipment, it is possible to help users browse and explore the information easily. To provide the quick query response, the CIM information is stored into a binary tree based on the underlying relationship among the hierarchical tress. The implementation can guarantee the optimal user experience.

The second part for query-driven one-line visualization is to develop a query engine for retrieving the model information from the database. Based on the ID number or name, the model information can be exhibited and expanded. Meanwhile, it allows users to retrieve the information of the topology connection.

After preparing the CIM model, the challenging part for the auto-generation of one-line diagram is to implement the layout of the graphical elements which are interoperated from the CIM model. A substation one-line diagram can display hundreds of equipment and their connections within a substation. Therefore, it is literally impossible to develop a specific program to tackle all possible substation layout configurations. Through the study of the real substation layout configurations, the pattern identification is to use for interoperating the CIM model and the substation layout builder can lay out one-line diagrams with three steps. The first step is to discover the overall layout through data clustering calculation. It can filter out hierarchical “block” information which contains the backbone of the layout. Furthermore, based on the block information, the display builder can select the proper block layout from the pre-designed block designs to build the display automatically. Finally, the last step is to tune the layout and make it perfect.

If the layout can be obtained automatically, the display may be converted into the Scalable Vector Graphics (SVG) format which is a widely-used standard display format. Since the SVG format allows user to define and add customized features into the display, the real-time data from the PI system can be integrated into the display. Finally, the SVG display can be visualized into the web browser seamlessly since the SVG display is compatible with all web browsers.

5.7.3 Implementation of Key Performance Indicators

A Key Performance Indicator (KPI) is a measurable value that demonstrates how effectively a company is achieving key business objectives. Although various data from different data sources have been integrated into the PI system, they may not fully fulfill the business requirements. Therefore, the implementation of KPIs is critical and urgent to exhibit and monitor the most important data in real time from any web-enable device, regardless of the user's locations. Thus, Visual KPI, which a third-party software of the PI system, has been deployed in DVP.

Taking advantage of Visual KPI which has tight connection with the PI system through adapters, it can maximize the value of the data, improve decision-making and increase performance. With real-time, actionable data, users can get 24/7 insight into organizational and asset performance. In Figure 5–15 and Figure 5–16, they show the battery monitoring in a substation.

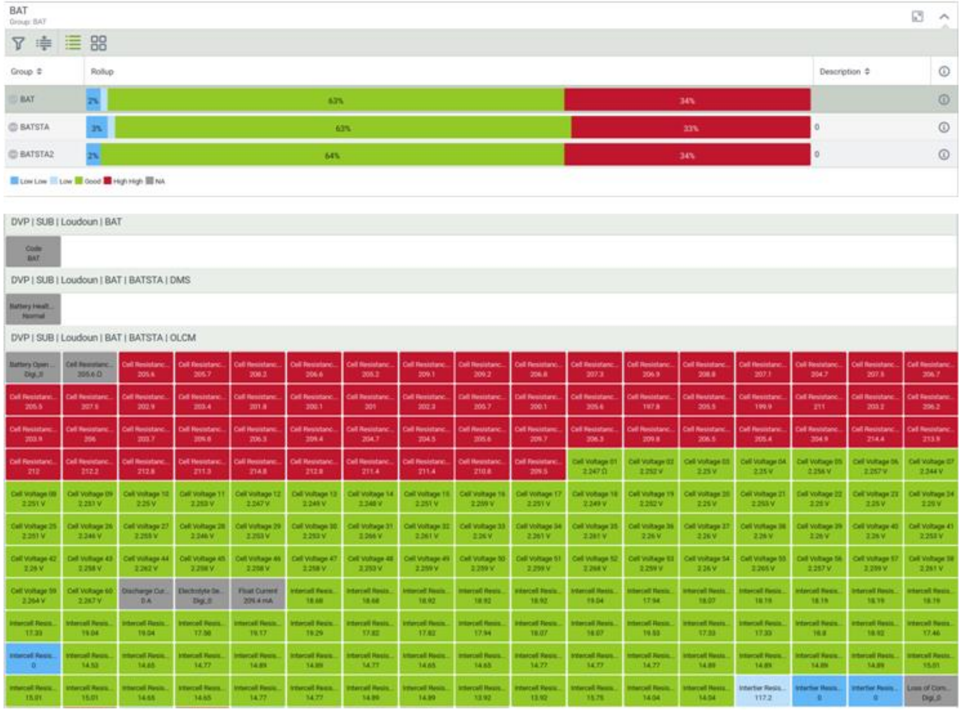

Figure 5–15 Overall battery monitoring

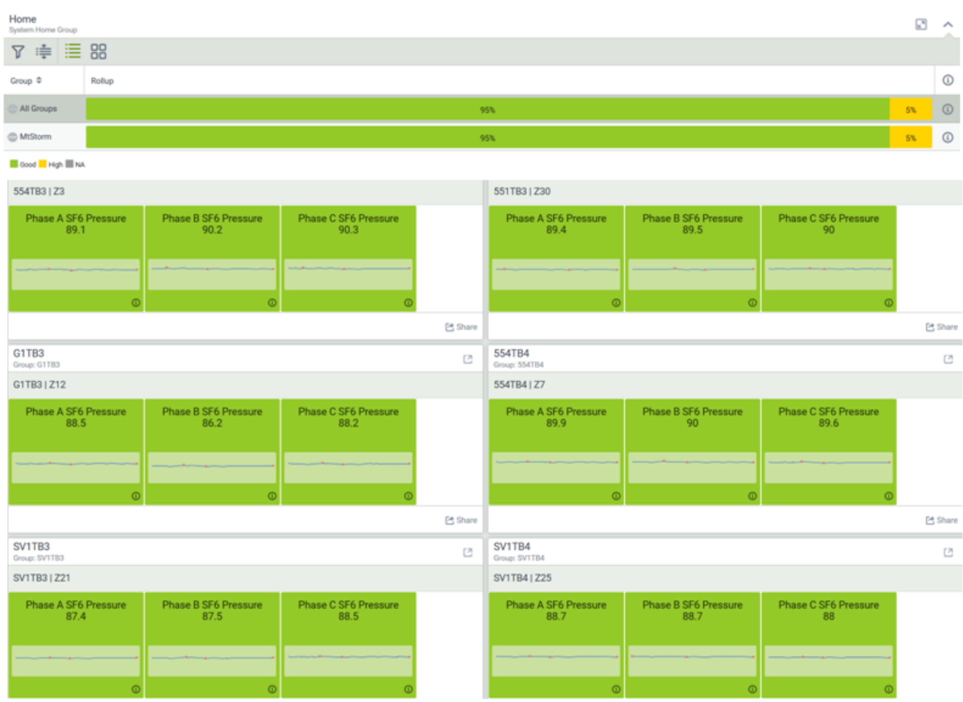

Figure 5–16 Battery monitoring of cells

With the popular using of mobile applications in smart phones, Visual KPI can be deployed through the web service of the PI system. Since most displays can be created and viewed on HTML5, users can see Visual KPI displays through cell phones or tablets they use.

5.8 Conclusion

Through the ongoing project in DVP, this chapter presents the entire solution for integrating, managing and analyzing big data in the power industry. The ultimate target is to build a highly reliable and flexible common data platform with the features of scalability, real time, high reliability and security within the enterprise. It is hopeful that DVP will see improvements in its business intelligence, asset management capabilities, and all-around usability of its data. It is hoped that users are presented with a system that allows them to conveniently build custom applications and dashboards with few barriers. Furthermore, this chapter may provide a good instance for peers who intend to enhance the capability of managing and utilizing big data to improve business intelligence.

CHAPTER 6 IDENTIFICATION OF TRANSMISSION-LINE PARAMETERS CONSIDERING TEMPERATURE IMPACT USING REAL-TIME DATA

6.1 Introduction

Accurate transmission-line parameters are of vital importance for various operation, planning and protection applications in power systems [73], [74]. The transmission-line parameters in today's power systems still depend on the calculation from the circuit model through conductor dimension, tower geometry, line length and other factors. However, transmission-line parameters can be affected by various factors like environment factors, modeling inaccuracies and even human errors. Moreover, once the values of the power system network parameters like resistance, shun admittance and reactance are determined by electrical utilities, these values may not be updated unless the physical devices would be updated. In power systems, transmission-line parameters are not constant, the actual parameters would be dynamic since the ambient temperature, mutual coupling and soil resistivity may have underlying relationship with these values [75]. According to reports for transmission-line parameters, the errors between calculated and actual values of transmission-line parameters may reach up to 30%. Unfortunately, it is impossible to detect and know the change of parameters since the inherent disadvantage of circuit models is that models cannot be updated promptly. In addition, the existing approach for measuring transmission-line parameters is to conduct the field test but it may cause the scheduled outage. Therefore, although electrical utilities have already realized the importance of re-calibrating transmission-line parameters, they do not have applicable approaches to implement.

To exhibit the variance of transmission-line parameters and derive reliable values which are close to the actual parameters, extensive research has proposed various measurement-driven approaches to estimate transmission-line parameters. In [76], [77], several approaches using linear and nonlinear equations with phasor measurements are proposed. Authors in [78] provide a method regarding online tracking of transmission-line parameters using SCADA data of the control center to computer values of transmission-line parameters. However, very few studies refer to the identification of transmission-line parameters considering temperature impact using actual real-time data. In fact, it is critical to demonstrate the impact of ambient temperature on the variance of transmission-line resistance since it correlates with the dynamic rating of transmission lines.

The remaining content of this chapter is organized as follows. The second part demonstrates the methodology of the identification of transmission-line parameters. In the third part, the methodology is validated by case studies with real synchrophasor data. The last part concludes this chapter.

6.2 Identification Methodology

6.2.1 Data-Driven Approach for Parameter Identification

A three-phase π model for a general transmission line is shown in Figure 6–1, where $V_{S(abc)}$, $V_{R(abc)}$, $I_{S(abc)}$, $I_{R(abc)}$ represent the three-phase voltage and current phasor vectors at both ends of the line while $Z_{(abc)}$ and $B_{(abc)}$ are the series impedance matrix and shunt admittance matrix. Based on the nodal analysis, the following equations can be written:

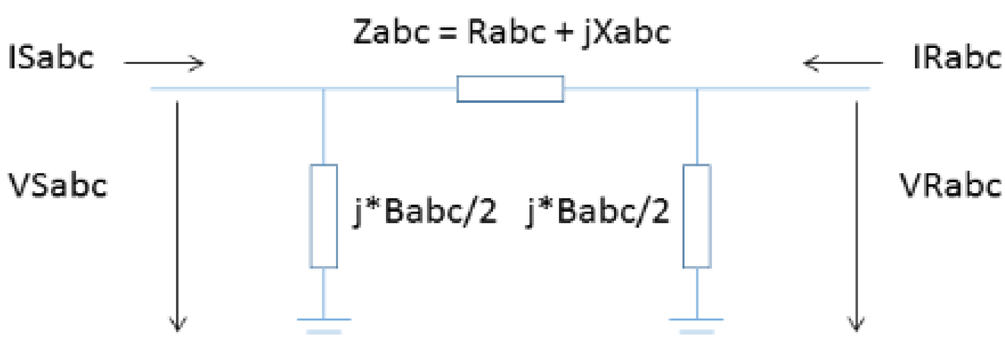

Figure 6–1 Transmission-line π model

$$\boldsymbol{V}_{\boldsymbol{S}(\boldsymbol{abc})} - \boldsymbol{V}_{\boldsymbol{R}(\boldsymbol{abc})} = (\boldsymbol{I}_{\boldsymbol{S}(\boldsymbol{abc})} - \boldsymbol{V}_{\boldsymbol{S}(\boldsymbol{abc})} * \frac{j}{2}\boldsymbol{B}_{(\boldsymbol{abc})}) * \boldsymbol{Z}_{(\boldsymbol{abc})} \tag{6–1}$$

$$\boldsymbol{I}_{\boldsymbol{S}(\boldsymbol{abc})} + \boldsymbol{I}_{\boldsymbol{R}(\boldsymbol{abc})} = \boldsymbol{V}_{\boldsymbol{S}(\boldsymbol{abc})} * \frac{j}{2}\boldsymbol{B}_{(\boldsymbol{abc})} + \boldsymbol{V}_{\boldsymbol{R}(\boldsymbol{abc})} * \frac{j}{2}\boldsymbol{B}_{(\boldsymbol{abc})} \tag{6–2}$$

For a transmission line, both impedance matrix $Z_{(abc)}$ and $B_{(abc)}$ are symmetrical. Equation (6–1) can be re-organized as:

$$\boldsymbol{V_{S(abc)}} - \boldsymbol{V_{R(abc)}} = \boldsymbol{I_{S(abc)}} * \boldsymbol{Z_{(abc)}} - \boldsymbol{V_{S(abc)}} * \frac{\boldsymbol{j}}{\boldsymbol{2}}\boldsymbol{B_{(abc)}} * \boldsymbol{Z_{(abc)}} \tag{6–3}$$

where define $B_{(abc)} * Z_{(abc)}$ as $P_{(abc)}$ which is complex

$$\boldsymbol{P_{(abc)}} = \boldsymbol{B_{(abc)}} * \boldsymbol{Z_{(abc)}} \tag{6–4}$$

Therefore, (6–3) can be written as:

$$\boldsymbol{V_{S(abc)}} - \boldsymbol{V_{R(abc)}} = \boldsymbol{I_{S(abc)}} * \boldsymbol{Z_{(abc)}} - \boldsymbol{V_{S(abc)}} * \frac{\boldsymbol{j}}{\boldsymbol{2}}\boldsymbol{P_{(abc)}} \tag{6–5}$$

Thus, (6–5) and (6–2) can be written as:

$$\begin{bmatrix} \Delta \boldsymbol{V_a} \\ \Delta \boldsymbol{V_b} \\ \Delta \boldsymbol{V_c} \end{bmatrix} = \begin{bmatrix} \boldsymbol{Z_a} & \boldsymbol{Z_{ab}} & \boldsymbol{Z_{ac}} \\ \boldsymbol{Z_{ab}} & \boldsymbol{Z_b} & \boldsymbol{Z_{bc}} \\ \boldsymbol{Z_{ac}} & \boldsymbol{Z_{bc}} & \boldsymbol{Z_c} \end{bmatrix} \begin{bmatrix} \boldsymbol{I_{S(a)}} \\ \boldsymbol{I_{S(b)}} \\ \boldsymbol{I_{S(c)}} \end{bmatrix} - \frac{\boldsymbol{j}}{\boldsymbol{2}} \begin{bmatrix} \boldsymbol{P_a} & \boldsymbol{P_{ab}} & \boldsymbol{P_{ac}} \\ \boldsymbol{P_{ab}} & \boldsymbol{P_b} & \boldsymbol{P_{bc}} \\ \boldsymbol{P_{ac}} & \boldsymbol{P_{bc}} & \boldsymbol{P_c} \end{bmatrix} \begin{bmatrix} \boldsymbol{V_{S(a)}} \\ \boldsymbol{V_{S(b)}} \\ \boldsymbol{V_{S(c)}} \end{bmatrix} \tag{6–6}$$

$$\begin{bmatrix} \Sigma \boldsymbol{I_a} \\ \Sigma \boldsymbol{I_b} \\ \Sigma \boldsymbol{I_c} \end{bmatrix} = \frac{\boldsymbol{j}}{\boldsymbol{2}} \begin{bmatrix} \boldsymbol{B_a} & \boldsymbol{B_{ab}} & \boldsymbol{B_{ac}} \\ \boldsymbol{B_{ab}} & \boldsymbol{B_b} & \boldsymbol{B_{bc}} \\ \boldsymbol{B_{ac}} & \boldsymbol{B_{bc}} & \boldsymbol{B_c} \end{bmatrix} \begin{bmatrix} \Sigma \boldsymbol{V_a} \\ \Sigma \boldsymbol{V_b} \\ \Sigma \boldsymbol{V_c} \end{bmatrix} \tag{6–7}$$

where $\Delta V_x = V^S - V^R$, $\sum I_x = I^S + I^R$, $\sum V_x = V^S + V^R$ and $x = a, b\ or\ c.$

Meanwhile, $P_x = S_x + j * T_x$. Thus, based on the definitions above, the equation can be derived as follows:

$$\boldsymbol{Z} = \boldsymbol{H} \cdot \boldsymbol{\beta} \tag{6–8}$$

where H is a matrix formulated from equations above and contains measurements while the measurement vector Z contains PMU voltage and current measurements. If (6–8) is solved, the transmission-line parameters may be derived.

6.2.2 Bad Data Detection

The classical method based on statistics is used for bad data detection after solving the constrained least-squares. Bad data identification is achieved by checking the normalized residuals of each measurement, which proceeds as follows:

Step 1: Solve the curve-fitting problem described in and obtain the residual for each measurement point:

$$\boldsymbol{r^i = z^i - H^i \beta}, \qquad \boldsymbol{i = 1, 2, \cdots, N} \tag{6–9}$$

Step 2: Compute the normalized residual as:

$$(\boldsymbol{r^i})^{\boldsymbol{norm}} = \frac{\boldsymbol{r_i}}{\sqrt{\boldsymbol{\Omega_{ii}}}}, \quad \boldsymbol{i = 1, 2, \cdots, N} \tag{6–10}$$

where Ω_{ii} is the diagonal element of the matrix Ω,

$$\boldsymbol{\Omega = H(H^T H)^{-1} H^T} \tag{6–11}$$

Step 3: Find the largest normalized residual $(r^i)^{norm}$ and check whether it is larger than a prescribed identification threshold c, c can be 3.0:

$$(\boldsymbol{r}^{\boldsymbol{i}})^{\boldsymbol{norm}} > \boldsymbol{c} \tag{6–12}$$

Step 4: If (6–12) does not hold, then no bad data will be suspected; otherwise, the data sample corresponding to the largest normalized residual is the bad data and should be removed from the data set.

Step 5: If bad data is detected and removed from the data set, the algorithm flow must return to Step 1 and the process above must be repeated. Otherwise, this process ends and solutions are found.

6.3 Case Study

The proposed approach can obtain very accurate transmission-line parameters through measurements. Furthermore, this study demonstrates the possibility to leverage the various existing information stored in the PI system to develop innovative applications through data mining technologies.

6.3.1 Identification Results

The identification of transmission-line parameters has been implemented to a 500kV transmission line in DVP system. The result during a one-day period is shown below in Figure 6–2, Figure 6–3 and Figure 6–4. The identification can obtain the more accuracy parameters than the current parameters in PSS®E and EMS after verifying the calculation results in EMS state estimation.

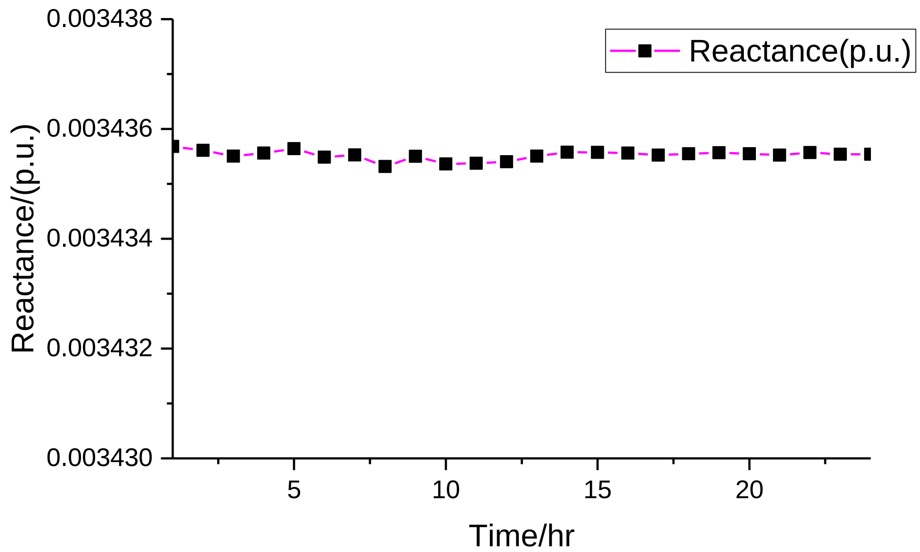

Figure 6–2 Identification results of the transmission-line reactance within 24hrs

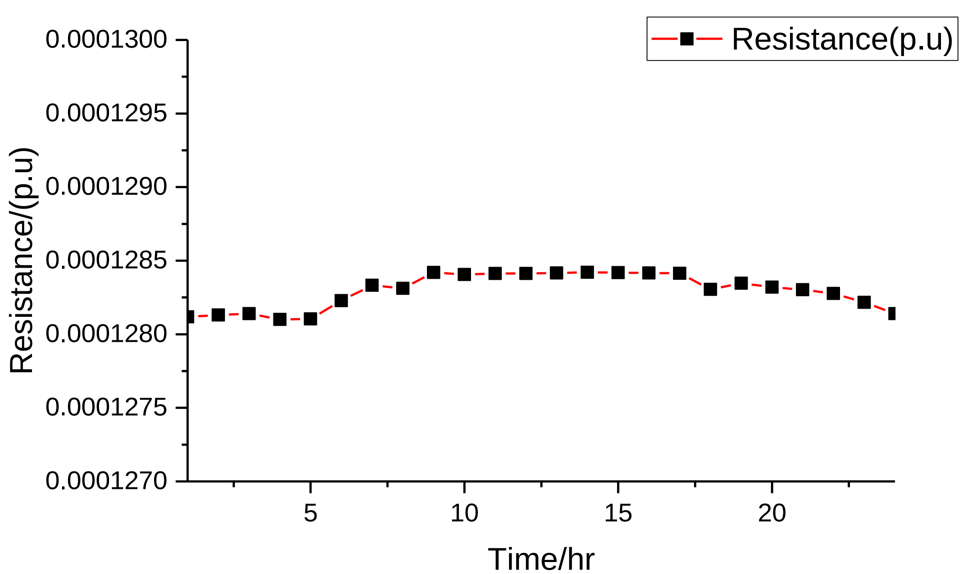

Figure 6–3 Identification results of the transmission-line resistance within 24hrs

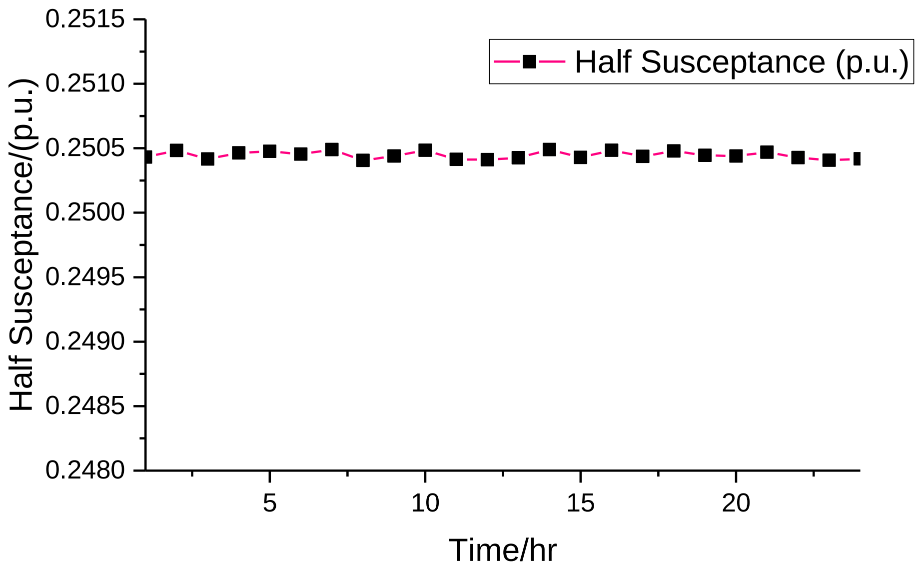

Figure 6–4 Identification results of the transmission-line susceptance within 24hrs

6.3.2 Comparison with Current Parameters

In practice, transmission-line parameters using in power system calculation tools and EMS are derived from the empirical parameters. Thus, it is possible that the EMS's line impedance values are significantly wrong. The identified parameters can be compared with the current parameters to verify the accuracy of transmission-line parameters using in EMS and other calculation software.

The approach for the parameter validation is to re-calculate state estimation base on Savecases in EMS to compare the results with current parameters and the results with identification parameters. From Figure 6–5 to Figure 6–16, they demonstrate that EMS state estimation results of 500kV LIN596 from current parameters and identified parameters in three separate days which are Jan 19, 2016, Mar 12, 2016 and May 26, 2016, respectively.

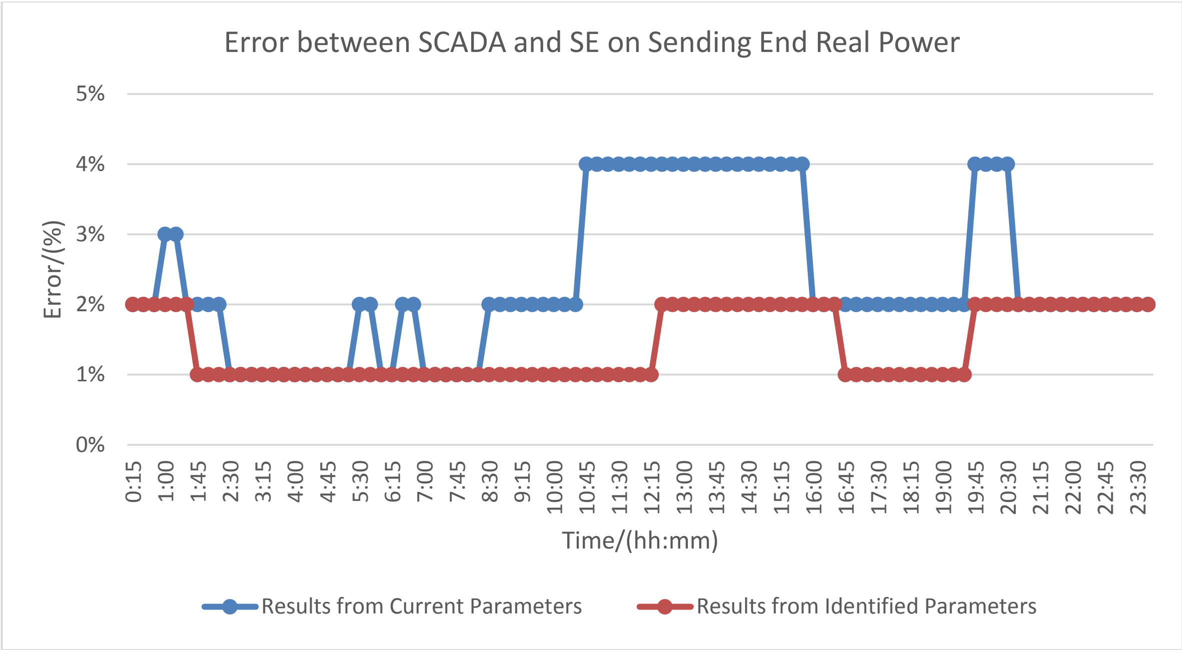

Figure 6–5 Comparison of real power of sending end on Jan. 19, 2016

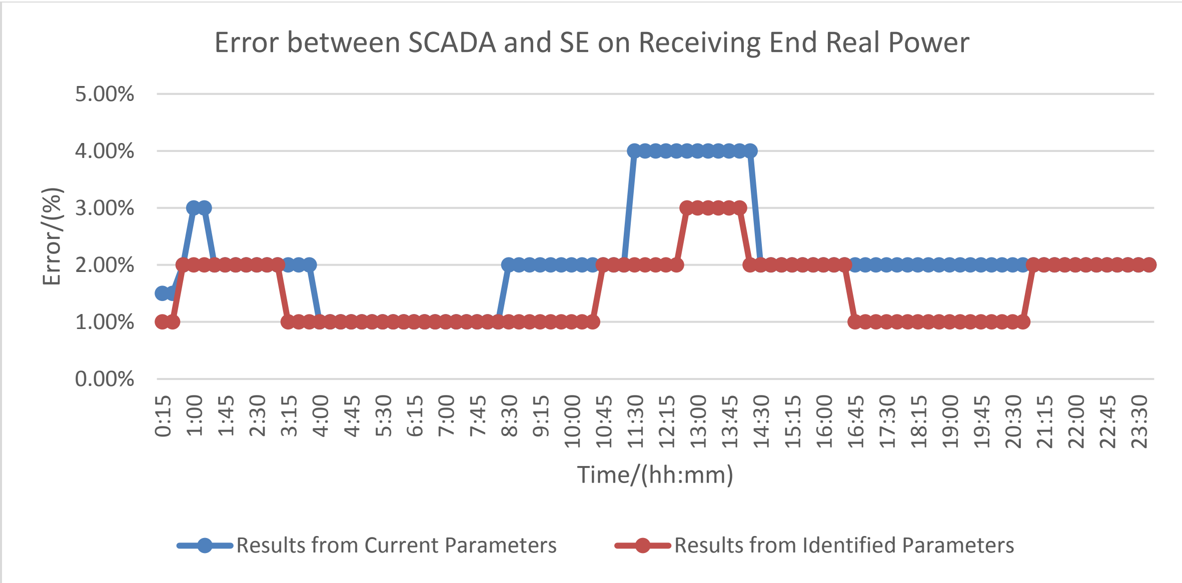

Figure 6–6 Comparison of real power of receiving end on Jan. 19, 2016

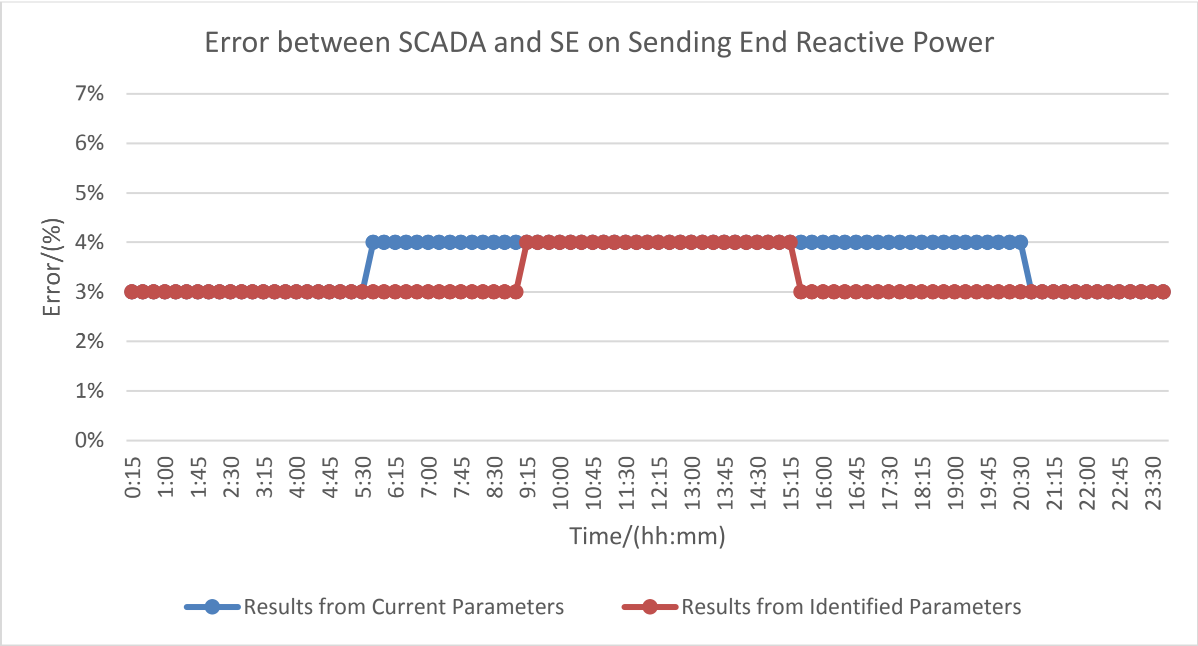

Figure 6–7 Comparison of reactive power of sending end on Jan. 19, 2016

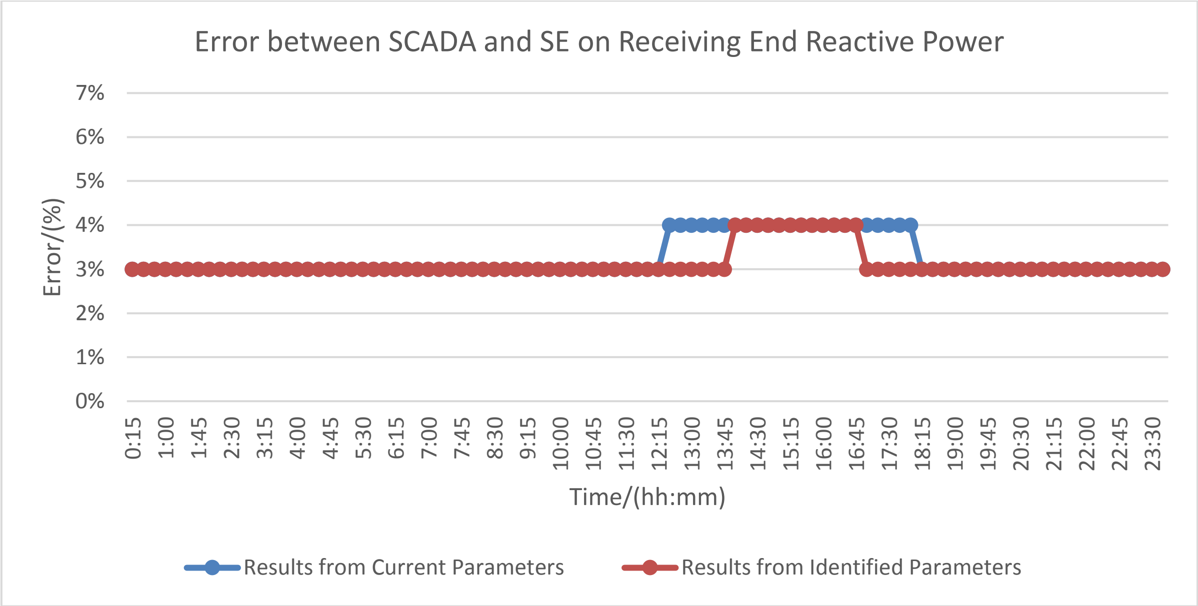

Figure 6–8 Comparison of reactive power of receiving end on Jan. 19, 2016

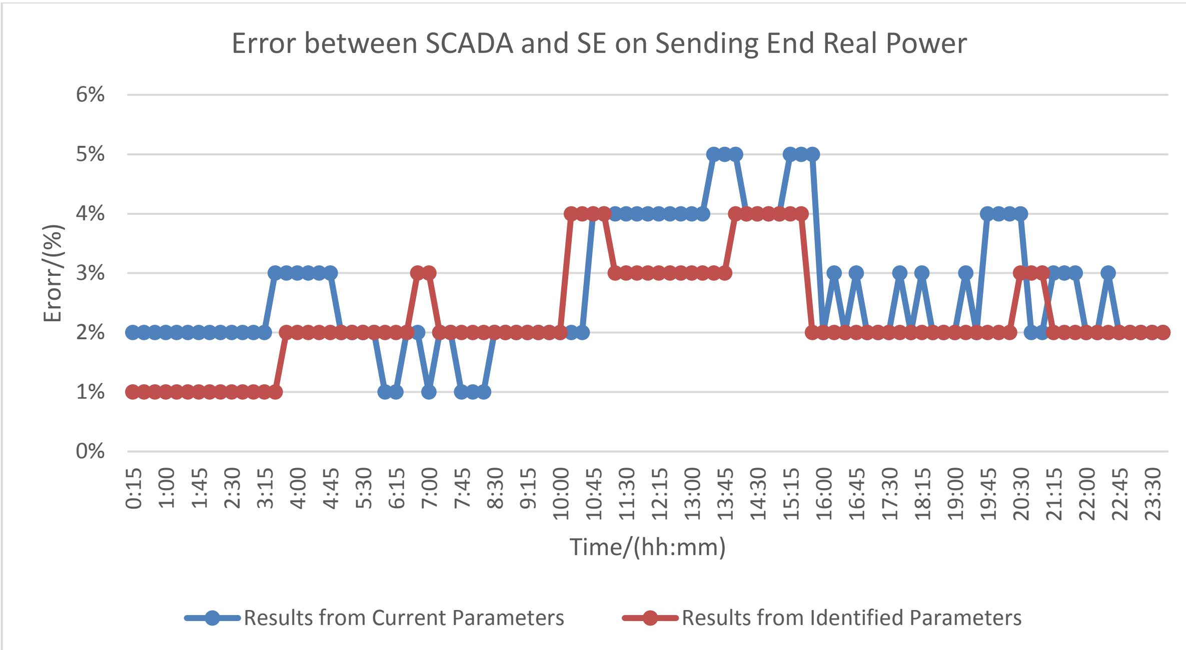

Figure 6–9 Comparison of real power of sending end on Mar. 12, 2016

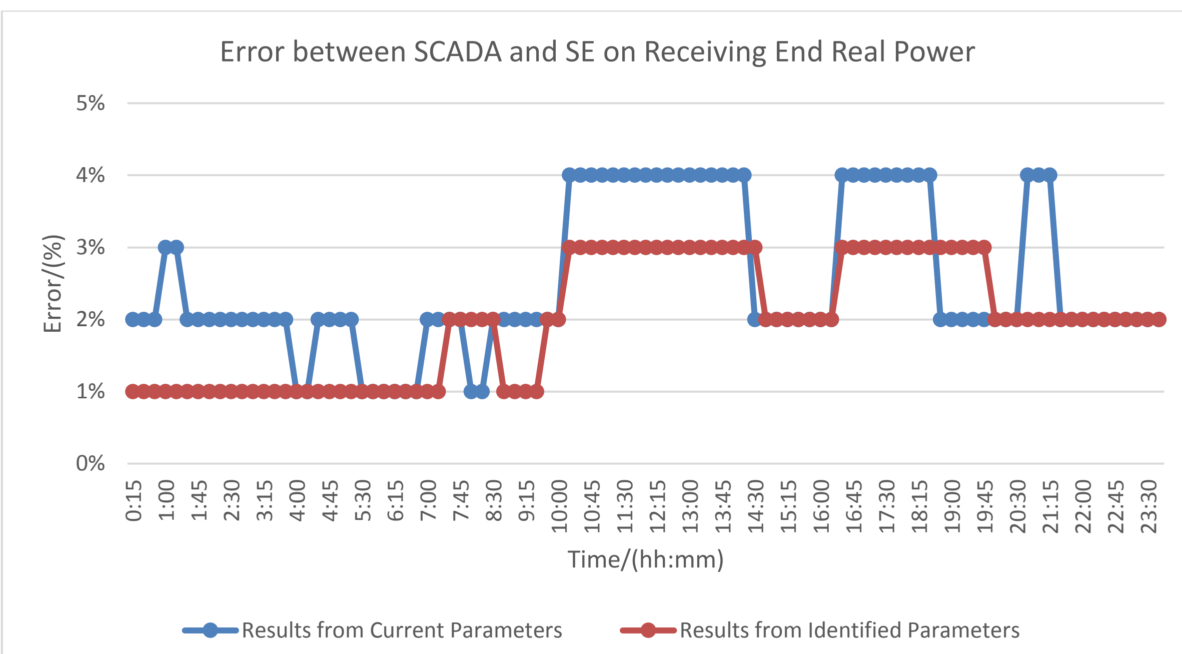

Figure 6–10 Comparison of real power of receiving end on Mar. 12, 2016

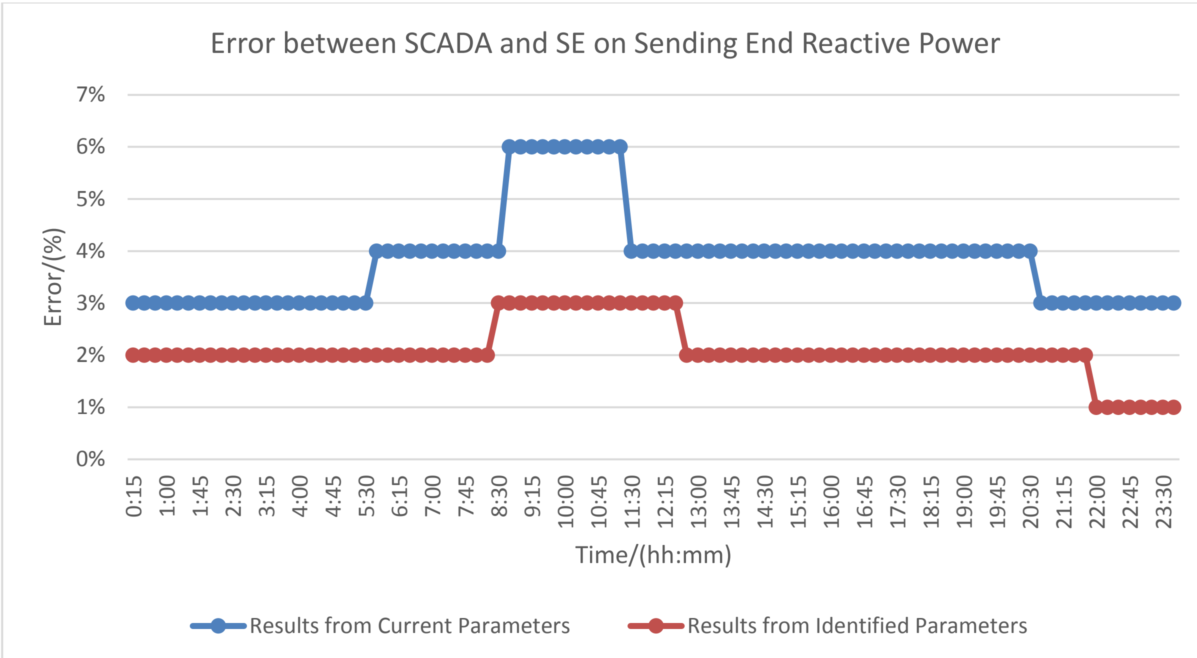

Figure 6–11 Comparison of reactive power of sending end on Mar. 12, 2016

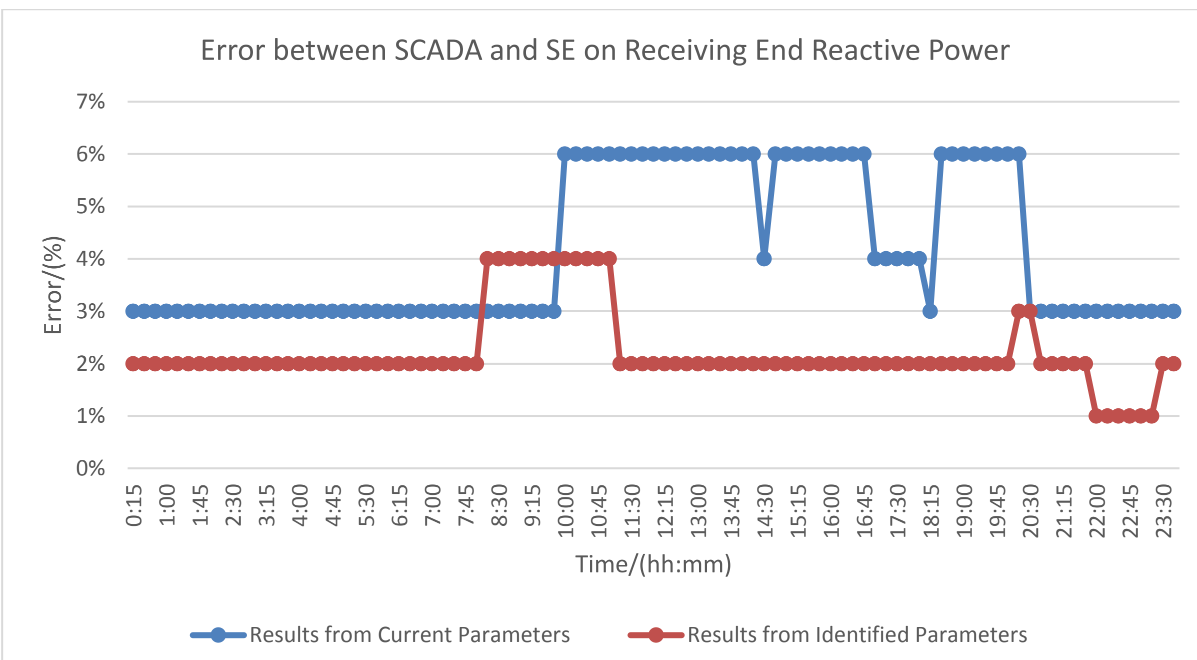

Figure 6–12 Comparison of reactive power of receiving end on Mar. 12, 2016

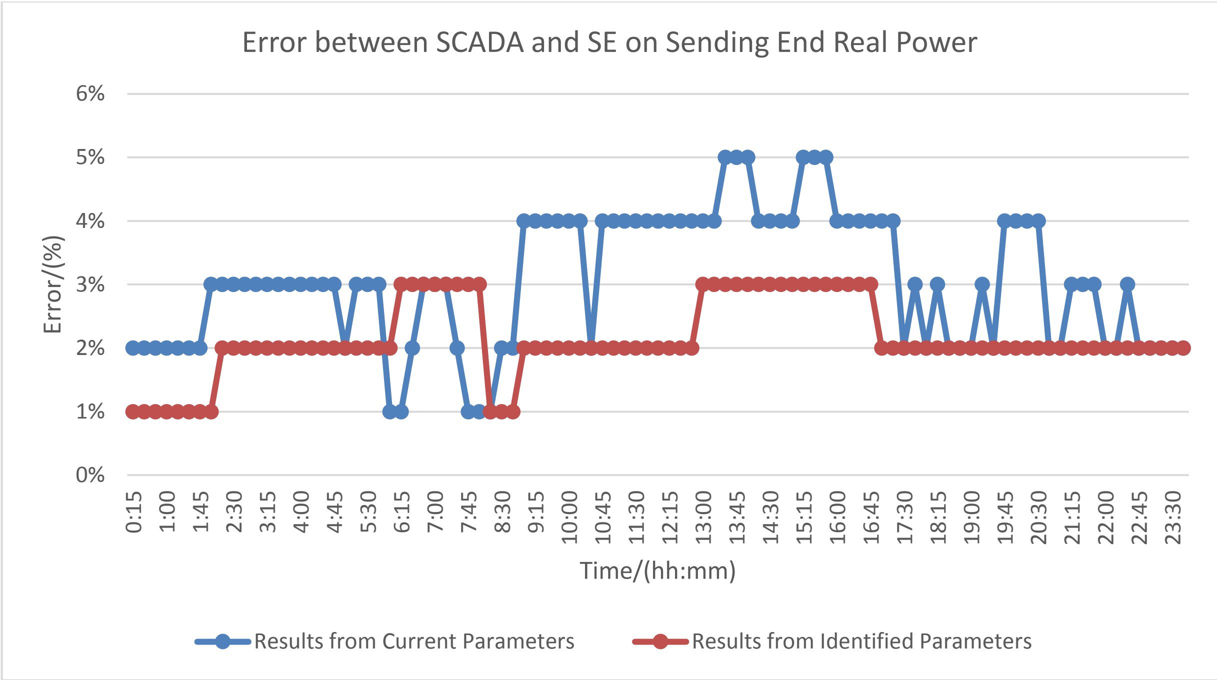

Figure 6–13 Comparison of real power of sending end on May. 26, 2016

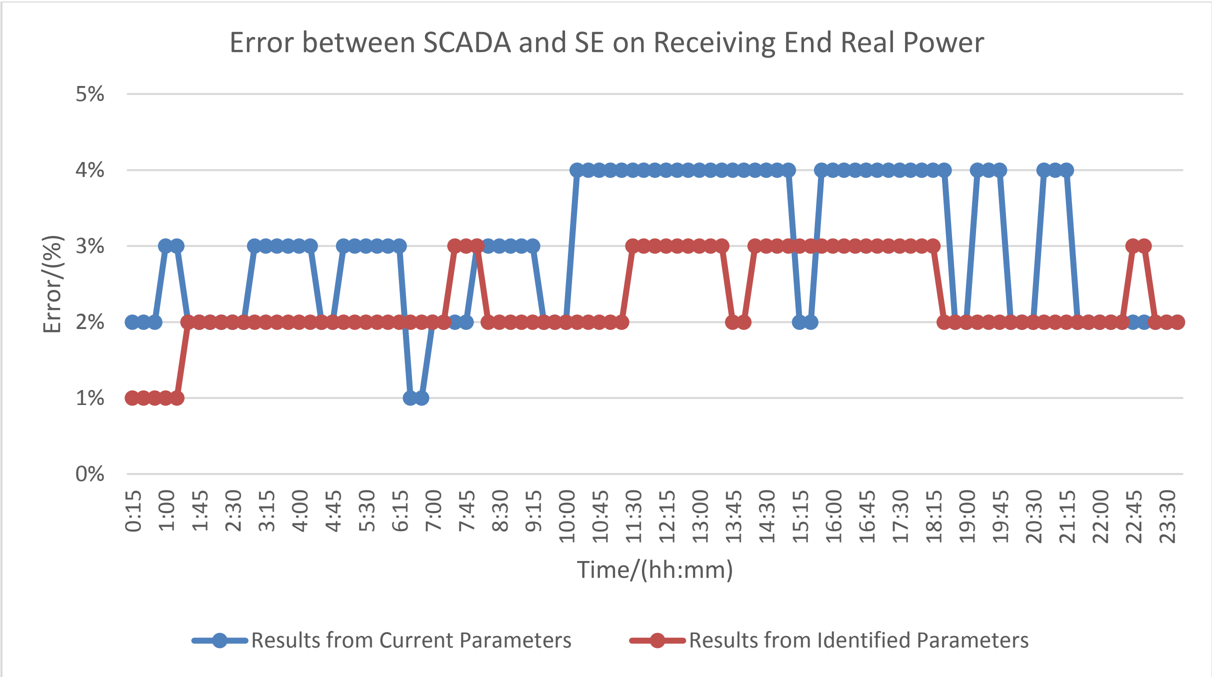

Figure 6–14 Comparison of real power of receiving end on May. 26, 2016

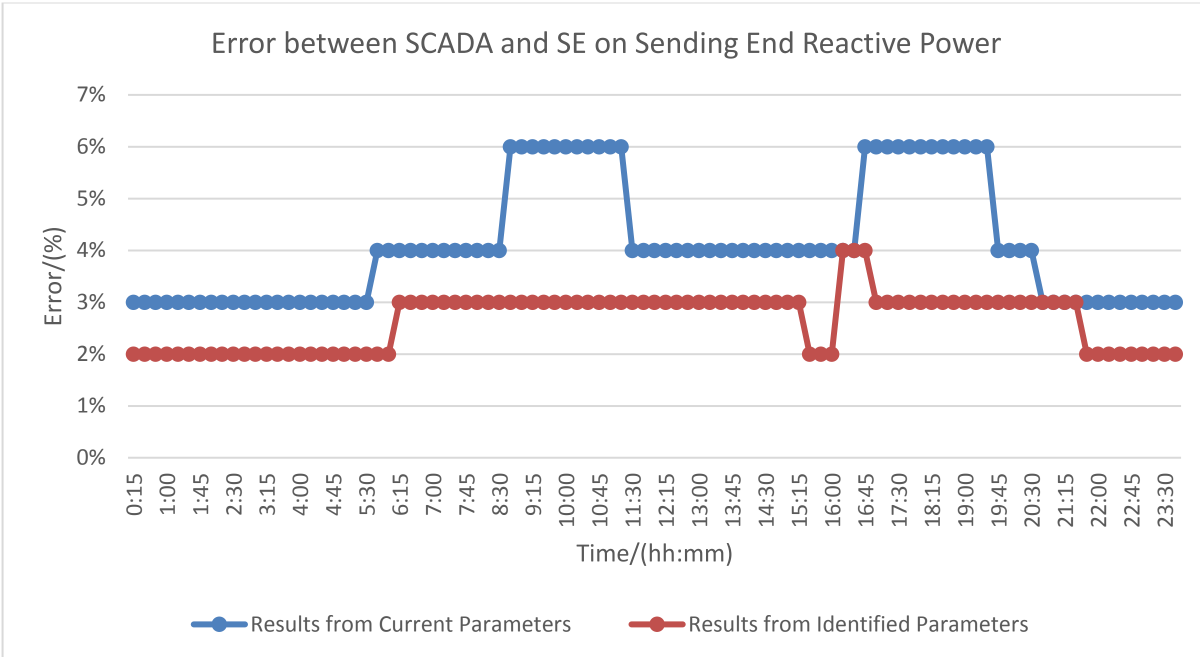

Figure 6–15 Comparison of reactive power of sending end on May. 26, 2016

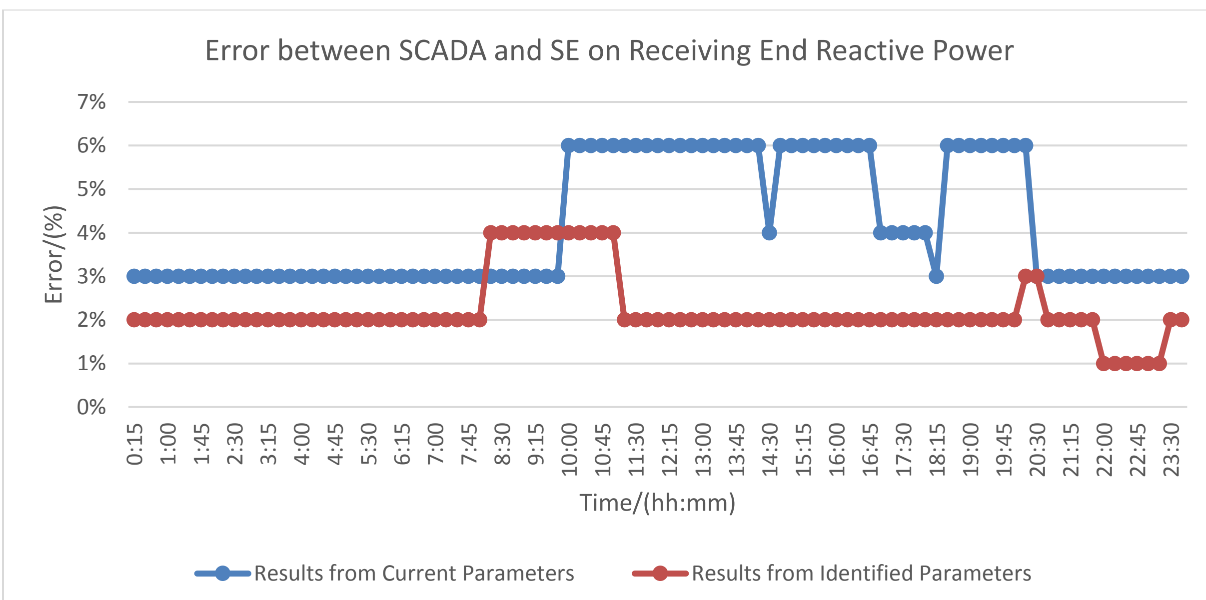

Figure 6–16 Comparison of reactive power of receiving end on May. 26, 2016

In figures, the blue lines with dots represent the state estimation from current parameters and the red lines with dots represent the state estimation from identified parameters. The susceptible data threshold of real power and reactive power in EMS state estimation configuration is 5%. That means that the data with error greater than 5% would be treated as bad data.

The entire comparison may be triggered in every 5 minutes in one day so that total 96 calculation results would be included in the comparison. The comparison results exhibit that the identified parameters can improve the accuracy of EMS state estimation significantly. Since the EMS state estimation would not exceed the susceptible threshold all the time, it is not easy for EMS engineers to detect and target the slight inaccuracy of transmission-line parameters before. Therefore, the proposed method may be very helpful for daily maintenance in control centers of power systems.

6.3.3 Impact of Ambient Temperature on Parameters

To observe the impact of ambient temperature on transmission-line resistance, the data from three days are used for parameters identification. Since the PI system in DVP stores the temperature information, the study of transmission-line parameters identification can utilize the temperature data in the PI system to observe and analyze the impact of the temperature on the transmission-line resistance in Figure 6–17, Figure 6–18 and Figure 6–19. From results of the identification of transmission-line parameters, the impact of temperature changes can be observed by the change of transmission-line resistance. Initially, the transmission-line resistance may be changed with the temperature variation. In addition, the significant variation of ambient temperature may cause the obvious change of the resistance. Likewise, the slight change of the resistance may be associated with the insignificant change of ambient temperature.

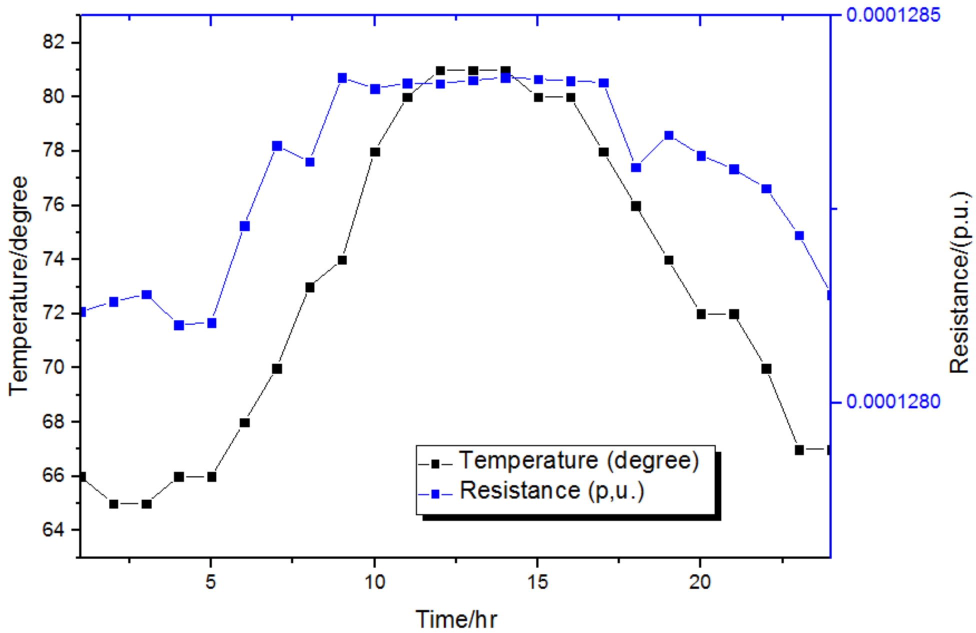

Figure 6–17 Impact of the temperature on resistance on May 26, 2016

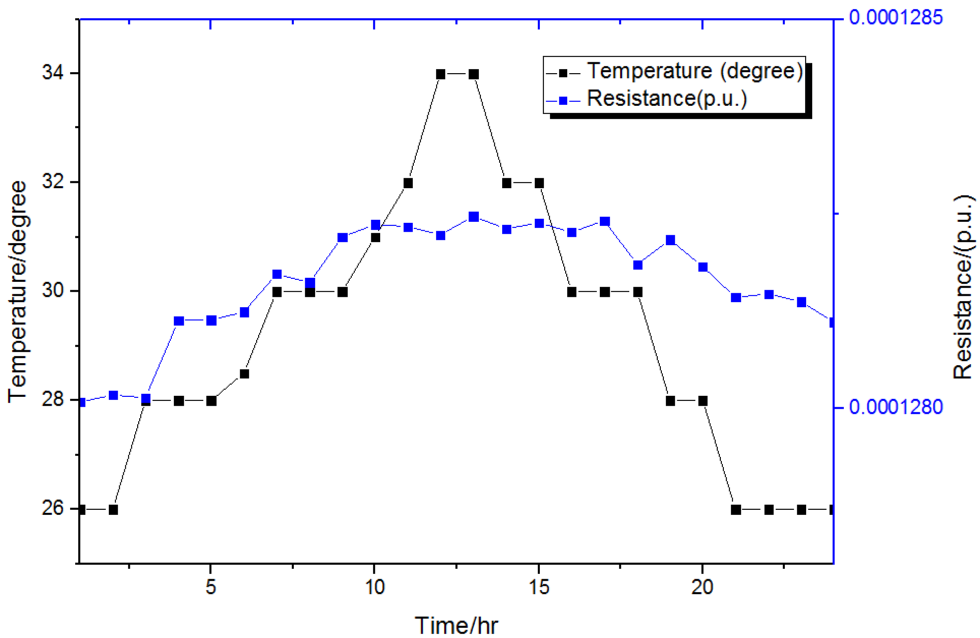

Figure 6–18 Impact of the temperature on resistance on Jan 19, 2016

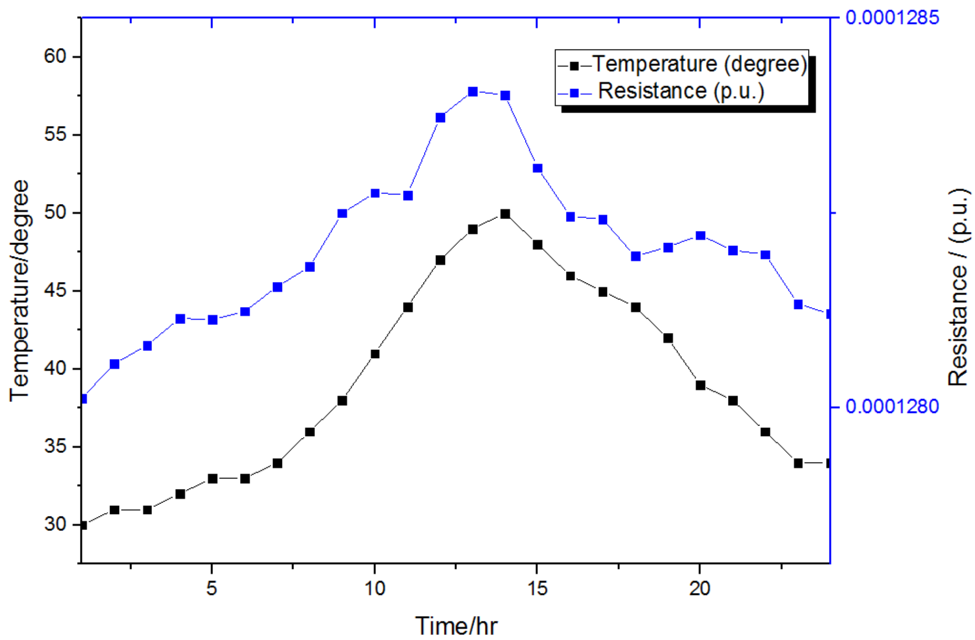

Figure 6–19 Impact of the temperature on resistance on Mar 12, 2016

6.4 Conclusion

Synchrophasor data have the potential to improve the accuracy of transmission-line parameters in the EMS database. More accurate parameter means to obtain more accurate power system models, target more accurate fault locations in the small timeframe as well as achieve more economic system operations. The following challenges may be noticed and lessons may be learnt during this development: 1) it was identified that although PMU are generally more accurate devices, measurement errors may come from the instrumentation channel due to various causes; 2) it is critical to identify the credibility of the calculated transmission-line impedance parameters for system operators in order to make the calculation useful; 3) the research utilizes the PI system with ambient temperature data so that the impact of ambient temperature on the variance of transmission-line resistance can be observed obviously; 4) a novel method is proposed to calculate the positive-sequence transmission-line impedance, and this approach can be extended to calculate the other sequence impedance as well.

CHAPTER 7 CONCLUSIONS AND FUTURE WORKS

7.1 Conclusions

This dissertation covered a wide variety of research topics about synchrophasor measurement and its applications, including the system dynamic response estimation, the measurement-driven model for adaptive wide-area damping controllers, the performance comparison of measurement-driven models as well as the development of DVP data historian and the identification of transmission-line parameters using DVP data historian.

At the very beginning, this dissertation provided the brief comparison between measurement-driven models and circuit-based models in power systems. Moreover, this dissertation also gave an introduction regarding measurement-driven approaches.

Secondly, taking advantage of wide-area real-time synchrophasor data collected by FDRs, this dissertation provided detailed information and methodology to implement the system dynamic response estimation by the ARX model. The approach has been verified by ring-down data and ambient data, respectively. Meanwhile, the ARX model can also update online promptly and avoid drawbacks of conventional circuit-based models. As the core functionality of early warning of impending instability, the accuracy index from the system dynamic response estimation can provide a good indicator for researchers and operators to monitor the operating condition of the entire system.

Thirdly, this dissertation proposed a transfer function model for designing adaptive wide-area damping controllers using wide-area synchrophasor data. In this work, based on a linear MIMO ARMAX model, a concept of developing the transfer function model for oscillation damping control was proposed and its overall performance was examined by various tests. Case studies also demonstrated that this method is effective to capture the dominant inter-area oscillation modes through estimating the transfer function of the system model. The wide-area adaptive damping controller may be designed by the transfer function.

After that, to compare the performance among different MIMO identification algorithms, this dissertation exhibited differences among algorithms in terms of the consumption time, order and accuracy. Based on the comparison results, the MIMO ARMAX model can derive the accurate low-order model with the rapid calculation speed.

This dissertation also discussed the ongoing DVP data historian project. Since the data mining and data analytics are critical for electric utilities and the ubiquitous challenges on data integration impede the implementation of advanced applications, the PI system provides a promising solution to reorganize the data stream, integrate the data at various resolutions and provide handy tools and services to end users. The implementation of data historian project enhances the business intelligence and leverages data-driven applications.

Taking advantage of abundant data in DVP data historian, the identification of transmission-line parameters can be implemented. Based on synchrophasor data from two ends of a transmission line, transmission-line parameters can be estimated by the data-driven model with LS algorithm. Compared to current parameters in EMS, the identified parameters through real measurement data are much more accurate. Meanwhile, based on the ambient temperature of the transmission line collected by the PI system, the impact of the temperature on transmission-line resistance can be observed.

7.2 Future Works

This dissertation explored some research topics around synchrophasor and its application. Though very promising results have been presented in this dissertation, a lot of interesting future work can be done in the future.

For the system dynamic response estimation by the ARX model, the methodology can be extended to estimate the load model. The load model which is derived from the measurement-based method would improve the accuracy of load modeling in circuit-based models.

In addition, based on the transfer function model created by the MIMO ARMAX model, the adaptive wide-area damping controller can be implemented and improved in the large hardware testbed with larger power systems.

For the data historian implementation, future applications using measurement data can be developed to benefit end users. Future work associated with measurement-driven visualization would be implemented in the PI system.

LIST OF REFERENCES

[1] J. De La Ree, V. Centeno, J. S. Thorp, and A. G. Phadke, "Synchronized Phasor Measurement Applications in Power Systems," *IEEE Trans. Smart Grid*, vol. 1, no. 1, pp. 20–27, Jun. 2010.

[2] Y. Liu, S. You, W. Yao, Y. Cui, L. Wu, D. Zhou, J. Zhao, H. Liu, and Y. Liu, "A Distribution Level Wide Area Monitoring System for the Electric Power Grid – FNET/GridEye," *IEEE Access*, vol. 3536, no. c, pp. 1–1, 2017.

[3] Y. Liu, W. Yao, D. Zhou, L. Wu, S. You, H. Liu, L. Zhan, J. Zhao, H. Lu, W. Gao, and Y. Liu, "Recent Developments of FNET/GridEye — A Situational Awareness Tool for Smart Grid," *CSEE J. Power Energy Syst.*, vol. 2, no. 3, pp. 19–27, 2016.

[4] Y. Zhang, P. Markham, T. Xia, L. Chen, Y. Ye, Z. Wu, Z. Yuan, L. Wang, J. Bank, J. Burgett, R. W. Conners, and Y. Liu, "Wide-Area Frequency Monitoring Network (FNET) Architecture and Applications," *IEEE Trans. Smart Grid*, vol. 1, no. 2, pp. 159–167, 2010.

[5] Z. Zhong, C. Xu, B. J. Billian, L. Zhang, S. J. S. Tsai, R. W. Conners, V. A. Centeno, A. G. Phadke, and Y. Liu, "Power System Frequency Monitoring Network (FNET) Implementation," *IEEE Trans. Power Syst.*, vol. 20, no. 4, pp. 1914–1921, 2005.

[6] D. Zhou, J. Guo, Y. Zhang, J. Chai, H. Liu, Y. Liu, C. Huang, X. Gui, and Y. Liu, "Distributed Data Analytics Platform for Wide-Area Synchrophasor Measurement Systems," *IEEE Trans. Smart Grid*, vol. 7, no. 5, pp. 1–9, 2016.

[7] L. Wang, J. Burgett, J. Zuo, C. C. Xu, B. J. Billian, R. W. Conners, and Y. Liu, "Frequency Disturbance Recorder Design and Developments," in *2007 IEEE Power Engineering Society General Meeting, PES*, 2007, pp. 1–7.

[8] P. Kundur, "*Power System Stability and Control*." McGraw-Hill, Inc, New York, 1994.

[9] D. N. Kosterev, C. W. Taylor, and W. a. Mittelstadt, "Model Validation for the August 10, 1996 WSCC System Outage," *IEEE Trans. Power Syst.*, vol. 14, no. 3, pp. 967–979, 1999.

[10] F. Hu, K. Sun, A. Del Rosso, E. Farantatos, and N. Bhatt, "Measurement-Based Real-Time Voltage Stability Monitoring for Load Areas," *IEEE Trans. Power Syst.*, vol. 31, no. 4, pp. 2787–2798, Jul. 2016.

[11] Y. Liu, S. Member, K. Sun, and Y. Liu, "Measurement-Based Power System Dynamic

Model for Response Estimation," no. 2, pp. 1–6, 2012.

[12] J. W. Pierre, "Initial Results in Electromechanical Mode Identification from Ambient Data," *IEEE Trans. Power Syst.*, vol. 12, no. 3, pp. 1245–1251, 1997.

[13] M. G. Anderson, N. Zhou, J. W. Pierre, and R. W. Wies, "Bootstrap-Based Confidence Interval Estimates for Electromechanical Modes from Multiple Output Analysis of Measured Ambient Data," *IEEE Trans. Power Syst.*, vol. 20, no. 2, pp. 943–950, 2005.

[14] L. Chen, P. N. Markham, and Y. Liu, "Wide-Area Dynamic Model Validation Using FNET Measurements," in *2012 IEEE PES Innovative Smart Grid Technologies (ISGT)*, 2012, pp. 1–7.

[15] F. Bai, Y. Liu, Y. Liu, K. Sun, E. Farantatos, N. Bhatt, A. Del Rosso, and X. Wang, "Measurement-Based Correlation Approach for Power System Dynamic Response Estimation," *IET Gener. Transm. Distrib.*, vol. 9, no. 12, pp. 1474–1484, Sep. 2015.

[16] K. Sun, K. Hur, and P. Zhang, "A New Unified Scheme for Controlled Power System Separation Using Synchronized Phasor Measurements," *IEEE Trans. Power Syst.*, vol. 26, no. 3, pp. 1544–1554, Aug. 2011.

[17] D. J. Trudnowski, "Estimating Electromechanical Mode Shape From Synchrophasor Measurements," *IEEE Trans. Power Syst.*, vol. 23, no. 3, pp. 1188–1195, Aug. 2008.

[18] H. Liu, H. Shi, X. Teng, and F. Yuan, "Hydro-Thermal AGC Generators Coordinated Optimization Control Strategy in Yunnan Power Grid," *Autom. Electr. Power Syst.*, vol. 20, pp. 96–99, 2009.

[19] Z. Wang, Y. Xie, C. Yin, and H. Liu, "Research on the Coordination of AGC and Primary Frequency Regulation Based on CPS," *Power Syst. Prot. Control*, vol. 19, pp. 22–25, 2009.

[20] H. Shi, and H. Liu, "Application of Security Active Power Real-Time Dispatching to AGC in Yunnan Electric Power Grid," *South. Power Syst. Technol.*, vol. 1, p. 48–50, 2010.

[21] H. Liu, W. Zhai, and Y. Liu, "The Plant-Level Load Coordinated Distribution System of Thermal Power Plants in Yunnan Power Grid," *South. Power Syst. Technol.*, vol. 5, no. Supplement 1, pp. 34–38, 2011.

[22] B. Pal, and B. Chaudhuri, *Robust Control in Power Systems*. Springer, 2005.

[23] M. E. Aboul-Ela, A. A. Sallam, J. D. McCalley, and A. A. Fouad, "Damping Controller Design for Power System Oscillations Using Global Signals," *IEEE Trans. Power Syst.*, vol. 11, no. 2, pp. 767–773, May 1996.

[24] W. Yao, L. Jiang, J. Wen, Q. H. Wu, and S. Cheng, "Wide-Area Damping Controller of FACTS Devices for Inter-Area Oscillations Considering Communication Time Delays," *IEEE Trans. Power Syst.*, vol. 29, no. 1, pp. 318–329, Jan. 2014.

[25] A. Fuchs, M. Imhof, T. Demiray, and M. Morari, "Stabilization of Large Power Systems Using VSC–HVDC and Model Predictive Control," *IEEE Trans. Power Deliv.*, vol. 29, no. 1, pp. 480–488, Feb. 2014.

[26] C. Zhu, M. Khammash, V. Vittal, and Wenzheng Qiu, "Robust Power System Stabilizer Design Using H/Sub ∞/ Loop Shaping Approach," *IEEE Trans. Power Syst.*, vol. 18, no. 2, pp. 810–818, May 2003.

[27] R. Majumder, B. C. Pal, C. Dufour, and P. Korba, "Design and Real-Time Implementation of Robust FACTS Controller for Damping Inter-Area Oscillation," *IEEE Trans. Power Syst.*, vol. 21, no. 2, pp. 809–816, May 2006.

[28] A. G. Phadke, "The Wide World of Wide-Area Measurement," *IEEE Power Energy Mag.*, vol. 6, no. 5, pp. 52–65, 2008.

[29] H. Liu, L. Zhu, Z. Pan, F. Bai, Y. Liu, Y. Liu, M. Patel, E. Farantatos, and N. Bhatt, "ARMAX-Based Transfer Function Model Identification Using Wide-Area Measurement for Adaptive and Coordinated Damping Control," *IEEE Trans. Smart Grid*, vol. 8, no. 3, pp. 1105–1115, May 2017.

[30] L. Ljung, *System Identification : Theory for the User*. Prentice-Hall, 1987.

[31] D. K. Chaturvedi, and O. P. Malik, "Generalized Neuron-Based Adaptive PSS for Multimachine Environment," *IEEE Trans. Power Syst.*, vol. 20, no. 1, pp. 358–366, Feb. 2005.

[32] J. Zhang, C. Y. Chung, C. Lu, K. Men, and L. Tu, "A Novel Adaptive Wide Area PSS

Based on Output-Only Modal Analysis," *IEEE Trans. Power Syst.*, vol. 30, no. 5, pp. 2633–2642, Sep. 2015.

[33] I. Kamwa, R. Grondin, and Y. Hebert, "Wide-Area Measurement Based Stabilizing Control of Large Power Systems-A Decentralized/Hierarchical Approach," *IEEE Trans. Power Syst.*, vol. 16, no. 1, pp. 136–153, 2001.

[34] R. Eriksson, and L. Soder, "Wide-Area Measurement System-Based Subspace Identification for Obtaining Linear Models to Centrally Coordinate Controllable Devices," *IEEE Trans. Power Deliv.*, vol. 26, no. 2, pp. 988–997, Apr. 2011.

[35] I. Kamwa, and L. Gerin-Lajoie, "State-Space System Identification-Toward MIMO Models for Modal Analysis and Optimization of Bulk Power Systems," *IEEE Trans. Power Syst.*, vol. 15, no. 1, pp. 326–335, 2000.

[36] N. Zhou, J. W. Pierre, and J. F. Hauer, "Initial Results in Power System Identification from Injected Probing Signals Using a Subspace Method," *IEEE Trans. Power Syst.*, vol. 21, no. 3, pp. 1296–1302, Aug. 2006.

[37] H. Ghasemi, C. A. Canizares, and A. Moshref, "Oscillatory Stability Limit Prediction Using Stochastic Subspace Identification," *IEEE Trans. Power Syst.*, vol. 21, no. 2, pp. 736–745, May 2006.

[38] S. A. Nezam Sarmadi, and V. Venkatasubramanian, "Electromechanical Mode Estimation Using Recursive Adaptive Stochastic Subspace Identification," *IEEE Trans. Power Syst.*, vol. 29, no. 1, pp. 349–358, Jan. 2014.

[39] R. W. Wies, J. W. Pierre, and D. J. Trudnowski, "Use of ARMA Block Processing for Estimating Stationary Low-Frequency Electromechanical Modes of Power Systems," *IEEE Trans. Power Syst.*, vol. 18, no. 1, pp. 167–173, Feb. 2003.

[40] L. Dosiek, and J. W. Pierre, "Estimating Electromechanical Modes and Mode Shapes Using the Multichannel ARMAX Model," *IEEE Trans. Power Syst.*, vol. 28, no. 2, pp. 1950–1959, May 2013.

[41] N. R. Chaudhuri, A. Domahidi, R. Majumder, B. Chaudhuri, P. Korba, S. Ray, and K. Uhlen, "Wide-Area Power Oscillation Damping Control in Nordic Equivalent System,"

IET Gener. Transm. Distrib., vol. 4, no. 10, pp. 1139, 2010.

[42] W. Yao, L. Jiang, J. Wen, Q. Wu, and S. Cheng, "Wide-Area Damping Controller for Power System Interarea Oscillations: A Networked Predictive Control Approach," *IEEE Trans. Control Syst. Technol.*, vol. 23, no. 1, pp. 27–36, Jan. 2015.

[43] N. Zhou, Z. Huang, L. Dosiek, D. Trudnowski, and J. W. Pierre, "Electromechanical Mode Shape Estimation Based on Transfer Function Identification Using PMU Measurements," in *2009 IEEE Power & Energy Society General Meeting*, 2009, pp. 1–7.

[44] D. J. Trudnowski, J. W. Pierre, Ning Zhou, J. F. Hauer, and M. Parashar, "Performance of Three Mode-Meter Block-Processing Algorithms for Automated Dynamic Stability Assessment," *IEEE Trans. Power Syst.*, vol. 23, no. 2, pp. 680–690, May 2008.

[45] F. Bai, H. Liu, L. Zhu, Y. Liu, K. Sun, X. Wang, M. Patel, and E. Farantatos, "A Measurement-Based Control Input-Output Signal Selection Approach to Damp Inter-Area Oscillations," in *2015 IEEE PES Asia-Pacific Power and Energy Engineering Conference (APPEEC)*, 2015, pp. 1–5.

[46] G. Rogers, *Power System Oscillations*. Boston, MA: Springer US, 2000.

[47] J. Turunen, J. Thambirajah, M. Larsson, B. C. Pal, N. F. Thornhill, L. C. Haarla, W. W. Hung, A. M. Carter, and T. Rauhala, "Comparison of Three Electromechanical Oscillation Damping Estimation Methods," *IEEE Trans. Power Syst.*, vol. 26, no. 4, pp. 2398–2407, Nov. 2011.

[48] L. Dosiek, N. Zhou, J. W. Pierre, Z. Huang, and D. J. Trudnowski, "Mode Shape Estimation Algorithms under Ambient Conditions: A Comparative Review," *IEEE Trans. Power Syst.*, vol. 28, no. 2, pp. 779–787, May 2013.

[49] Z. Tashman, H. Khalilinia, and V. Venkatasubramanian, "Multi-Dimensional Fourier Ringdown Analysis for Power Systems Using Synchrophasors," *IEEE Trans. Power Syst.*, vol. 29, no. 2, pp. 731–741, Mar. 2014.

[50] M. L. Crow, and A. Singh, "The Matrix Pencil for Power System Modal Extraction," *IEEE Trans. Power Syst.*, vol. 20, no. 1, pp. 501–502, Feb. 2005.

[51] A. K. Singh, and B. C. Pal, "IEEE PES Task Force on Benchmark System for Stability

Controls Report on the 68- Bus, 16-Machine, 5-Area System. Version 3.3.” [Online]. Available: http://www.sel.eesc.usp.br/ieee/index.htm.

[52] Institute of Electrical and Electronics Engineers., and IEEE-SA Standards Board., *IEEE Standard for Synchrophasor Data Transfer for Power Systems*. Institute of Electrical and Electronics Engineers, 2011.

[53] L. Zhu, H. Liu, Y. Ma, Y. Liu, E. Farantatos, M. Patel, and S. McGuinness, “Adaptive and Coordinated Oscillation Damping Control Using Measurement-Driven Approach,” in *2016 Power Systems Computation Conference (PSCC)*, 2016, pp. 1–7.

[54] L. Zhu, H. Liu, Z. Pan, Y. Liu, E. Farantatos, M. Patel, S. McGuinness, and N. Bhatt, “Adaptive Wide-Area Damping Control Using Measurement-Driven Model Considering Random Time Delay and Data Packet Loss,” in *2016 IEEE Power and Energy Society General Meeting (PESGM)*, 2016, pp. 1–5.

[55] L. Yang, X. Zhang, Y. Ma, J. Wang, L. Hang, K. Lin, L. M. Tolbert, F. Wang, and K. Tomsovic, “Hardware Implementation and Control Design of Generator Emulator in Multi-Converter System,” *Conf. Proc. - IEEE Appl. Power Electron. Conf. Expo. - APEC*, pp. 2316–2323, 2013.

[56] H. Liu, L. Zhu, Z. Pan, J. Guo, J. Chai, W. Yu, and Y. Liu, “Comparison of MIMO System Identification Methods for Electromechanical Oscillation Damping Estimation,” in *2016 IEEE Power and Energy Society General Meeting (PESGM)*, 2016, pp. 1–5.

[57] J. Guo, H. Liu, D. Zhou, J. Chai, Y. Zhang, and Y. Liu, “Real-Time Power System Electromechanical Mode Estimation Implementation and Visualization Utilizing Synchrophasor Data,” in *2016 IEEE/PES Transmission and Distribution Conference and Exposition (T&D)*, 2016, pp. 1–5.

[58] J. Zhang, C. Lu, and Y. Han, “MIMO Identification of Power System with Low Level Probing Tests: Applicability Comparison of Subspace Methods,” *IEEE Trans. Power Syst.*, vol. 28, no. 3, pp. 2907–2917, Aug. 2013.

[59] P. Van Overschee, and B. De Moor, “Subspace Algorithms for the Stochastic Identification Problem,” in *1991 Proceedings of the 30th IEEE Conference on Decision*

and Control, pp. 1321–1326.

[60] H. Liu, J. Guo, W. Yu, L. Zhu, Y. Liu, T. Xia, R. Sun, and R. M. Gardner, "The Design and Implementation of the Enterprise Level Data Platform and Big Data Driven Applications and Analytics," in *2016 IEEE/PES Transmission and Distribution Conference and Exposition (T&D)*, 2016, pp. 1–5.

[61] A. Bose, "Smart Transmission Grid Applications and Their Supporting Infrastructure," *IEEE Trans. Smart Grid*, vol. 1, no. 1, pp. 11–19, Jun. 2010.

[62] M. Kezunovic, L. Xie, and S. Grijalva, "The Role of Big Data in Improving Power System Operation and Protection," in *2013 IREP Symposium Bulk Power System Dynamics and Control - IX Optimization, Security and Control of the Emerging Power Grid*, 2013, pp. 1–9.

[63] J. Guo, S. You, C. Huang, H. Liu, D. Zhou, J. Chai, L. Wu, Y. Liu, J. Glass, M. Gardner, and C. Black, "An Ensemble Solar Power Output Forecasting Model through Statistical Learning of Historical Weather Dataset," in *2016 IEEE Power and Energy Society General Meeting (PESGM)*, 2016, pp. 1–5.

[64] S. You, L. Zhu, Y. Liu, H. Liu, Y. Liu, M. Shankar, R. Robertson, and T. King, "A Survey on Next-Generation Power Grid Data Architecture," in *2015 IEEE Power & Energy Society General Meeting*, 2015, pp. 1–5.

[65] J. Liu, X. Li, D. Liu, H. Liu, and P. Mao, "Study on Data Management of Fundamental Model in Control Center for Smart Grid Operation," *IEEE Trans. Smart Grid*, vol. 2, no. 4, pp. 573–579, Dec. 2011.

[66] J. Wang, and H. Zhou, "Conceptual Design and the Future Development for Operation Smart System in China Southern Power Grid," *IEEE Trans. Smart Grid*, vol. 4, no. 3, pp. 1621–1629, Sep. 2013.

[67] B. Wang, B. Fang, Y. Wang, H. Liu, and Y. Liu, "Power System Transient Stability Assessment Based on Big Data and the Core Vector Machine," *IEEE Trans. Smart Grid*, vol. 7, no. 5, pp. 2561–2570, Sep. 2016.

[68] B. Yan, B. Wang, L. Zhu, H. Liu, Y. Liu, X. Ji, and D. Liu, "A Novel, Stable, and

Economic Power Sharing Scheme for an Autonomous Microgrid in the Energy Internet," *Energies*, vol. 8, no. 11, pp. 12741–12764, Nov. 2015.

[69] D. Wei, B. Wang, G. Lin, D. Liu, Z. Dong, H. Liu, and Y. Liu, "Research on Unstructured Text Data Mining and Fault Classification Based on RNN-LSTM with Malfunction Inspection Report," *Energies*, vol. 10, no. 3, p. 406, Mar. 2017.

[70] Z. Pan, X. Wang, G. Mei, Y. Liu, W. Yao, H. Liu, and X. Wen, "A Transformer Neutral Current Balancing Device to Restrain Half-Cycle Saturation Induced by HVDC Monopolar Operations," *Electr. Power Syst. Res.*, vol. 132, pp. 104–114, 2016.

[71] X. Dong, and D. Srivastava, "Big Data Integration," in *2013 IEEE 29th International Conference on Data Engineering (ICDE)*, 2013, pp. 1245–1248.

[72] J. Zhu, E. Zhuang, C. Ivanov, and Z. Yao, "A Data-Driven Approach to Interactive Visualization of Power Systems," *IEEE Trans. Power Syst.*, vol. 26, no. 4, pp. 2539–2546, Nov. 2011.

[73] Q. Shi, H. Hu, W. Xu, and J. Yong, "Low-Order Harmonic Characteristics of Photovoltaic Inverters," *Int. Trans. Electr. Energ. Syst.*, vol. 26, no. 2, pp. 347–364, Feb. 2016.

[74] Q. Shi, H. Cui, F. Li, Y. Liu, W. Ju, and Y. Sun, "A Hybrid Dynamic Demand Control Strategy for Power System Frequency Regulation," *CSEE J. Power Energy Syst.*, vol. 3, no. 2, pp. 17-26, Jun. 2017.

[75] H. Saadat, *Power System Analysis*. PSA Pub, 2010.

[76] X. Zhao, H. Zhou, D. Shi, H. Zhao, C. Jing, and C. Jones, "On-Line PMU-Based Transmission Line Parameter Identification," *CSEE J. Power Energy Syst.*, vol. 1, no. 2, pp. 68–74, Jun. 2015.

[77] D. Shi, D. J. Tylavsky, N. Logic, and K. M. Koellner, "Identification of Short Transmission-Line Parameters from Synchrophasor Measurements," in *2008 40th North American Power Symposium*, 2008, pp. 1–8.

[78] Y. Wang, W. Xu, and J. Shen, "Online Tracking of Transmission-Line Parameters Using SCADA Data," *IEEE Trans. Power Deliv.*, vol. 31, no. 2, pp. 674–682, Apr. 2016.

VITA

Hesen Liu was born in Shandong, China. He got his B.S. degree in Department of Electrical Engineering from North China Electric Power University, Beijing, China, in 2005. He worked for Yunnan Power Grid Company, Kunming, Yunnan, China, from 2005 to 2011. After that, he earned the M.S. degree in Department of Electrical Engineering and Computer Science from the University of Tennessee, Knoxville, TN, USA, in 2015. He is working towards his Ph.D. degree in the Department of Electrical Engineering and Computer Science, University of Tennessee, Knoxville, with graduation in August 2017.

His research interests include wide-area power system measurement and power system dynamics and control.